Preliminary, uncorrected copy

LBL-2144

"Физика ионов высокой энергии не решает проблем физики элементарных частиц"
В. К. Ланцос

PHYSICS RESEARCH WITH HIGH ENERGY HEAVY IONS*

Herbert Steiner

Department of Physics and
Lawrence Berkeley Laboratory
University of California
Berkeley, California 94720
USA

Lectures prepared for the "Adriatic Meeting on Particle Physics"
Rovinj, Yugoslavia
September 23--October 5, 1973

*Work done under the auspices of the U.S. Atomic Energy Commission.

TABLE OF CONTENTS

I. INTRODUCTION

In the past few years it has become possible to accelerate various heavy ions -- from deuterons and alpha particles up to ^{20}Ne -- to energies of several GeV per nucleon. It will soon be possible to accelerate even heavier ions (at least up to Fe) to relativistic energies. In these lectures we will be discussing the physics interest in experiments involving such heavy ions. One is immediately faced with a curious fact; namely, most high energy elementary particle physicists tend to consider complicated objects like deuterons and alpha particles, not to speak of the heavier ions, as too complex and messy to deal with. As a colleague of mine once told me: "The idea of throwing mudpies at each other doesn't really interest me." On the other hand the nuclear physicist tends to be rather apprehensive about the complexity and cost of high energy experiments, and generally feels more comfortable with lower energy experiments having more or less traditional interpretations. Thus high energy heavy ion physics finds itself in a no-man's land somewhere between elementary particle physics and nuclear physics. To make matters even worse it turns out that the language used by particle physicists to describe high energy processes is almost incomprehensible to nuclear physicists and visa versa. I hope to show in these lectures that experiments with high energy heavy ions are likely to have an important impact on both high energy elementary particle physics and nuclear physics. They will also provide useful new information about processes having astrophysical implications. Although these lectures will confine themselves to questions of physics, it must be pointed out that heavy ion beams will also play important roles in biomedical research and therapy, and in the production of superheavy elements.

A bit of history might be in order. It has been possible for quite some time now to accelerate heavy ions to energies of several MeV/nucleon, and a very active research program has evolved with these particles, including Coulomb excitation studies, production of heavy elements and new isotopes, etc. Many of the early cyclotrons were capable of accelerating deuterons and alpha particles to energies of tens of MeV per nucleon. The 184" synchrocyclotron at Berkeley has for a long time had the capability of producing beams of 10^{11} 450 MeV deuterons/sec, or a similar intensity of 915 MeV alpha particles. These beams were used both for physics and biomedical research. But it was only in 1970-71 that four accelerators in the multi-GeV class -- the Princeton-Penn Proton Synchrotron, the Dubna Synchrophasotron, the proton synchrotron SATURNE at Saclay, and the LBL Bevatron began to accelerate ions heavier than protons.

In discussing experimental programs in these lectures, I will confine myself mainly to those at the Bevatron, although some recent results from SATURNE will also be mentioned. In Table I is a summary of parameters of the presently available heavy ion beams at the Bevatron. During the next year it is planned to couple the Super Hilac accelerator to the Bevatron as an injector of even heavier ions. The expected beam parameters are also shown in Table I. Up to now most of the experiments have been of the rather simple exploratory type, but more refined experimental programs are starting to be undertaken.

It is important to emphasize a kinematical fact which plays a crucial role in many of these experiments. The availability of very energetic projectiles makes it possible to study their fragmentation in

TABLE I.

PROPERTIES OF HEAVY ION BEAMS AT THE BEVATRON

ION	ENERGY PER NUCLEON	PRESENTLY AVAILABLE FLUX (particles per pulse)	ANTICIPATED FLUX WITH BEVALAC (1974) (particles per pulse)
$^{1}_{H}$	0.1 - 2.5 GeV	5×10^{12}	--
$^{2}_{H}$	"	2×10^{11}	--
$^{3}_{He}$	"	1×10^{11}	--
$^{4}_{He}$	"	2×10^{10}	3×10^{10}
$^{6}_{Li}$	"	--	3×10^{10}
$^{10}_{B}$	"	--	3×10^{10}
$^{12}_{C}$	"	1×10^{8}	6×10^{10}
$^{14}_{N}$	"	1×10^{7}	3×10^{10}
$^{16}_{O}$	"	1.5×10^{7}	3×10^{10}
$^{20}_{Ne}$	"	10^{5}	10^{10}
$^{40}_{Ar}$	"	--	5×10^{8}
$^{84}_{Kr}$	"	--	5×10^{4}

Energy spread: 300 KeV/nucleon FWHM

Spill: 0.2 - 1.0 sec

Pulse frequency: 10 - 17 pulses/minute

the laboratory system even though the fragments have little or no energy relative to the projectile. Thus for example information about the fragmentation of ^{12}C can be obtained in a ^{12}C (projectile) + p (target) collision which could not be obtained in the corresponding p (projectile) + ^{12}C (target) interaction because in the latter case many of the fragments would find it difficult or even impossible to get out of a finite-sized target. As we will see shortly, it has become possible to make detailed studies of the fragmentation of energetic projectiles into pieces having very low velocities relative to the projectile -- measurements which heretofore were impossible. A related consideration is that the fragmentation of fast projectiles tends to cause the various pieces to go into a rather narrow cone in the forward direction, thus making it quite straightforward to make detailed momentum analyses of the fragments with a magnetic spectrometer having a relatively small solid angle acceptance in the laboratory system and to detect most of them with detectors of modest size. These factors, though of no great theoretical significance, are very important indeed from the experimental point of view.

What then can one hope to learn from experiments with energetic heavy ions? As we will see, the experiments bear on such topics as high energy interaction mechanisms, fragmentation processes, particle production, nuclear and hypernuclear structure, and cross sections for processes having astrophysical implications. We will examine the theoretical models that have been proposed to describe high energy heavy ion processes, and in particular we will try to focus on the similarities and differences between heavy ion interactions and the corresponding interactions of high energy pions, kaons, and nucleons both from the experimental and the theoretical points of view.

In attempting to present a rather new subject like this it soon becomes painfully clear that there are as yet few if any experts, nor a great deal of solid reference material. I have tried to include in the bibliography a sampling of some typical experimental and thooretical papers dealing with the topics discussed in these lectures.

II. WHAT CAN WE HOPE TO LEARN FROM EXPERIMENTS WITH ENERGETIC HEAVY IONS?

A. High Energy Interaction Mechanisms and Nuclear Structure

At the outset one has to define the term "high energy". What may be high energy in one domain of physics will certainly not be high energy in another. One has to introduce a scale. In atomic physics that scale may be characterized by the level spacings of atomic energy levels, in nuclear physics the spacing between nuclear levels, and in elementary particle physics the spacing between resonances. In terms of constituent models the characteristic energies could also be related to the binding of the various pieces. Asymptotic considerations apply when the interaction energies are large compared to such characteristic energies. Of course, a given system can have several quite distinct characteristic energies; thus, for example, a nucleus may have characteristic energies corresponding to possible coherent excitations of the whole nucleus, as well as those related to resonant excitations of the individual nucleons comprising the nucleus. It may not be unreasonable to expect that asymptotic considerations will be applicable to hadronic systems at various levels. In particular, the fragmentation of several GeV/nucleon nuclei by various targets can be expected to show some of the same kinds of limiting distributions that have been postulated for and observed in "elementary" particle interactions at NAL and ISR. It seems likely that the closely related concepts of scaling and/or factorization may also be applicable to nuclear systems at high energy. Two important consequences follow if these conjectures are true: (1) High energy heavy ion experiments would provide an extremely powerful means of studying nuclear correlations inside nuclei.

In the limiting case the fragmentation of such nuclei should reflect very closely the "parton" structure of the projectile independent of energy and target. (2) Such experiments (at a few GeV/nucleon) could conceivably provide important tests of high energy interaction models. The additional degree of freedom introduced by allowing the baryon number to vary puts additional constraints on models of high energy collisions, and may provide new insights into the nature of such interactions.

As an example let us consider the question of factorizability of total cross sections. The principle of factorization implies that

$$\sigma_{AA}\sigma_{BB} = (\sigma_{AB})^2 .$$

Thus,

$$\sigma_{AA} = \frac{(\sigma_{pA})^2}{\sigma_{pp}} .$$

Since

$$\sigma_{pA} \propto A^{2/3} ,$$

one would expect

$$\sigma_{AA} \propto A^{4/3} .$$

It has been pointed out by Gribov[1] that such a behavior is not in conflict with theory at sufficiently high energy if the nucleus becomes larger and at the same time more transparent. Still it is a rather strange result and it would be very surprising indeed to see such an A-dependence at a few GeV per nucleon. Specific models, such as for example Glauber-type models or even geometric models predict quite different relations between total cross sections. It is worth keeping in mind that such tests of factorization are difficult in the case of B = 0,1 systems because of the very limited number of possible experimentally accessible

combinations of stable projectiles and targets. The use of $B \geq 2$ particles will greatly increase the experimentally feasible tests of factorization.

B. Astrophysical Considerations

Among the most important and still unanswered questions in astrophysics are those pertaining to the nature of cosmic ray sources and the lifetimes of the cosmic rays. Practically all models of cosmic ray source abundances that have been proposed suffer from a lack of accurate cross section data for the fragmentation of various heavy ions by the hydrogen and helium in the interstellar medium. The availability of beams of heavy ions with energies of a few hundred to a few thousand MeV/nucleon should make possible measurements of a number of cross sections of interest, including those for some unstable heavy ions. The question of cosmic ray lifetimes might be resolved by measurement of production, interaction and electron attachment cross sections of ^{10}Be and ^{53}Mn. These are typical examples of K-capturing nuclear species, and their abundance can be related to cosmic ray lifetimes once the relevant cross sections are known.

C. Chew's Conjecture

Chew has conjectured that "whenever the available energy becomes large there should be manifested general strong interaction characteristics that are independent of baryon number. None of the known hadrons, after all, can be regarded as 'elementary', the composite nature of any hadron becoming more and more prominent as the energy increases."[2] He argues the concept of "nuclear democracy" is incompatible with assigning a

preferred status to any hadronic species.[3] Although he recognizes that there are certain experimental distinctions, between B = 0,1 and B $\geq$ 2 systems such as for example the density of level spacings, he maintains that most of the experimentally measurable parameters vary rather smoothly and monotonically with baryon number, and that common theoretical foundations underlie all hadronic systems. In his view the traditional theoretical distinction between "nuclear" and "particle" physics is rather artificial, and arises more from the failure of theorists to properly merge non-relativistic and relativistic considerations than from any inherent difference between them.[4]

Chew divides our present understanding of strong interactions into the following three categories: "(1) General principles; (2) Models of manifestly limited capacity that approximately describe restricted ranges of phenomena; (3) Principles that currently are applied only in an approximate sense but that show promise of eventually achieving a general status." Examples of the first category are such general S-matrix principles as Poincare invariance (implying conservation of energy, momentum, and angular momentum, as well as equivalence of different inertial frames of reference), unitarity, causality, isospin symmetry, hypercharge conservation, and the connection between spin and statistics. In the second category he places quark models, the potential (optical) model and the dual resonance (Veneziano) model. Examples of the third category are SU(3) symmetry and Regge asymptotic behavior. He then observes that in such a classification no sharp line can be drawn on the basis of baryon number, and he asks the question of whether category 2 and 3 principles are general enough to encompass B $\geq$ 2 phenomena. It is through experiments

with energetic heavy ions that we may hope to learn whether or not B = 0 and 1 systems constitute an aristocratic class obeying a distinct set of physical laws or if we are dealing with true nuclear democracy.

III. TYPES OF THEORETICAL APPROACHES TO HIGH ENERGY HEAVY ION INTERACTIONS

The existing theoretical models can be classified into three groups:

(1) Macroscopic, geometric, optical, hydrodynamic, statistical.

(2) Microscopic, e.g., interaction of constituents, multiple scattering, cascade processes.

(3) Regge and Particle Type Models, e.g., multiperipheral bootstrap, Regge asymptotic models, pole dominance.

Not only are these theoretical approaches of interest in themselves, but also the connections between them have yet to be clearly formulated.

A. Macroscopic Models

There are various types of macroscopic models. Common to all of them is the underlying basis that in the interactions of energetic heavy ions the principal features can be described in terms of parameters characterizing the macroscopic properties of the colliding systems. For example, Bowman, Swiatecki and Tsang[5] use the geometric picture of two colliding spheres which partially overlap according to the impact parameter between them. For relativistic ions these Lorentz-contracted spheres then interact with each other in the region where they overlap. They use the term "abrasion" to describe the process of shearing off nuclear matter in the overlap region. The residual target and/or projectile nuclei may then be grossly distorted objects with much higher than normal surface energy. These highly excited objects deexcite by boiling off nucleons in a second stage process which they characterize by the term "ablation". They have refined this simple picture by introducing a "friction" parameter whose

role it is to modify the clean abrasion by allowing a friction between the target and projectiles to partly heat nuclear matter in target and projectile and to cause it to drag chunks of nuclear matter out of one system or the other in the collision process. Their simple model has been quite successful in describing the general features of the limited fragmentation data that is now available. It will be interesting to experimentally determine how strong is the correlation between the fragmentation of the target and the projectile. With this model, naively one might expect to find a strong correlation in the sense that a big piece knocked out of the projectile should more often than not be accompanied by a big piece knocked out of the target. A geometrically interesting configuration would be the case if a small projectile were to drill a small hole out of a larger target. At this stage this type of theoretical model is largely phenomenological in that the parameters are determined by comparison to experiment or by crude estimation. Its main virtue is the simplicity of the geometrical picture used.

Another type of macroscopic model is one in which the projectile generates a shock wave inside the target (or visa versa), and the fragmentation or particle production is the result of such shock phenomena. This type of model was suggested many years ago by Glassgold, Heckrote, and Watson,[6] and might be applicable to high energy nucleus-nucleus processes. It is worth keeping in mind that the velocity of sound in nuclear matter is a significant fraction of the velocity of light so that relativistic collisions are needed to produce such shock phenomena. Detailed calculations are needed to establish the usefulness of this type of model in high energy heavy ion collisions.

role it is to modify the clean abrasion by allowing a friction between the target and projectiles to partly heat nuclear matter in target and projectile and to cause it to drag chunks of nuclear matter out of one system or the other in the collision process. Their simple model has been quite successful in describing the general features of the limited fragmentation data that is now available. It will be interesting to experimentally determine how strong is the correlation between the fragmentation of the target and the projectile. With this model, naively one might expect to find a strong correlation in the sense that a big piece knocked out of the projectile should more often than not be accompanied by a big piece knocked out of the target. A geometrically interesting configuration would be the case if a small projectile were to drill a small hole out of a larger target. At this stage this type of theoretical model is largely phenomenological in that the parameters are determined by comparison to experiment or by crude estimation. Its main virtue is the simplicity of the geometrical picture used.

Another type of macroscopic model is one in which the projectile generates a shock wave inside the target (or visa versa), and the fragmentation or particle production is the result of such shock phenomena. This type of model was suggested many years ago by Glassgold, Heckrote, and Watson,[6] and might be applicable to high energy nucleus-nucleus processes. It is worth keeping in mind that the velocity of sound in nuclear matter is a significant fraction of the velocity of light so that relativistic collisions are needed to produce such shock phenomena. Detailed calculations are needed to establish the usefulness of this type of model in high energy heavy ion collisions.

Statistical or thermodynamic models in which the interaction is described in terms of temperature and partition of energy according to the principles of statistical mechanics are also likely to find applicability in the fragmentation of energetic nuclei. The density of possible final states is sufficiently high in this case that statistical considerations should play an important role. Here again methods of calculation exist but detailed comparisons with actual experimental situations are largely non-existent.

Optical models in which the projectile (or the target) is considered as an optical medium with complex refractive index have been widely used to describe small angle nucleon-nucleus scattering and should aslo provide a good description of certain types of nucleus-nucleus collisions. The basic problem here is to properly describe the optical properties of the system. Müllensiefen[7] uses the opaqueness of the nucleon and the density distribution of the A nucleons which follows from the measured nuclear electric form factor to determine the nuclear opaqueness, $\rho_A(x,y,z)$. The nucleon opaqueness is determined from elastic nucleon-nucleon scattering. Thus, although the theory itself is macroscopic, the input parameters are determined in part from microscopic considerations. In essence Müllensiefen's calculations as well as those of Czyz and Maximon[8] are extensions of the Chou-Yang model for pp scattering[9] to nucleus-nucleus collisions.

B. Microscopic Models

Here the basic premise is that the scattering of two complex objects can be related in a straightforward way to the scatterings of the various constituents out of which these complicated objects are built. The most frequently used models are all extensions or elaborations of the original

Glauber model. Implicit in most calculations of this type are: (1) The nucleons inside a nucleus are uncorrelated; (2) Spin effects are neglected; (3) In combining the effects of multiple scatterings the phases involved are simply added; (4) The results of such calculations are valid only for small angle scattering; (5) The passage of the projectile is fast compared to the rotation frequency of a deformed target nucleus. For example, Tekou has applied the Glauber model to both deuteron-nucleus scattering,[10] and nucleus-nucleus scattering[11] at high energy.

The elastic scattering amplitude of a wave through a medium can be written

$$f = \frac{ik}{2\pi} \int d^2\vec{b} \, [1 - e^{iX(b)}] \, e^{i\vec{q}\cdot\vec{b}}$$

where $\vec{b}$ is the impact parameter

$\vec{q}$ is the momentum transfer

$\vec{k}$ is the momentum of the wave.

The phase X(b) is then constructed from the phases of the individual nucleon-nucleon scattering terms. This type of calculation is well-known and will not be repeated here. For a plane wave through a system with a large number of constituents,

$$\frac{dI}{dx} = -\rho\sigma I \tag{2}$$

where I is the intensity of the wave,

$$\frac{d\psi}{dx} = ik\psi - \frac{\rho\sigma}{2}\psi(1-i\alpha) \tag{3}$$

where the factor

$$\alpha = \frac{\text{Re } f(0^\circ)}{\text{Im } f(0^\circ)} \tag{4}$$

then

$$iX(b) = -\int_{-\infty}^{\infty} dz \, \rho(b,z) \, \frac{\sigma}{2} \, (1 - i\alpha) \quad . \tag{5}$$

For two composite systems:

$$iX(\vec{b}_1 - \vec{b}_2) = -\frac{\sigma}{2} \, (1 - i\alpha) \int d^2\vec{s} \; D_1(\vec{s} - \vec{b}_1) \; D_2(\vec{s} - \vec{b}) \tag{6}$$

where

$$D_1(s_1) = \int dz \; \rho_1(s_1, z) \tag{7a}$$

$$D_2(s_2) = \int dz \; \rho_2(s_2, z) \tag{7b}$$

and

$$\int d^3r_1 \rho_1(r_1) = A_1 \tag{8a}$$

$$\int d^3r_1 \rho_2(r_2) = A_2 \quad . \tag{8b}$$

In this case

$$f = \frac{ik}{2\pi} \int d^2b_1 \; d^2b_2 \; [1 - e^{i \, X(\vec{b}_1 - \vec{b}_2)}] \; e^{i\vec{q} \cdot (\vec{b}_1 - \vec{b}_2)} \tag{9}$$

In the limit of many constituents the Glauber theory goes over to the eikonal optical model discussed previously. In all cases where such Glauber-type calculations have been made with sufficient care the results have agreed very well with experiment down to energies < 500 MeV. However, up to now most of these calculations have involved primarily total and small angle elastic cross sections. It would be very useful to have this type of calculation extended to larger angles and to such inelastic channels as pion production and fragmentation of heavy ions into nucleons and other pieces. It may be difficult to do so because, although Glauber theory can be used to calculate nuclear excitations, it may be difficult to use it to predict specific deexcitation mechanisms.

In principle it is possible to use Glauber theory to study the detailed interactions of every nucleon in the target with every nucleon in the projectile, and even include the effects of inelastic processes. However, such calculations are still much too complicated to be practical. Instead various types of classical (non-quantum mechanical) cascade calculations bave been made using Monte Carlo methods. A weakness of such calculations is that it is difficult to take into account coherent effects in which several nucleons participate in a collision. Up to now relativistic effects have been largely ignored in such calculations. Despite these shortcomings such cascade calculations[12,13] have agreed quite well with certain experimental observations of light fragment emission resulting from proton, deuteron and ^{4}He bombardment of silver and uranium at energies of several GeV per nucleon.

C. Regge Type Models (High Energy Particle Theories)

As Chew suggests is is tempting to apply Regge ideas to the collision of energetic nuclei. One of the first practical aspects of this is to introduce the proper kinematical variables. As we will see shortly when we discuss the experimental results, the rapidity variable $y = \tanh \frac{v_{\parallel}}{c}$ and the scaling variable $x' = \frac{p^*_{\parallel}}{(p^*_{\parallel})_{max}}$ are very well suited to describe the interactions of relativistic heavy ions. This is because the rapidity variable, y, has the property of (1) continuing to grow as the particle's energy increases in contrast to the velocity which approaches its asymptotic limit whenever the kinetic energy becomes comparable to the mass, and (2) providing a description of particle interactions in which the differences in rapidity between particles is independent of Lorentz frame. At 2 GeV/nucleon

the rapidity difference between target and projectile is just a little less than two units. Use of the invariant cross sections $E\frac{d^3\sigma}{dp^3}$, $\frac{d^2\sigma}{dtdm^2}$, $\frac{d^3\sigma}{dyd^2p}$, etc., are useful in displaying the experimental results. Relations between these cross sections and between the various types of kinematical variables commonly used in relativistic particle collisions can be found for example in References 14 and 15.

Chew[2] defines Regge behavior as follows: Consider a collision process in which one can divide incoming and outgoing momenta into two groups (as shown in diagram below).

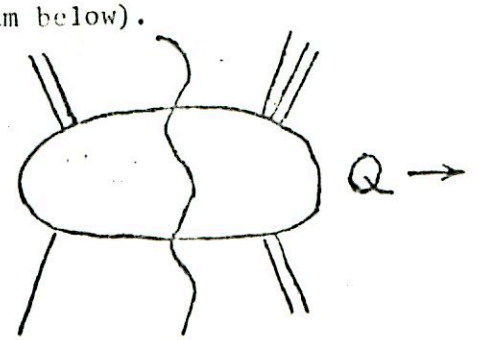

Diagram 1

Q is the four momentum transfer between the right and left groupings. Two sets of "internal" variables x_L and x_R characterize the left and right groups of particles. When the rapidity difference $\zeta = \tanh\frac{v_{LR}}{c}$ is large and all other variables -- x_L, x_R and $t = Q^2$ -- are held fixed, the amplitude has the asymptotic form:

$$A(x_L, x_R, t, \zeta) \underset{\zeta\to\infty}{\sim} \sum_i g_i(x_L, x_R, t)\, e^{\alpha_i\zeta} \qquad (10)$$

where i may contain continuous as well as discrete components.

Froissart has shown that for $t = 0$

$$\mathrm{Re}\,\alpha_i \leq 1.$$

Those values of α_i with the largest real parts are asymptotically dominant.

In particular it has been experimentally observed that when t is near zero and the internal quantum numbers in the direction of the momentum transfer vector Q (in Diagram 1) are those of the vacuum there is an important contribution to the expansion[10] from $\alpha_i = 1$. This is the so-called Pomeranchuk contribution -- the "pomeron".

Chew then goes on to define a Regge pole as being a discrete value of α_i that depends only on t (not on x_R and x_L) and whose coefficient has a factorizable dependence on x_L and x_R; i.e.,

$$A(x_L, x_R, t, \zeta) \underset{\zeta\to\infty}{\sim} \sum_i g_{iL}(x_L,t)\, g_{iR}(x_R,t)\, e^{\alpha_i(t)\zeta} \qquad (11)$$

The question of how the pomeron is related to Regge poles, and if it factorizes is still not experimentally settled. However, if we assume that for rapidity gaps $\zeta \geq 2$ a factorizable pomeron dominates for both large and small baryon number we can examine what experimental consequences this has in the case of high energy heavy ion interactions.

We have shown earlier the experimental implication of factorizability in the case of total cross sections, i.e., $\sigma_{AA}\sigma_{BB} = (\sigma_{AB})^2$. In the case of diffractive dissociation of AB → A*B* where there is a large rapidity gap between AA* and BB* as shown in Diagram 2

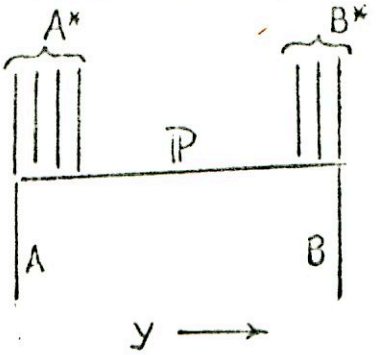

Diagram 2

factorization implies that

$$s^2 \frac{d\sigma}{dt}(AB \to A^*B^*) \underset{\left(\frac{s}{m_{A^*}^2 m_{B^*}^2}\right)\text{large}}{\sim} A_{A\mathbb{P}\to A^*} \left(\frac{s}{m_{A^*}^2 m_{B^*}^2}\right)^{2\alpha_{\mathbb{P}}(t)} A_{B\mathbb{P}\to B^*}$$

where $A_{A\mathbb{P}\to A^*}$ and $A_{B\mathbb{P}\to B^*}$ are factors which are related to the cross sections $\sigma(A\mathbb{P}\to A^*)$ and $\sigma(B\mathbb{P}\to B^*)$, and s is the square of the total c.m. energy.

For the special case when $AB \to A'$ + anything as in Diagram 3,

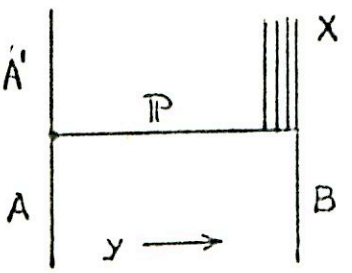

Diagram 3

when only the final particle A' is detected, we are dealing with a single particle inclusive experiment. Again, if there is a large rapidity gap, and if no quantum numbers are exchanged, it is tempting to assume "pomeron" dominance. In this case the right hand vertex is proportional to the total "pomeron" + B cross section which in turn is related to the so-called triple pomeron vertex whose value and behavior as a function of t is of great current interest (see Diagram 4).

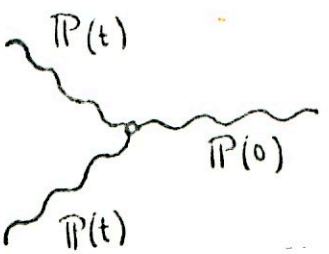

Diagram 4

If the aspects of Regge behavior described above are valid for large baryon numbers as well as for small, there will be a vast increase in the variety of experiments that shed light on the triple-pomeron vertex. Of course, we don't know yet if the energies available at present for these experiments

would be sufficiently high to cleanly isolate the "pomeron" contribution. Thus another question of interest is at what energies do Regge asymptotic approximations become valid? If the spacing between levels were to determine the scale then the scattering of large baryon number systems may be asymptotic much sooner than the corresponding "elementary" particle processes.

In inclusive experiments of the type sketched in Diagram 4 pomeron factorization implies that what happens at the AA'P vertex depends asymptotically only on the momentum transfer but not on the PB X vertex; i.e., not on the nature of B nor on the energy. It would also be of interest to see how the coupling of the pomeron to B depends on the mass of B and on the momentum transfer, and how this coupling relates to the "pomeron"-nucleon coupling. As we will see in the next section, the experiments of Heckman, et al., indicate that the fragmentation of energetic nitrogen and oxygen ions is approximately proportional to the (mass of the target)$^{1/4}$.

It seems likely that in diffractive dissociation processes of heavy ions with energies of several GeV per nucleon, the rapidity distributions of the fragments will be somewhat different from those observed in pp experiments at higher energies. This is because the loose binding of the constituents of the heavy targets and projectiles may cause projectile and target fragmentation to be more copious than "pionization." In other words the production of particles in the interior regions of the multiperipheral chain can be expected to be suppressed relative to dissociation of the external particles. Experimental evidence from the interaction of 2.1 GeV ^{16}O ions in emulsion indicate the following relative probabilities for each of the fragmentation processes sketched below.[16]

Diagram (5a) ∿16%

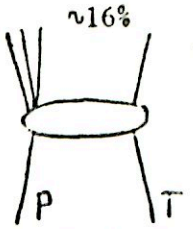

Projectile Fragmentation

(5b) ∿22%

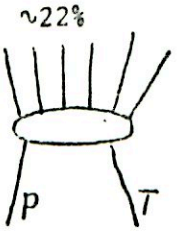

"Nucleation"

(5c) ∿51%

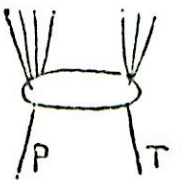

Projectile and Target Fragmentation

(5d) ∿11%

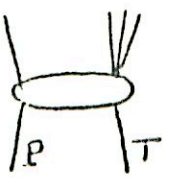

Target Fragmentation

It will be interesting to see how well these results can be reproduced by Regge and other models.

D. Relationships Between Macroscopic, Microscopic, and Regge Type Models

The success of any model must ultimately be based on how well predictions agree with experiment. If these three types of models were to all describe the experimental observations then it seems reasonable that there must exist a close connection between them. We have already seen an example of this in the case of the Glauber type model which goes over to an eikonal type optical model when the number of target and projectile constituents gets to be very high. The relationship between Glauber and Regge models is not quite so clear. Trefil[17] has used a Glauber type approximation to show that if nucleon-nucleon interactions scale, then nucleon-nucleus collisions and even nucleus-nucleus collisions should also scale. Experiments with energetic heavy ions may shed some additional light on how these various models interrelate. It is certainly an important theoretical problem to establish the connection between these different approaches.

The validity of such concepts as limiting fragmentation, scaling and factorization are not necessarily tied to any one particular model, and one of the crucial and as yet unanswered questions is: Where do the predictions of the different models really differ enough so that experiments can distinguish between them.

IV. EXPERIMENTAL RESULTS

In Table II is a summary of experimental heavy ion activities at the Bevatron taken from Heckman's talk[18] at the Uppsala Conference on High Energy Physics and Nuclear Structure. In this discussion of recent experimental results I will confine myself to three subjects: (1) Fragmentation of ^{16}O nuclei at 2.1 GeV/nucleon (at LBL); (2) Single particle inclusive spectra resulting from the collision of relativistic protons, deuterons, and alpha particles with nuclei (at LBL); and (3) missing mass spectra resulting from np, dp, and dd collisions (at Saclay).

TABLE II

CURRENT HEAVY ION PHYSICS RESEARCH PROGRAM AT BEVATRON

Heavy Ion Fragmentation: Single Particle Inclusive Spectra at Forward Angles

Heavy Ion Total Cross Section Measurements

Range and Ionization Studies

Positive and Negative Particle Production: Search for Coherent Pion Production

Nuclear Fragmentation of Heavy Target Nuclei Induced by High Energy Heavy Ions

d-p Backward Elastic Scattering

Production and Study of a Tagged, Mono-energetic Neutron Beam

Production of High Energy Hypernuclei

Emulsion Studies of Target Fragmentation, Spallation and Heavy Ion Cross Sections

Calibration of Particle Detection and Identification Systems for Satellite and Balloon Flight Experiments

A. Heavy Ion Fragmentation of ^{16}O Nuclei at 2.1 GeV/nucleon*

H. H. Heckman, Lawrence Berkeley Laboratory
G. E. Greiner, University of California, Space Sciences Laboratory
P. J. Lindstrom
F. S. Bieser

The experiment on the fragmentation of ^{16}O nuclei by Heckman, et al continue and extend earlier work on the 0^o- fragmentation of ^{14}N beam nuclei at 2.1 GeV/nucleon.[18] The first experimental results gave evidence that the single particle inclusive spectra are independent of the target nucleus. Another striking feature of the fragmentation process is that, within the measurement error, the forward going fragments of the beam projectile have mean velocities equal to the velocity of the incident beam. It is this last property that has proven extremely useful in the production of well defined secondary beams of isotopes.

Figure 1 is a scale drawing of the 0^o heavy-ion magnetic spectrometer that has been designed and brought into operation to carry out the 0^o-fragmentation experiments. The spectrometer focuses magnetically analysed beam fragments, produced within 12.5 mr of the beam direction, onto charge-measuring solid-state detector telescopes placed along the focal plane of the spectrometor. The rigidity $R(GV/c) = p/z$ of the fragments is given by the expression $R = K(D)/D$, where D is the deflection distance and K(D) is a slowly varying function of D. Salient features of the isotopic identification are:

i) Rigidity resolution (rms)
$\Delta R/R = 0.6\ \Delta D/D \quad (130 \leq D \leq 400 cm)$

ii) Charge resolution (rms)
$\Delta Z = \pm 0.1e$

iii) Time of flight (FWHM)
$\Delta t = 100$ psec

---

* The description of this experiment is taken from Heckman's paper given at the Fifth Conference on High Energy Physics and Nuclear Structure, Uppsala, Sweden, June, 1973. I thank Dr. Heckman for permission to include his paper in these lectures.

Because the beam fragments have well defined velocities, the magnetic spectrometer effectively becomes a Z/A ($\propto$D) spectrometer. How the isotopes are spatial separated along the guide rail is illustrated in Figure 2 where the distance D is indicated for all isotopes with A $\leq$ 16. Figure 3 presents the measured spectrum of the carbon isotopes as a function of D produced by the fragmentation of ^{16}O beam nuclei at E = 2.1 GeV/nucleon in a beryllium target. If we now take the N(D) spectrum and express it in terms of longitudinal momentum, we obtain the distribution $N(p_{\parallel})$ shown in Figure 4 . Qualitative properties of the carbon spectrum are:

i) the peak intensity occurs at A = 12,
ii) the envelope of the spectrum diminishes monotonically as $|A - 12|$ increases, and
iii) the spectral shape in momentum space of the various isotopes are the same.

To the accuracy of the measurements, a characteristic of all such spectra, helium through oxygen, is that the maximum for each isotope occurs at a momentum corresponding to the beam velocity.

The curves drawn through the individual carbon isotope spectra are Gaussian functions of momentum $P_{\parallel}$, all having equal standard deviations. When these distributions are transformed to the projectile frame (where the beam projectile is at rest), the momentum distribution conduce to a single (Gaussian) distribution of form $N(P_{\parallel})_{proj} \propto \exp[-P^2_{\parallel}/2(m_{\pi}c)^2]$. This is illustrated in Figure 5 where we have plotted the longitudinal momentum distributions $N(P_{\parallel})$ versus $P_{\parallel}$ for a sample of isotopes of the elements Z = 1 to 8 produced by the fragmentation of ^{16}O nuclei (Be target) at 2.1 GeV/nucleon. (The sample was selected on a criterion of minimal statistical accuracy for the spectrum of each isotope.) Within the indicated typical error, the distributions $N(P_{\parallel})$ are remarkably consistent with a

unique Gaussian function with $\sigma = m_\pi c = 140$ MeV/C.

To complement these longitudinal momenta data, we present in Figures 6 [a, b, c] our first measurements of transverse momenta. These distributions were derived from the analysis of particle trajectories using a pair of 3-plane (120^o) multiwire chambers (128 wires, 1 mm wire spacing) placed behind the detector telescopes. The data presented for ^{15}N, ^{14}C and ^{13}C are the projected transverse momentum distributions $N(P_\perp)$ as measured. Both x- and y- components of $P_\perp$, normal to, and in the plane of the spectrometer, were measured and are shown in the figure ($P_\parallel$ is along the z-axis). We anticipate that uncertainties in the incident beam direction, multiple scattering in the target and spatial resolution of the wire chambers will affect a 5 - 10% correction to the standard deviations of the $N(P_\perp)$ spectra.

As was done for the longitudinal momentum distributions given in Figure 5, we compare the perpendicular momentum distributions for ^{15}N, ^{14}C and ^{13}C to Gaussian functions. The solid curve has a standard deviation $\sigma = 140$ MeV/C, the dashed curves --- 100 and 180 MeV/c. The hash-marks in the vicinity of 500 MeV/c in each figure indicate the maximum value of $P_\perp$ that is transmitted by the spectrometer system for the laboratory momentum of each isotope. These $P_\perp$ (max) correspond to a 12.5 mrad production angle at the target. Although the data are preliminary, they clearly indicate that no significant differences are apparent between the longitudinal and transverse momentum distributions. Both can be characterized by Gaussian functions with widths $\sigma \approx m_\pi c$. In Figure 6 [c], we have included the longitudinal momentum distribution for ^{13}C (see Figure 5) to exhibit the similarity between the parallel and perpendicular momentum distributions.

At this stage, the experimental results strongly suggest that, in the projectile frame, the longitudinal and transverse momentum distributions of the fragmentation products of heavy ion beams at 2.1 GeV/nucleon are the same, with a characteristic width approximately $m_\pi c$.

Furthermore, these distributions appear to be independent of the atomic mass of the fragment.

That the fragmentation of relativistic heavy ions via the nucleus-nucleus interaction proceeds with a minimal value of momentum transfer suggests that theories pertaining to single particle inclusive spectra, may be applicable to heavy ion fragmentations. Of immediate relevancy is the concept of the factorization of cross-sections. Factorization states that in the reaction A + B → X + ----, the partial cross sections factor according to the rule $\sigma_{AB}^{X} \rightarrow \gamma_A^X \gamma_B$ where the function $\gamma^X(A)$ depends on the beam nucleus A and its fragmentation product X and γ_B is a function of the target nucleus B only.

As previously mentioned, the first high energy fragmentation experiments performed at the Bevatron gave evidence for such factorization, i.e., the modes of fragmentation are independent of the target nucleus.

In a conventional transmission experiment, we have measured the total cross sections for the production of B, C, and N from ^{16}O ions and B from ^{12}C ions at E = 2.1 GeV/nucleon in targets of CH_2, C, S, Cu and Pb. In this experiment, only the initial (Z = 6 or 8) and final (effective) charge Z^* of the products were measured. Figure 7 is a plot of the target factor γ_B, versus the mass of the target. If it is assumed that γ_B is of the form $\gamma_B = M^n$, where M is in atomic mass units, then γ_A^X is equal to the total cross section for the production of X from beam nucleus A in hydrogen. With a fitted target factor exponent of n = 0.256, the factorable cross section becomes $\sigma_{AB}^X = \sigma_A^X M^{0.256}$, an expression that fits the data to a confidence level of 0.6

B. Single Particle Inclusive Spectra Resulting from the Collision of Relativistic Protons, Deuterons, and Alpha Particles with Nuclei**

J. Jaros, J. Papp, L. Schroeder, J. Staples,
H. Steiner, and A. Wagner

Lawrence Berkeley Laboratory

We report here some preliminary results of an experiment to measure single particle inclusive spectra resulting from the collisions of 1.05-4.2 GeV (kinetic energy) protons, and 1.05 and 2.1 GeV/nucleon deuterons and alpha particles with targets of Be, C, Cu, and Pb. The yields of $\pi^{\pm}$, p, d, ^{3}H, ^{3}He, and ^{4}He were measured as a function of momentum at a fixed laboratory angle, $\theta = 2.5°$. The initial motivation for this experiment was to measure negative pion production from a variety of targets bombarded by relativistic deuterons and alpha particles to search for very energetic pions; pions with energies considerably larger than those which could be produced in a collision of a single nucleon with a nucleus. A second phase of the experiment consisted of reversing the polarity of our spectrometer and measuring positive particle yields. It was thought that the high energy fragmentation of deuterons and alpha particles might provide a heretofore unexploited means of studying particle momentum distributions and correlations inside these projectiles. It seemed quite possible that the fragmentation of these particles, even in the range of 1-2 GeV/nucleon, would already have reached some kind of limiting or asymptotic distribution, and that measurements of these fragmentation spectra might thus also afford rather interesting tests of such concepts as limiting fragmentation, scaling, and factorization. We were curious to see to what extent the various mechanisms proposed to describe very high energy elementary particle collisions could be applied to deuteron and alpha particle interactions at these energies. In this context, a series of questions present themselves:

**The description of this experiment is taken from our paper submitted to the Aix-en-Provence Conference on Elementary Particles (September, 1973).

(1) What is the role of diffractive dissociation, Regge or Pomeron exchange processes, multiperipheralism, fireballs, and other similar concepts in the collisions of high energy heavy ions with complex targets?

(2) Is there any relation between the characteristic energies of a system (e.g., the spacing of the energy levels) and the energy at which asymptotic considerations become valid?

(3) What can be learned about the "parton" structure of these particles in experiments of this type? After all we are dealing with systems whose nuclear structure is thought to be reasonably well understood, and so we should be able to test some of these ideas in a more familiar context, namely, the decomposition of a nuclear particle into its constituents.

Although we cannot answer all of these questions completely with the data presented here, we would like to indicate how our measurements bear on some of these concepts.

The experiment was performed in the external beam of the Bevatron. Fluxes of particles ranged from 10^{9}-10^{10} per pulse for alphas, and 10^{10}-10^{11} per pulse for deuterons. A double focusing spectrometer was used to momentum analyze the secondary particles and to transmit them to our detecting system. The detection system was extremely simple, consisting of two scintillation counters to measure the time-of-flight of the secondaries over a 15 meter flight path, and a pair of scintillation counters to record their pulse heights and in this way to distinguish between singly and doubly charged particles. The time-of-flight spectra were stored in a 400 channel

analyzer and then read onto magnetic tape. Data were typically taken at momentum/charge intervals of 0.25 GeV/c over the range, $0.5 \leq k \leq 5.0$ GeV/c. No attempts were made to make measurements below 0.5 GeV/c because in the case of pions the lepton contamination and the decay corrections became too large to be easily manageable. For protons and heavier fragments the multiple scattering and energy loss considerations made it impracticable to go to lower momenta. The upper limit of 5 GeV/c was set by limitations on the current in the magnets of the beam transport system. A monitor telescope (three scintillation counters in coincidence) was placed about 3 meters from the production targets at about 90° to the incident beam. The monitor counts, which were proportional to the amount of beam striking a given target, were used during the experiment as a relative normalization for our yields. To obtain an absolute normalization the monitor counts for each target were periodically calibrated against the beam intensity as measured with both an ionization chamber and a secondary emission monitor which were located in the primary beam just upstream of the production targets. Some unresolved questions still exist about these calibrations, and also about the effective solid angle acceptance of our spectrometer, so that the absolute normalization of our particle yields are not final. The momentum dependence of these yields for each target is not affected by these uncertainties. During the course of running, a scintillation screen viewed by a TV camera was moved into the beam to check the spot size of the beam at our production target and to see that the beam had not wandered off the target.

We turn first to the results on negative pion production. In Fig. 8 we show the single particle inclusive π^- spectra at 2.5° (Lab) resulting from the collision of 1.05, 1.73, 2.10, 2.66, 3.50, and 4.20 GeV protons

with a 0.64 cm long Be target. Similar spectra, not shown here, were obtained with C, Cu, and Pb targets. In these spectra as well as in all of the other pion yields to be reported here the results were corrected for lepton contamination in the beam (as measured with a gas-filled Cherenkov counter), decay in flight, and effects due to the finite lengths of the targets used. Except for the points at the very tails of these distributions the statistical errors are very small, and do not constitute the major uncertainty in our results. Systematic effects due to focusing and steering the primary beams onto our targets constituted the main source of error outside of the aforementioned monitor calibration problems. When these results are replotted in terms of the Lorentz Invariant cross section $\frac{E}{k^2}\frac{\partial^2\sigma}{\partial\Omega\partial k}$ versus the scaling variable $x' = \frac{k_{\parallel}^*}{(k_{\parallel}^*)_{max}}$ (where $k_{\parallel}^*$ is the longitudinal momentum of the outgoing pion as measured in the overall center-of-mass system) a rather remarkable result appears (Fig.9). All of the spectra tend to fall on top of each other. This scaling property, where the pion yield becomes a function only of the single scaling variable x', usually at a fixed $k_{\perp}$ and independent of the total energy, is familiar at higher energies, but here we see that even at 1 GeV the scaling behavior is quite well satisfied. It should be kept in mind that because the experiment was done at a fixed angle in the laboratory system ($\theta_L = 2.5°$) the transverse momentum, $k_{\perp}$, is not strictly constant ($22 \leq k_{\perp} \leq 220$ MeV/c). However, especially at the lower momenta $k_{\perp}$ stays small and does not vary much in an absolute sense. At the higher momenta (e.g. 3-4 GeV/c) this variation of $k_{\perp}$ may well be responsible for the observed differences in the various spectra.

The laboratory cross section, $\frac{\partial^2\sigma}{\partial\Omega\partial k}$, as a function of pion momentum,

k, for pion production by 1.05 GeV/nucleon and 2.10 GeV/nucleon protons, deuterons, and alpha particles on Be is shown in Figs.10 and 11. Two features stand out:

1) Pions are produced more copiously be deuterons and alphas than by protons, and
2) The pion spectra induced by deuterons and alphas extend to higher momenta than those induced by protons.

Preliminary attempts to fit the observed deuteron and alpha induced pion production spectra with a model in which the nucleons moving inside the projectile collide individually and independently with the target nucleus have so far been unsuccessful in reproducing the observed results. Although more refined calculations with better input data are necessary our results seem to suggest that the effects of multiple scattering terms or equivalently some sort of collective process in which several nucleons in the projectile act jointly are not negligible, and should be included in such calculations.

The Lorentz Invariant cross sections $\frac{E}{k^2}\frac{\partial^2\sigma}{\partial\Omega\partial k}$ vs x' for pion production by deuterons and alpha particles is shown in Figs. 12 and 13. Again the scaling property of these distributions seems to be satisfied. It is also interesting to note that these distributions fall much more steeply with x' as the mass of the projectile is increased. This feature is not unexpected since a complicated loosely-bound object like an alpha particle probably has a much harder time transferring a large fraction of its energy to a single pion than does a proton.

In Fig. 14 we show the pion yield as a function of laboratory momentum for 2.1 GeV/nucleon alpha particles on various targets. It is seen that the shape of these spectra is almost independent of target material. This feature is true of all the pion spectra measured in this experiment, except

at the very lowest momenta where a slight target dependence becomes noticeable. As shown in Fig. 15 the pion production cross sections for 2.1 GeV/nucleon alpha particles (as well as those for other projectiles and energies) are proportional to $A^{1/3}$ when $k \gtrsim 1$ GeV/c.

Next we turn to the results on the fragmentation of protons, deuterons, and alpha particles into positively charged particles. A large amount of data was amassed (incident energies: 1.05 and 2.10 GeV/nucleon; incident particles: protons, deuterons and alpha particles; targets: Be, C, CH_2, Cu, Pb; fragments: π^+, p, d, ^{3}H, ^{3}He, ^{4}He.) As an example in Fig. 16 is shown the fragmentation of 1.05 GeV/nucleon alpha particles by a Be target. The "parton" structure of the alpha particle is clearly displayed. Not only does ^{4}He consist of proton and neutron constituents, but also deuterons, ^{3}H, and ^{3}He. We thus expect that high energy diffractive dissociation of alpha particles in reactions of this type should provide us with a reasonably clean "snapshot" of nucleon correlations and momentum distributions without having the interaction itself seriously disturb the pre-existing conditions in the projectile. Care should be exercised in interpreting the magnitudes of the various peaks, because as has been pointed out previously the data were taken at fixed $\theta_{lab} = 2.5°$, and consequently different transverse momenta are involved in these distributions. These effects can be significant since typical Fermi momenta are 100 to 200 MeV/c and at $\theta_{lab} = 2.5°$ a k = 2 GeV/c particle has a transverse momentum of $\sim$100 MeV/c. In any case, it is evident that the fragmentation of ^{4}He into deuterons has a cross section comparable to that for fragmentation into protons. It should also be noted that the position of the proton, deuteron, and ^{3}H, ^{3}He peaks occur as expected at one-fourth, one-half,

and three-fourths of the momentum of the incident alpha particle. These facts are neatly summarized in a plot of the Lorentz Invariant cross section $\frac{E}{k^2}\frac{\partial^2\sigma}{\partial\Omega\partial k}$ versus y_c, the rapidity of the outgoing fragment. Such a plot is shown in Fig. 17. Several features stand out:

1) The peaks of the rapidity distributions all coincide with the rapidity of the incident alpha particle projectile.
2) The heavier the fragment the more sharply peaked (i.e., the narrower) the distribution.
3) The diffractive dissociation peak is cleanly separated from other identifiable regions of the rapidity distribution, i.e., it is well separated from the rapidity of the target, and stands out clearly from the central ("pionization") region. Again, this feature is not unexpected. On the contrary it would be surprising to find large numbers of these fragments in the central region, and the bulk of the particles resulting from target fragmentation are too low in momentum to be detected by our detecting system.
4) Because of the 0.5 GeV/c lower limit on the momentum of particles detected in this experiment the rapidity distribution of the pions (because of their small mass) extends to much higher values of rapidity than do the distributions of the heavy fragments.

In Figs. 18 and 19 are shown the laboratory cross sections and the Lorentz Invariant rapidity distributions resulting from the fragmentation of 1.05 GeV/nucleon deuterons on Be. The momentum distribution of the protons is again centered at the same point as in the case of the alpha particle, but here the distribution is significantly narrower. This is not unreasonable since the deuteron is a much more loosely bound system

than ^{4}He. This can also be seen by comparing the rapidity distributions. The shape of the deuteron spectrum is reminiscent of other inelastic scattering processes, and it may well be that rather similar theoretical considerations apply to all of these processes.

Finally, in Figs. 20 and 21 are presented the laboratory cross sections and the Lorentz Invariant rapidity distributions of protons resulting from the fragmentation of 2.1 GeV/nucleon deuterons and alpha particles by Be. Again the protons from the alpha fragmentation have a broader momentum (and rapidity) distribution than do the protons from deuteron disintegration. At first sight a comparison of Figs. 17, 19, and 21 would seem to indicate that these proton distributions have not yet attained any kind of limiting characteristic, but here again the pitfall of measurements at a fixed laboratory angle must be taken into account. Although a definitive statement about limiting distributions in this case must await further experimental investigation, it seems likely that the observed distributions are indeed at some kind of asymptotic limit.

Lack of space and time prevents us from showing the detailed behavior of these distributions for different targets. In practically all cases, however, the shapes of the distributions shown above for the case of Be are almost identical to those of the other targets. Only in the case of very low momentum heavy fragments do target dependent effects manifest themselves.

In this paper we have tried to show that single particle inclusive spectra resulting from the interactions of relatively modest-energy protons, deuterons, and alpha particles with nuclear targets show many of the features

such as scaling and limiting fragmentation that are characteristic of very high energy elementary particle interactions, and that experiments of the type discussed here may shed additional light not only on the nuclear physics aspects of these reactions but also on possible high energy interaction mechanisms.

We thank Dr. Hermann Grunder and the Bevatron Staff for their important contributions to this experiment. We also thank J. Wiss for help with the data analysis.

C. Missing Mass Spectra Resulting from np, dp and dd Collisions (at Saclay)***

The following types of reactions have been studied:

(1) $d + p \to d + (mm)^+$ at 2.94 - 3.41 and 3.48 GeV/c[19];

(2) $d + p \to {}^3He + \pi^0$, $d + p \to {}^3H + \pi^+$, $d + p \to {}^3He + \eta^0$ for $2.83 \leq p_d \leq 3.82$ GeV/c[20];

(3) $n + p \to d + (mm)^0$ and the "ABC" effect[21];

(4) $d + p \to {}^3He + (mm)^0$ and the parameters of the "ABC" and "DEF" effects[22];

(5) $d + d \to {}^4He + (mm)^0$ at 2.49, 3.34, and 3.82 GeV/c.[23]

(1) $d + p \to d + (mm)^+$

In this reaction one of the objectives was to look for T = 1/2 isobars. A single arm spectrometer was used to momentum analyze the outgoing deuteron. Some typical results are shown in Fig. 22[19]. Care must be taken in interpreting the peaks because of kinematical effects associated with plotting $\frac{d\sigma}{d\Omega dp}_{lab}$. The arrow on the first peak shows the position of the π mass in the reaction $N + p \to d + \pi$ for incident nucleons having half the momentum of the deuteron beam. The peak at a mass of 1150 MeV does not seem to move with angle or energy although its magnitude decreases at the larger angles. No evidence for higher mass T = 1/2 N*'s is seen. There are various possible mechanisms which can be used to explain the experimental observations. Among these the one-particle exchange contributions

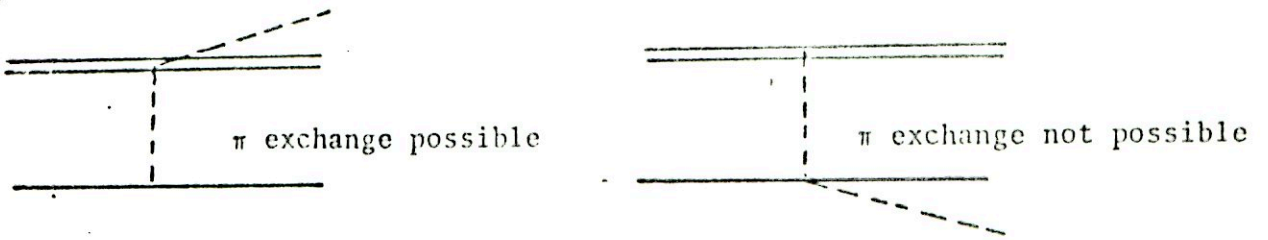

***Recent results of these experiments have been presented at Uppsala (June, 1973), Berkeley (August, 1973), and Aix-en-Provence (September, 1973).

are likely to be important. No claim is made that the observed peak is a new T = 1/2 baryon resonance.

(2) $d + p \to {}^3He + \pi^0$, $d + p \to {}^3H + \pi^+$, $d + p \to {}^3He + n^0$

Here the main objective was to measure the relevant cross sections and thereby to shed some light on possible meson production mechanisms. The first two reactions also afford yet another test of charge independence in hadronic interactions.[20]

(3) $n + p \to d + (mm)^0$ and the "ABC" effect

A monoenergetic neutron beam from deuteron stripping was used and a large "ABC" effect was observed as shown in Figs. 23 and 24. Confirming evidence comes from the deuteron spectrum resulting from the reaction $d + p \to d + (mm)^0 + p$ which can be interpreted to occur in part as

$$[p_{spectator} + n] + p \to p_{spectator} + d + (mm)^0$$

and $$[n_{spectator} + p] + p \to n_{spectator} + d + (mm)^+$$

(4) The "ABC" and the "DEF" effects in the reaction $d + p \to {}^3He + (mm)^0$

Thirteen spectra in the ranges of incident momenta $2.8 \leq p \leq 3.8$ GeV/c and laboratory angles $0 \leq \theta_L \leq 11°$ were obtained by the Saclay group for the above reaction as well as two spectra for the conjugate reaction $d + p \to {}^3H + (mm)^+$. An example of the results obtained by them is shown in Fig. 25. The authors conclude:

(a) The "ABC" effect exists and has I = 0.

(b) The central mass of the "ABC" varies between 300 ± 12 and 365 ± 23 MeV depending on kinematical conditions.

(c) The "ABC" has an intrinsic width of 50 ± 10 MeV.

(d) The angular distribution of the production cross section in the c.m. system is strongly peaked forward and backwards in contrast to π^0 and η^0 production.

(e) The production cross section of the "ABC" at 180° varies rapidly with total energy in the c.m. system and has a maximum near $W^* = 3.38$ (See Fig. 26).

(f) That there is a new bump, which they call "DEF", with a mass of 450 ± 20 MeV.

(g) That the "DEF" has I = 0.

(h) That the production cross section for the "DEF" has the same angular and energy dependence as the "ABC".

A number of mechanisms have been postulated to explain the observations[25,26] but up to now none of these are completely satisfactory. Thus the exact nature of the "ABC" effect, and now also perhaps the "DEF", still remains to be elucidated.

(5) $d + d \rightarrow {}^4He + (mm)^o$ at 2.49, 3.34, and 3.82 GeV/c.

The observed spectra show two broad peaks (Fig. 27). One corresponds to "ABC", the other to the ω^0. This reaction is of interest for several reasons: (1) One is dealing here with two T = 0 deuterons and a T = 0 alpha particle, so that if isospin symmetry is valid only T = 0 $(mm)^o$ states should be produced. No π^0's have been seen. (2) The reaction $dd \rightarrow He + \gamma$ can be studied ~~has been observed~~ and can be compared with the inverse process $\gamma + He \rightarrow d + d$ and thus afford a test of detailed balance.

The foregoing serve as illustrations of results that have so far been obtained in experiments involving $B \geq 2$ projectiles. It is clear that the interpretation of these experiments presents new difficulties and challenges. But it is also clear that experiments of this general type are likely to provide useful new information about the nature of strong interactions.

V. OTHER PHYSICS EXPERIMENTS AND THEIR POTENTIAL SIGNIFICANCE

Let us look briefly at a number of other types of experiments, some of which are even now being undertaken.

A. Total and Small Angle Differential Cross Section Measurements

Among other things the object here is to test factorization and to check the validity of Glauber model predictions. A complicating factor is introduced by the presence of rather strong Coulomb amplitudes which interfere with the nuclear scattering.[27] It may be very difficult to cleanly separate the Coulomb and nuclear effects.

B. Experiments with Monoenergetic Neutrons from Stripped Deuterons

The availability of energetic deuteron beams has made it possible to obtain high intensity, essentially monoenergetic neutron beams by stripping the deuterons. A further refinement is to tag the neutron's energy by momentum analyzing the stripped proton in coincidence with the neutron. Such monoenergetic neutron beams can be used in a number of experiments such as $n + p \to d + \pi$, $n + p \to p + n$, $n + p \to d + (mm)^0$, etc.

C. Polarized Neutrons from Stripped Polarized Deuterons

If polarized deuterons can be successfully accelerated to high energy the stripped protons or neutrons would also be polarized and could be used for example to study spin dependent effects in elastic and inelastic np scattering. Use in conjunction with a polarized target would permit high energy polarization correlation measurements which have a bearing on the

principle of factorization and on the establishment of the nature of the nucleon-nucleon scattering amplitudes at high energy. It should be easier to accelerate polarized deuterons to high energy than polarized protons because of their smaller magnetic moment. Polarized or even aligned deuterons would also be very useful in making detailed tests of Glauber theory.

D. Hypernuclei and Superstrange Nuclei

The use of energetic heavy ion beams to produce hypernuclei offers an interesting new probe of nuclear structure. The Arizona group[28] has made preliminary measurements of the reaction $^{16}O + p \rightarrow {}^{17}_{\Lambda}O + K^+$ in hopes of using this type of two body final state to produce unique species of hyperfragments whose decays could subsequently be studied. Unfortunately the cross sections are small. A more prolific source of energetic hyperfragments would result from the fragmentation of a relativistic projectile into a K^+ and a hyperfragment. The presence of the K^+ could be used to trigger the hyperfragment detectors. The time-dilation associated with the lifetime of relativistic hyperfragments may make possible detailed measurements of decay parameters and lifetimes. Kerman and Weiss[29] have pointed out that it should be possible to produce superstrange nuclei with beams of energetic heavy ions. Very roughly the cross sections in heavy nuclei are calculated to decrease by factors of about 10 for each additional unit of strangeness.

E. Spin Correlation Measurements in the Fragmentation of B ≥ 2 Nuclei

An interesting test of diffractive dissociation and a novel probe of nuclear structure is possible through the determination of spin correlations of fragments produced in particle interactions at high energy. The idea can best be illustrated for the case of deuteron fragmentation. In the diffractive dissociation of a deuteron the $^3S_1$ nature of the neutron-proton system should be left intact. Thus there should be a definite correlation between the spins of the neutron and the proton fragments. This can be measured in those cases where both the neutron and the proton are rescattered in such a way that the scatterings analyze the polarizations. Then for example there should be a preponderance of neutron scatters to the left whenever left-scattered protons are detected. Similarly right-right, up-up, down-down, should be more probable than up-down, right-left, etc. Here we have another manifestation of the so-called Einstein-Rosen-Podalsky Paradox. The idea can be turned around by assuming that spin flip is unimportant in the fragmentation of high energy projectiles. Then such measurements would bear on the spin correlations of the constituents of the fragmenting nucleus.

F. Measurements of Pion Multiplicities

It would be very interesting to determine if anomalously high pion multiplicities result from nucleus-nucleus collisions at high energies. After all, a very large amount of energy could sometimes be deposited into a rather small volume and this might manifest itself in the form of pions. From another point of view high pion multiplicities could also result from coherent effects between production amplitudes of the various nucleon-nucleon

scatterings. In any case such measurements should provide interesting tests of high energy interaction models.

G. Fragment Correlation Experiments (Multiparticle Inclusive and Exclusive Reactions

As pointed out previously fragment correlation measurements should provide important tests of theoretical models. Several types of correlations are of interest: (1) Correlations between target and projectile fragments. This tests geometric models and factorization. (2) Correlation between projectile fragments. This is particularly important from the standpoint of nuclear structure. For example, when ^{12}C fragments into ^{4}He is the residue most often two more α particles or some other configuration? (3) Correlation between fragments clustering near the rapidity of the projectile and those which dome from the middle of the rapidity interval. Are the "central" fragments really independent of both projectile and target as might be naively expected from a multiperipheral type model? Such rapidity correlations play an important role in high energy interaction theories.

H. Coherent Excitations of Nuclei

Nuclear levels can be selectively excited in processes where the exchange of quantum numbers can be selectively controlled. For example $\alpha + (A,Z) \rightarrow \alpha + X$ requires that X has to have the same isospin as (A,Z). Although such reactions have been extensively studied at lower energies, the availability of high energy projectiles allows such measurements to be extended.

VI. A FEW CONCLUDING COMMENTS AND SPECULATIONS

I have tried to show that experiments with high energy heavy ions are likely to yield interesting new information about the nature of high energy processes and about nuclear structure. It is a new field with many more questions than answers.

It is amusing to speculate about some "far out" aspects of heavy ion collisions:

(1) For example, what happens when two heavy ions come together to form a system with $Z_{eff} > 137$? Will quantum electrodynamics survive?

(2) At very high energies the lifetime of virtual states (e.g., that of N*'s) inside nuclei increases by a factor m/E. What is the effect of such virtual states?

(3) What would happen in heavy ion interactions at ISR energies? Farley[30] speculates about possible new types of phenomena when high energy densities (say ∿10 GeV/nuclear volume) are produced. Would such a system have a Hagedorn limiting temperature? Could one get pion condensation? Could such a system be a breeding ground for new types of complex systems? Quantum number restrictions may be less severe.

(4) It seems likely that central collisions of high energy heavy ions will be more interesting than peripheral processes. It is not really clear what happens when two massive relativistic objects hit head-on.

(5) Can we expect any unusual phenomena to be associated with the very large angular momenta available in such processes?

I hope these comments will serve to stimulate more thinking about physics with high energy heavy ions.

VII. ACKNOWLEDGMENTS

In preparing these lectures I benefited greatly from notes taken durng a recent two-week LBL summer study on heavy ion physics. Discussions with many colleagues, especially G. F. Chew, A. Goldhaber, and L. Bertocchi were particularly valuable. H. Heckman and his group, as well as L. Schroeder have been very helpful in providing summaries of recent experimental papers. To all of them, and to Miss Suzie Sayre who worked beyond the call of duty in helping me get this report written on time I express my sincere thanks.

VIII. REFERENCES

1. V. N. Gribov, Soviet Journal of Nuclear Physics 9, 369 (1969).

2. G. F. Chew, "Large and Small Baryon Numbers in High Energy Collision Theory", LBL Internal Report, p.2, May 21, 1973 (unpublished).

3. G. F. Chew, "High Energy Heavy Ion Beams as Tests of Nuclear Democracy and as a Tool to Clarify Regge Asymptotic Behavior", LBL Internal Report, March 10, 1972 (unpublished).

4. G. F. Chew, "Nuclear and Particle Physics: Two Different Subjects?". Comments on Nuclear and Particle Physics 2, 107 (1968).

5. J. D. Bowman, W. J. Swiatecki, and C. F. Tsang, "Abrasion and Ablation of Heavy Ions", LBL Internal Report, July, 1973, (unpublished).

6. A. E. Glassgold, W. Heckrote, K. M. Watson, Ann. Phys. 6 1 (1959).

7. A. Mullensiefen, Nucl. Phys. B28 368 (1971).

8. W. Czyz and L. C. Maximon, Phys. Letters 27B 354 (1968), Ann Phys. 52, 59 (1969).

9. T. T. Chou and C. N. Yang, Phys. Rev. 170, 1591, (1968); Phys. Rev. Letters 20, 1213 (1968).

10. A. Tékou, Nucl. Phys. B46, 141 (1972).

11. A. Tékou, Nucl. Phys. B46, 152 (1972).

12. A. Pozkanzer, H. Bertini, private communication.

13. G. W. Barry, "Inclusive Reactions Involving Nuclei", Purdue Univ. Preprint (1973), (unpublished).

14. J. Kasman, "Inclusive Spectra: Kinematics and Phenomenology", Part III of "A Compilation of Data on Inclusive Reactions", LBL-80, August, 1972. Obtainable from the Particle Data Group, LBL.

15. W. R. Frazer, L. Ingber, C. H. Mehta, C. H. Poon, D. Silverman, K. Stowe, P. D. Ting and H. J. Yesian, Rev. Mod. Phys. 44 284 (1972).

16. D. Greiner, private communication.

17. J. S. Trefil, "A Survey of the Theory of Inclusive Reactions on Nuclei", (A summary of discussions at the LBL Summer Study on Heavy Ion Physics) July, 1973, unpublished.

18. a) H. H. Heckman, "High Energy Heavy Ions: A New Area for Physics Research", LBL-2052, to be published in the Proceedings of the Vth Conference on High Energy Physics and Nuclear Structure" held in Uppsala, Sweden, June, 1973.

b) H. H. Heckman, D. E. Greiner, P. J. Lindstrom, and F. S. Bieser, Phys. Rev. Letters, 28 926 (1972).

19. J. Banaigs, J. Berger, L. Goldzhal, L. Vu-Hai, M. Cotterau, C. LeBrun, F. L. Fabbri, P. Picozza,"High Energy Coherent Interaction of Deuterons on Protons", contributed paper to Fifth Conference on High Energy Physics and Nuclear Structure", Uppsala, June, 1973.

20. J. Banaigs, J. Berger, L. Goldzahl, T. Risser, L. Vu-Hai, M. Cotterau, C. LeBrun, "A Study of the Reaction $d + p \rightarrow {}^3He + \pi^0$, $d + p \rightarrow {}^3He + \pi^+$, and $d + p \rightarrow {}^3He + \eta^0$", contributed paper to Fifth Conference on High Energy Physics and Nuclear Structure, Uppsala, June, 1973.

21. G. Bizard, F. Bonthonneau, M. Cotterau, J. L. Laville, C. LeBrun, F. Lefebvres, J. C. Malherbe, R. Regimbart, J. Berger, J. Duflo, L. Goldzahl, F. Plouin, L. Vu-Hai, "Observation of the "ABC" Effect in $n + p \rightarrow d + (mm)^o$, contributed paper to Fifth Conference on High Energy Physics and Nuclear Structure, Uppsala, June, 1973.

22. J. Banaigs, J. Berger, L. Goldzahl, T. Risser, L. Vu-Hai, M. Cotterau, C. LeBrun, "'ABC' and 'DEF' Effects: Position, Width, Isospin, Angular and Energy Distributions", contributed paper to Fifth Conference on High Energy Physics and Nuclear Structure, Uppsala, June, 1973.

23. J. Banaigs, J. Berger, L. Goldzahl, T. Risser, L. Vu-Hai, M. Cotterau, C. LeBrun, F. L. Fabbri, P. Picozza, "A Study the Reaction $d + d \rightarrow {}^4He + (mm)^o$, contributed paper to Fifth Conference on High Energy Physics and Nuclear Structure, Uppsala, June, 1973.

24. M. D. Shuster, T. Risser, I. Bar-Nir, "On the Nature of the ABC Effect", contributed paper to Fifth Conference on High Energy Physics and Nuclear Structure, Uppsala, 1973.

25. M. Bleszynski, F. L. Fabbri, P. Picchi, P. Picozza, "Nucleus Excitation Model for ABC Effect", contributed paper to Fifth Conference on High Energy Physics and Nuclear Structure, Uppsala, June, 1973.

26. J. C. Anjos, D. Levy and A. Santoro, "Dynamical Model for the ABC Effect", contributed paper to the Fifth Conference on High Energy Physics and Nuclear Structure, Uppsala, June, 1973.

27. See for example, V. Franco, Phys. Rev. D7, 215 (1973).

28. T. Bowen, G. Cable, D. A. Delise, E. W. Jenkins, R. M. Kalbach, K. J. Nield, R. C. Noggle and A. E. Pifer, "Production of Hypernuclei in a 2.1 GeV/nucleon Oxygen Beam", Reported by H. H. Heckman at Uppsala, (see Reference 18).

29. A. Kerman and M. Weiss, "Superstrange Nuclei", LLL preprint (January, 1973) (unpublished).

30. F. J. M. Farley , "Speculations on Nucleus-Nucleus Collisions at the ISR", CERN-NP Internal Report 70-26 (1970).

IX. FIGURE CAPTIONS

Fig. 1. Magnetic spectrometer for the 0°-fragmentation experiment. Fragments of heavy ion beam (^{16}O) produced within 12.5 mr of the beam direction are focused along guide rail according to charge and momentum.

Fig. 2. Deflection distance D vs Z and A of isotopes produced at 0° and at beam velocity.

Fig. 3. Observed count-rate vs D of the carbon isotopes produced by the fragmentation of ^{16}O nuclei at 2.1 GeV/nucleon.

Fig. 4. Momentum spectrum for the carbon isotopes produced by the fragmentation of ^{16}O nuclei at 2.1 GeV/nucleon.

Fig. 5. Longitudinal momentum distributions in projectile frame.

Fig. 6. Transverse momentum distributions for a) ^{15}N; b) ^{14}C and c) ^{13}C isotopes produced by fragmentation of ^{16}O at 2.1 GeV/nucleon. Transverse components in, and normal to, the plane of the magnetic spectrometer are shown. The longitudinal momentum spectrum for ^{13}C is also shown for comparison in c).

Fig. 7. Target factor $\gamma(B)$ vs M(amu) of target, the solid line denoted $\gamma(B) = M^{0.256}$.

Fig. 8. $\left(\frac{\partial^2\sigma}{\partial\Omega\partial k}\right)_{lab}$ for π^- production by protons on Be as a function of pion momentum. $\theta = 2.5°$ (lab). The different points correspond to different proton energies. The curves have no theoretical significance and were drawn only to aid the eye in connecting the points at each energy.

Fig. 9 π^- production by protons on Be. $\theta = 2.5°$ (lab). The data of Fig. 8 plotted in terms of the Lorentz Invariant cross section $\frac{E}{k^2}\frac{\partial^2\sigma}{\partial\Omega\partial k}$ vs the scaling variable $x' = \frac{k_{\pi}^*}{(k_{\pi}^*)_{max}}$.

Fig. 10 $\left(\frac{\partial^2\sigma}{\partial\Omega\partial k}\right)_{lab}$ for π^- production by 1.05 GeV/nucleon protons, deuterons, and alphas on Be. $\theta = 2.5°$ (lab).

Fig. 11. $\left(\frac{\partial^2\sigma}{\partial\Omega\partial k}\right)_{lab}$ for π^- production by 2.10 GeV/nucleon protons, deuterons, and alphas on Be. θ = 2.5° (lab)

Fig. 12. The Lorentz Invariant cross section $\frac{E}{k^2}\frac{\partial^2\sigma}{\partial\Omega\partial k}$ vs the scaling variable $x' = \frac{k_{\parallel}^*}{(k_{\parallel}^*)_{max}}$ for pion production by 1.05 GeV/nucleon and 2.1 GeV/nucleon deuterons. θ = 2.5° (lab).

Fig. 13. The Lorentz Invariant cross section $\frac{E}{k^2}\frac{\partial^2\sigma}{\partial\Omega\partial k}$ vs the scaling variable $x' = \frac{k_{\parallel}^*}{(k_{\parallel}^*)_{max}}$ for pion production by 1.05 GeV/nucleon and 2.1 GeV/nucleon alphas. θ = 2.5° (lab).

Fig. 14. $\left(\frac{\partial^2\sigma}{\partial\Omega\partial k}\right)_{lab}$ vs pion momentum k for π^- production by 2.1 GeV/nucleon alpha particles for three different targets: Be, C, and Pb. θ = 2.5° (lab)

Fig. 15. $\left(\frac{\partial^2\sigma}{\partial\Omega\partial k}\right)_{lab}$ vs A_{Target} for π^- production by 2.10 GeV/nucleon alpha particles for different pion momenta. θ = 2.5° (lab).

Fig. 16. Fragmentation cross sections, $\left(\frac{\partial^2\sigma}{\partial\Omega\partial k}\right)_{lab}$, vs fragment momentum for dissociation of 1.05 GeV/nucleon alpha particles into protons, deuterons, ^{3}H, ^{3}He, and ^{4}He. θ = 2.5° (lab). Be target.

Fig. 17. The data of Fig. 9 plotted in terms of the Lorentz Invariant cross section $\frac{E}{k^2}\frac{\partial^2\sigma}{\partial\Omega\partial k}$ vs the rapidity variable y_c. Arrows indicate the rapidity of the target and the incident alpha particle projectile. θ = 2.5° (lab).

Fig. 18. Proton and deuteron production cross sections $\left(\frac{\partial^2\sigma}{\partial\Omega\partial k}\right)_{lab}$ vs fragment momentum resulting from the interaction of 1.05 GeV/nucleon deuterons in Be. θ = 2.5° (lab).

Fig. 19. The data of Fig. 18 replotted in terms of the Lorentz Invariant cross section $\frac{E}{k^2}\frac{\partial^2\sigma}{\partial\Omega\partial k}$ vs the rapidity variable y_c.

Fig. 20. Fragmentation cross sections $\left(\frac{\partial^2\sigma}{\partial\Omega\partial k}\right)_{lab}$ vs momentum for protons resulting from 2.10 GeV/nucleon deuteron and alpha particle interactions in Be. $\theta = 2.5°$ (lab).

Fig. 21. The data of Fig. 20 replotted in terms of the Lorentz Invariant cross section $\frac{E}{k^2}\frac{\partial^2\sigma}{\partial\Omega\partial k}$ vs the rapidity variable y_c.

Fig. 22. Missing mass spectra at various angles and incident energies resulting from the reaction $d + p \rightarrow d + (mm)^o$. Saclay Group.[19]

Fig. 23. Missing mass spectrum resulting from the reaction $n + p \rightarrow d + (mm)^o$. Saclay Group.[21]

Fig. 24. Missing mass spectrum resulting from the reaction $d + p \rightarrow d + (mm)^o + p_{spectator}$. Saclay Group[21].

Fig. 25. Missing mass spectrum resulting from the reaction $d + p \rightarrow {}^3He + (mm)^o$. Saclay Group.[22]

Fig. 26. Backward differential cross section as a function of energy for producing the "ABC" in the reaction $d + p \rightarrow {}^3He + $ "ABC". Saclay Group[22].

Fig. 27. Missing mass spectrum resulting from the reaction $d + d \rightarrow {}^4He + (mm)^o$. Saclay Group.[23]

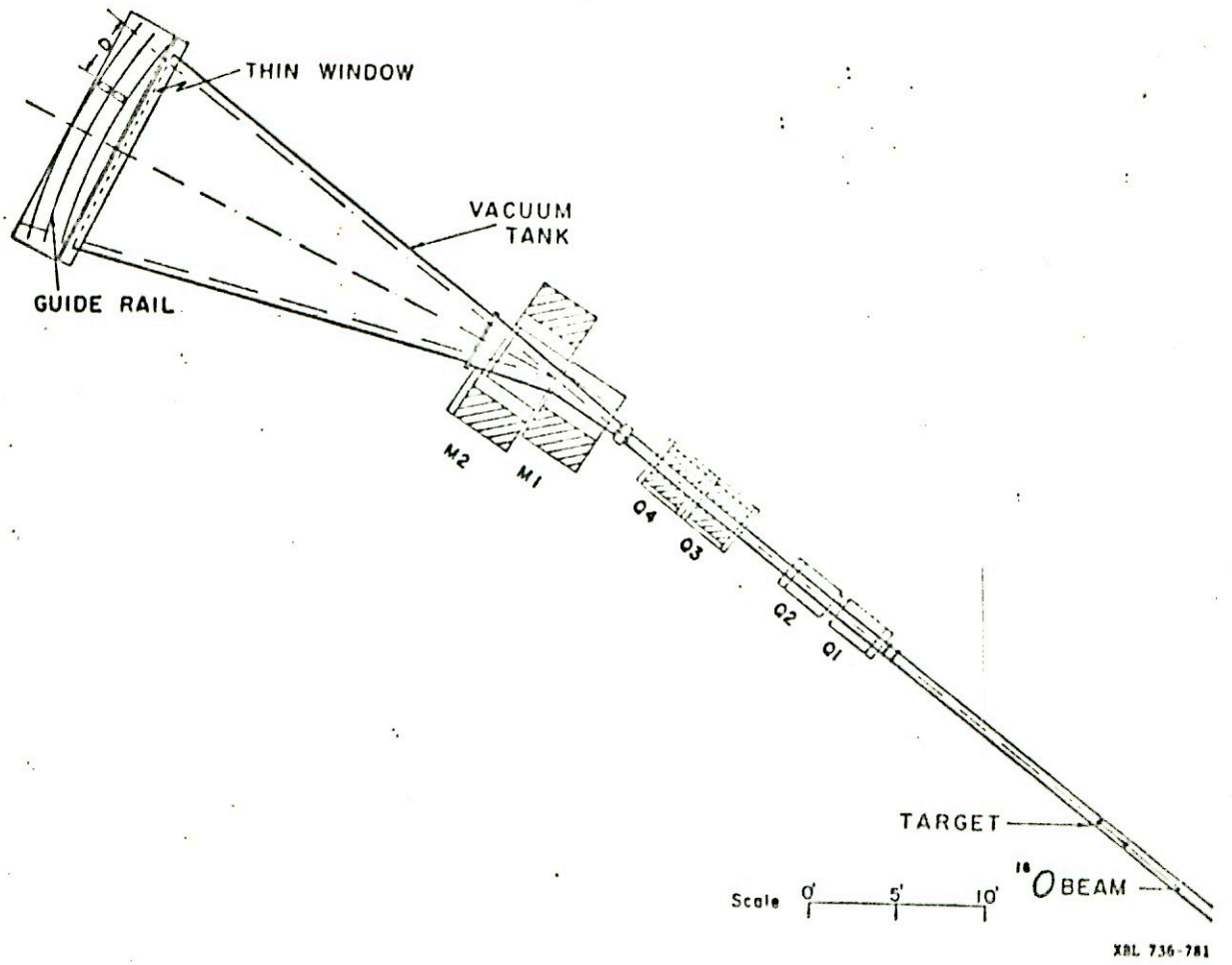
THIN WINDOW
VACUUM TANK
GUIDE RAIL
M2
M1
Q4
Q3
Q2
Q1
TARGET
^{18}O BEAM
Scale 0' 5' 10'
XBL 736-781

Fig. 1.

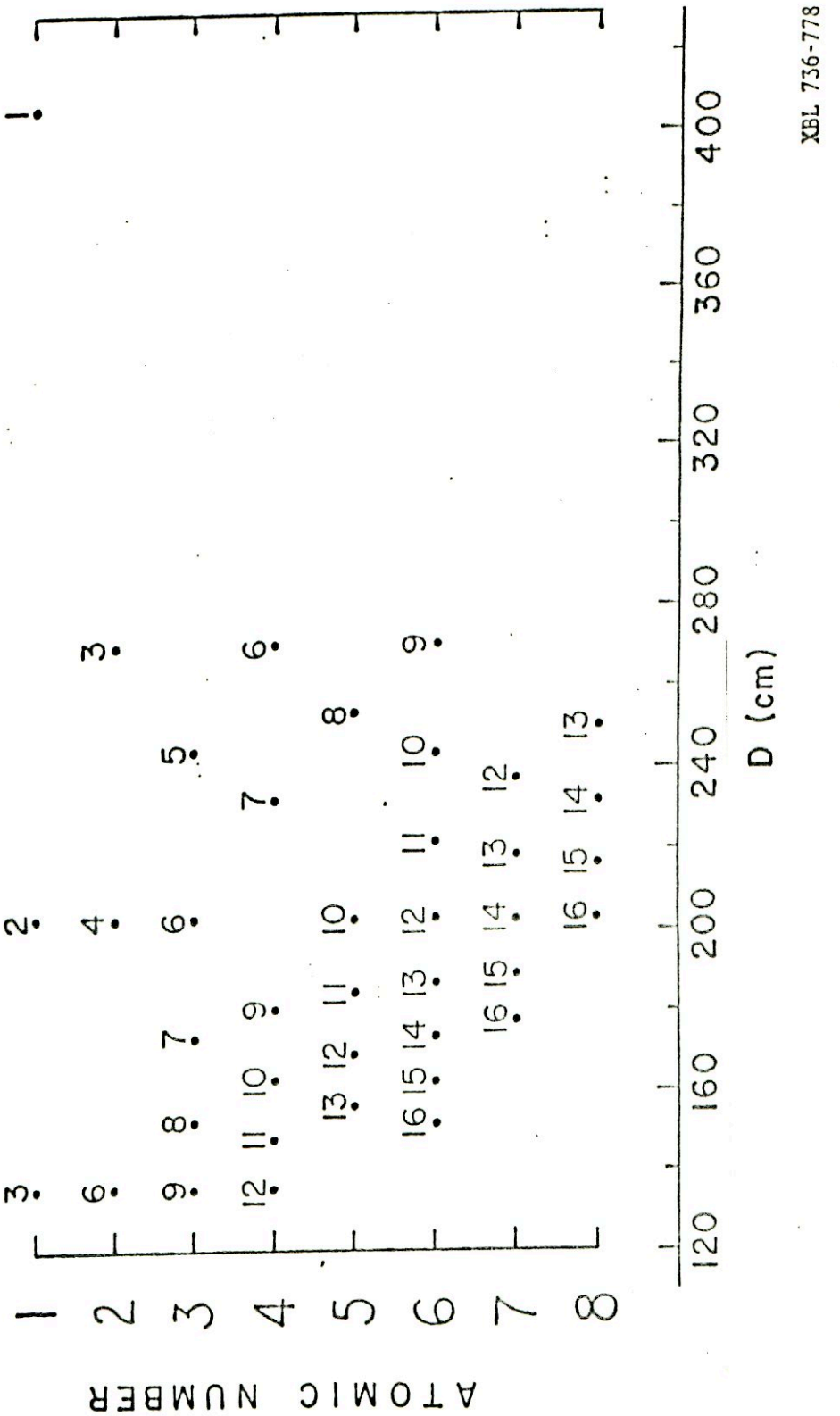

XBL 736-778

Fig. 2.

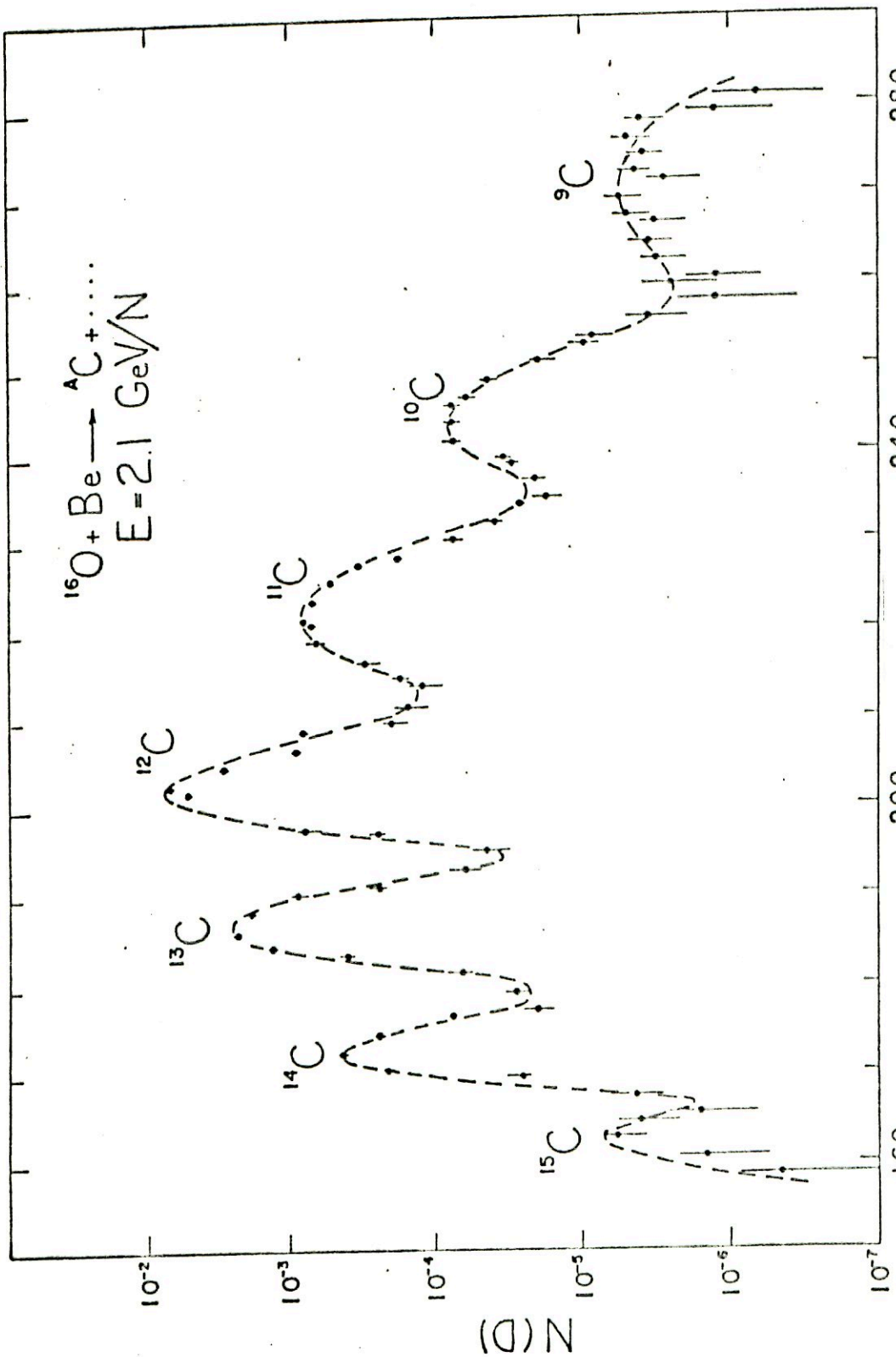

XBL 736-783

Fig. 3.

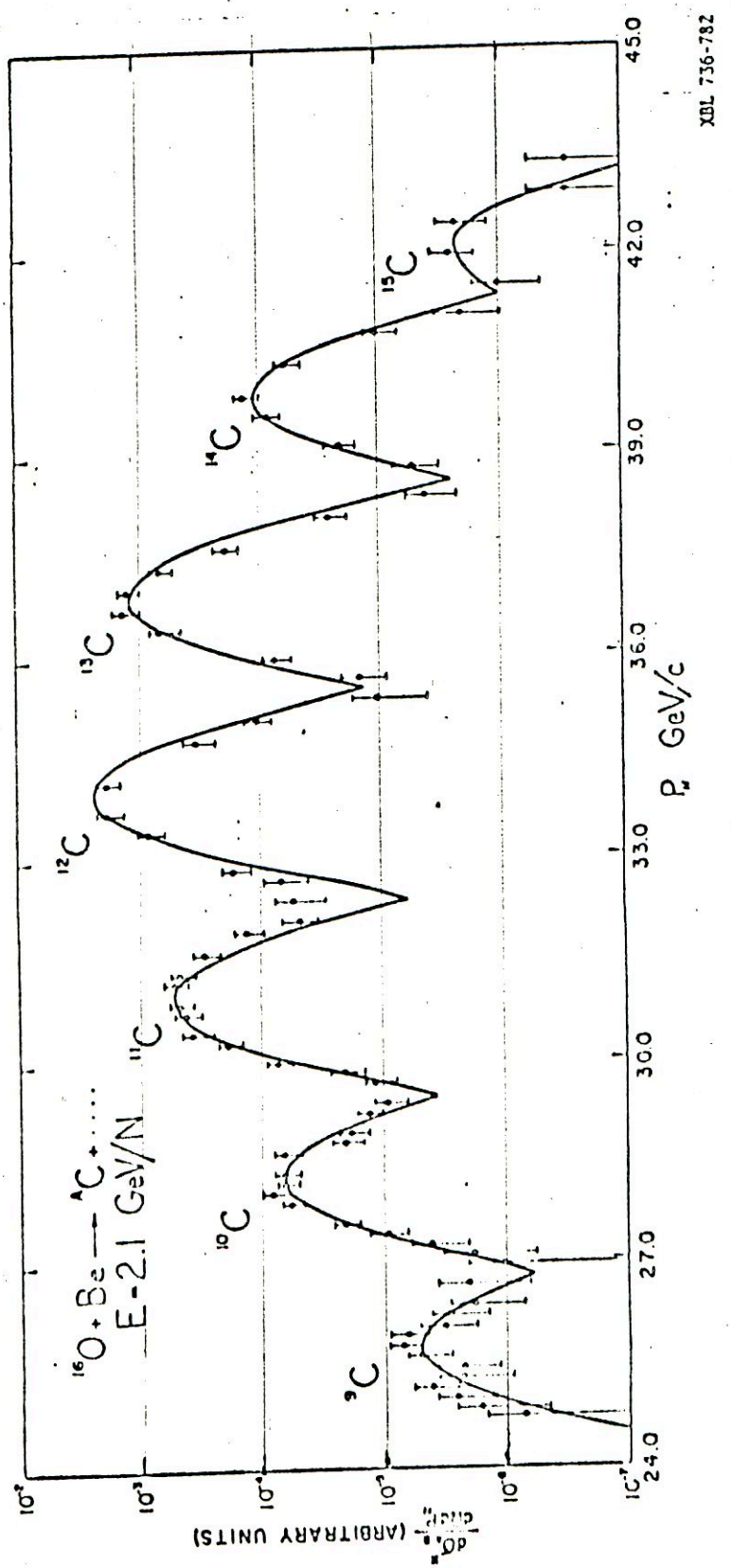
$^{16}O + Be \rightarrow {}^{A}C + \ldots$
E-2.1 GeV/N
^{9}C
^{10}C
^{11}C
^{12}C
^{13}C
^{14}C
^{15}C
$\frac{d\sigma}{d(p/c)}$ (ARBITRARY UNITS)
p, GeV/c
XBL 736-782

Fig. 4.

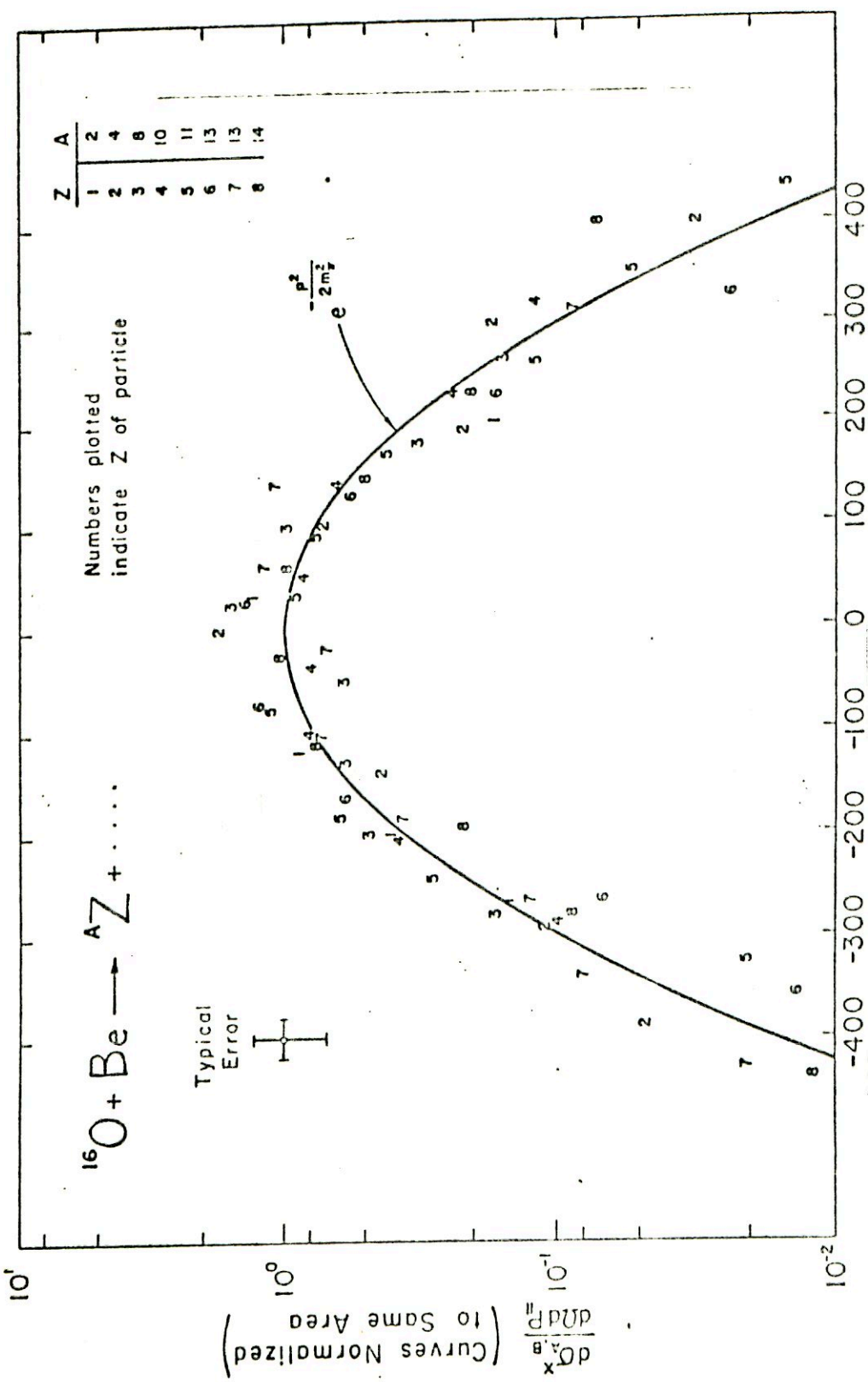
$^{16}O + Be \longrightarrow {}^{A}Z + \ldots$
Numbers plotted indicate Z of particle
Z A
1 2
2 4
3 8
4 10
5 11
6 13
7 13
8 14
$e^{-\frac{p^2}{2m_z}}$
Typical Error
$\frac{d\sigma}{d\Omega dP_{\parallel}}$ (Curves Normalized to Same Area)
$P_{\parallel}$ (MeV/c) Projectile Frame
XBL 736-779

Fig. 5.

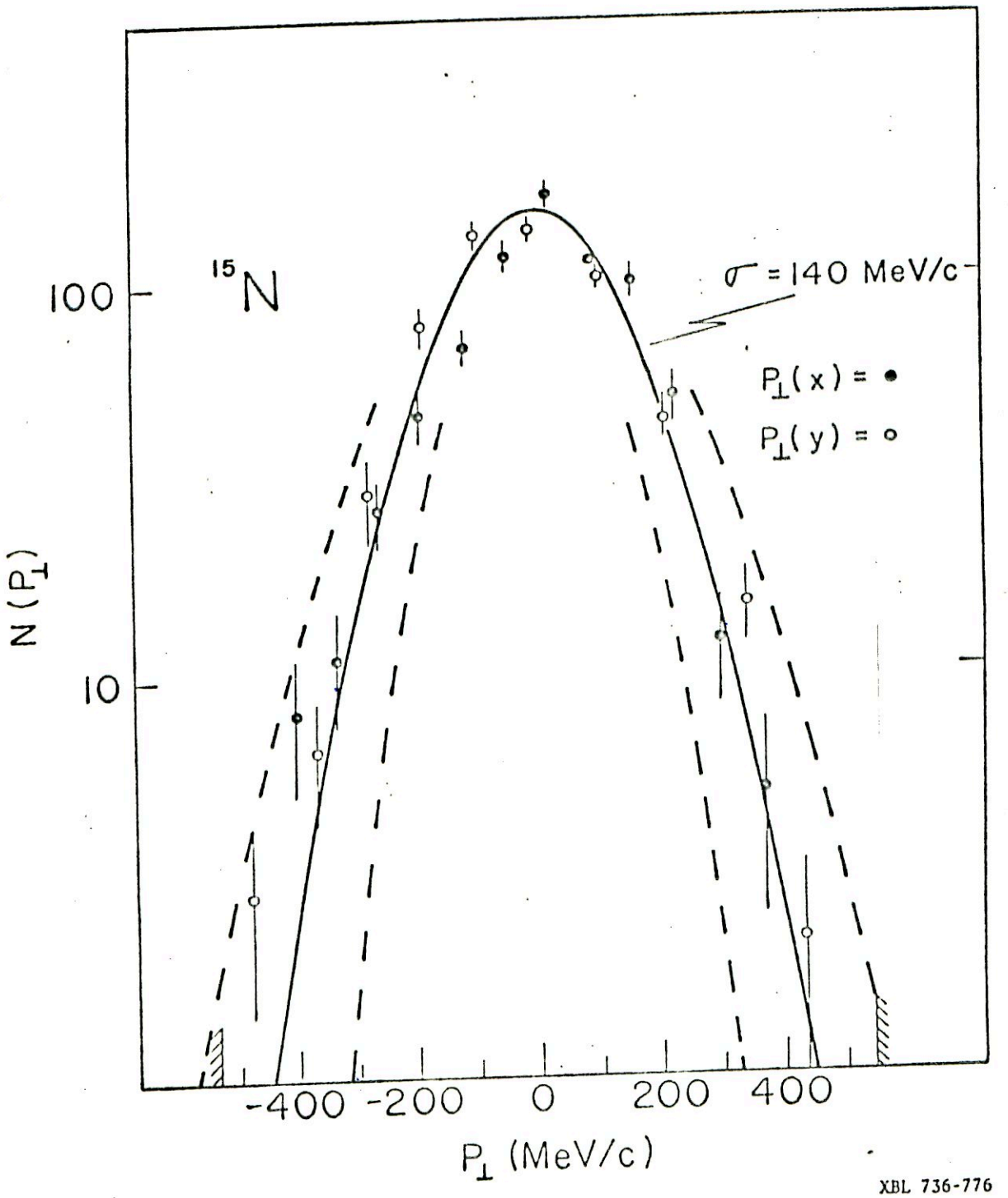

Fig. 6.
(a)

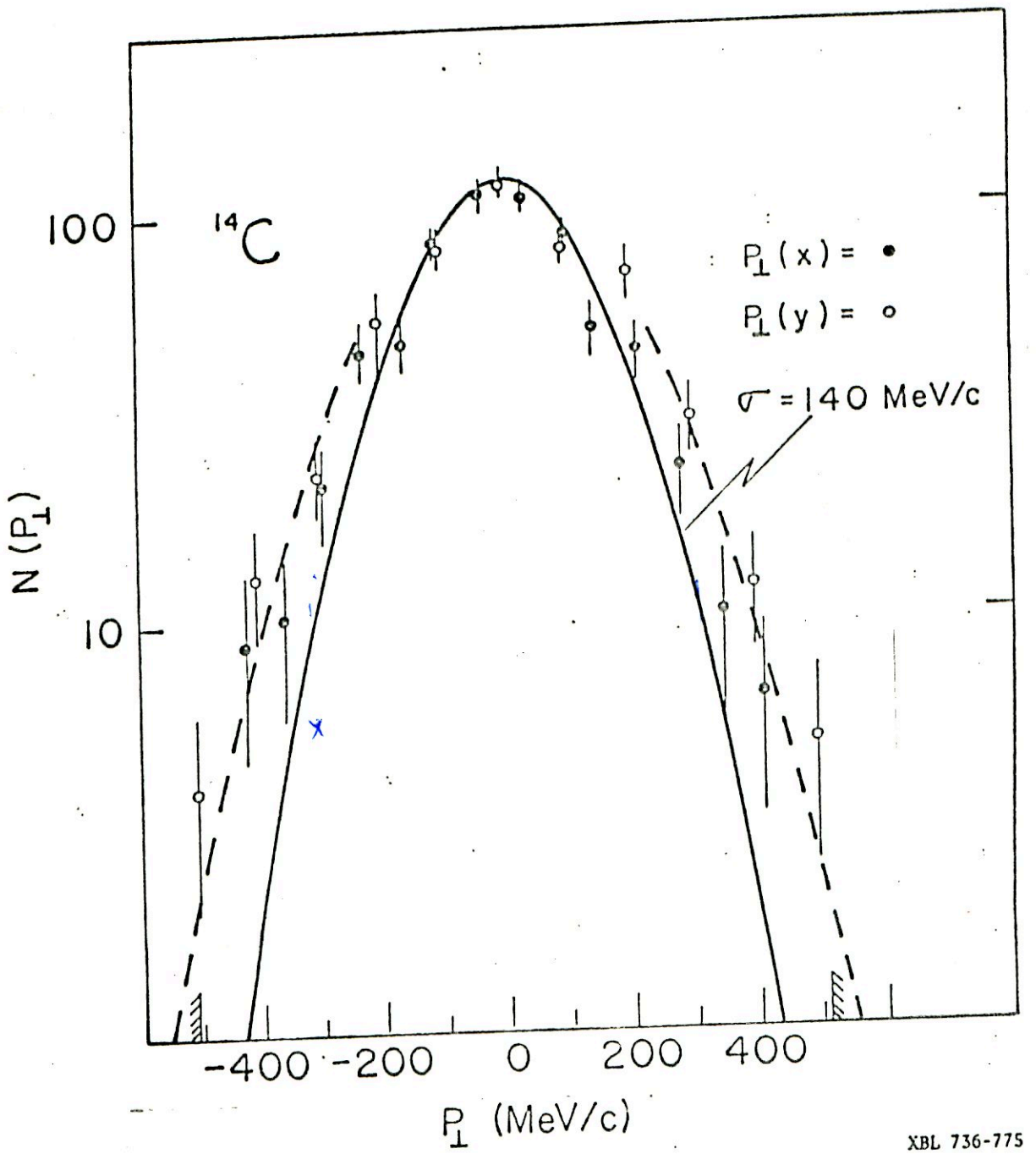
100
10
^{14}C
$P_\perp(x)$ = •
$P_\perp(y)$ = o
σ = 140 MeV/c
N($P_\perp$)
-400 -200 0 200 400
$P_\perp$ (MeV/c)
XBL 736-775

Fig. 6.
(b)

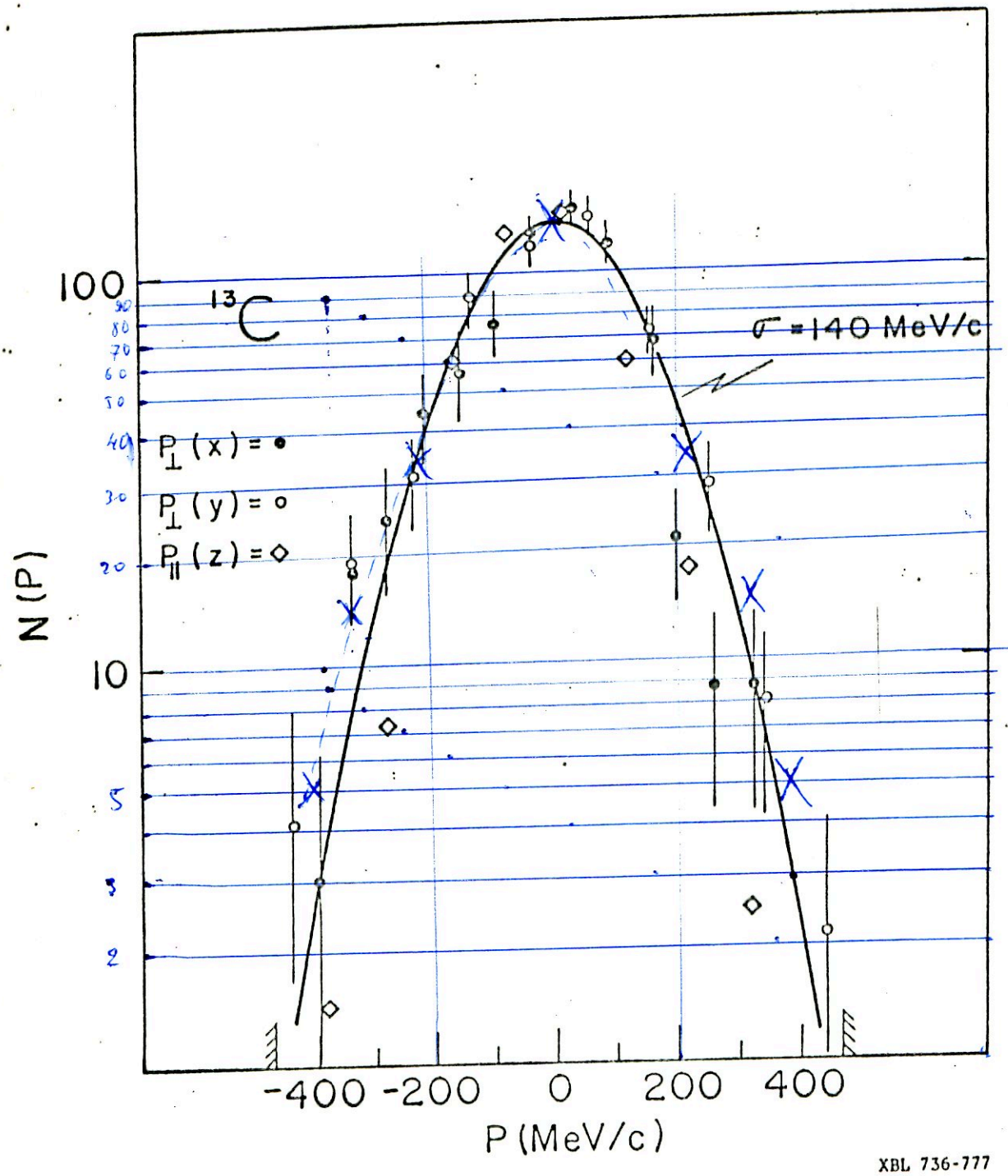
100
80
70
60
50
40
30
20
10
5
3
2
N(P)
^{13}C
σ = 140 MeV/c
$P_\perp(x)$ = •
$P_\perp(y)$ = o
$P_\parallel(z)$ = ◇
-400
-200
0
200
400
P (MeV/c)
XBL 736-777

Fig. 6.
(c)

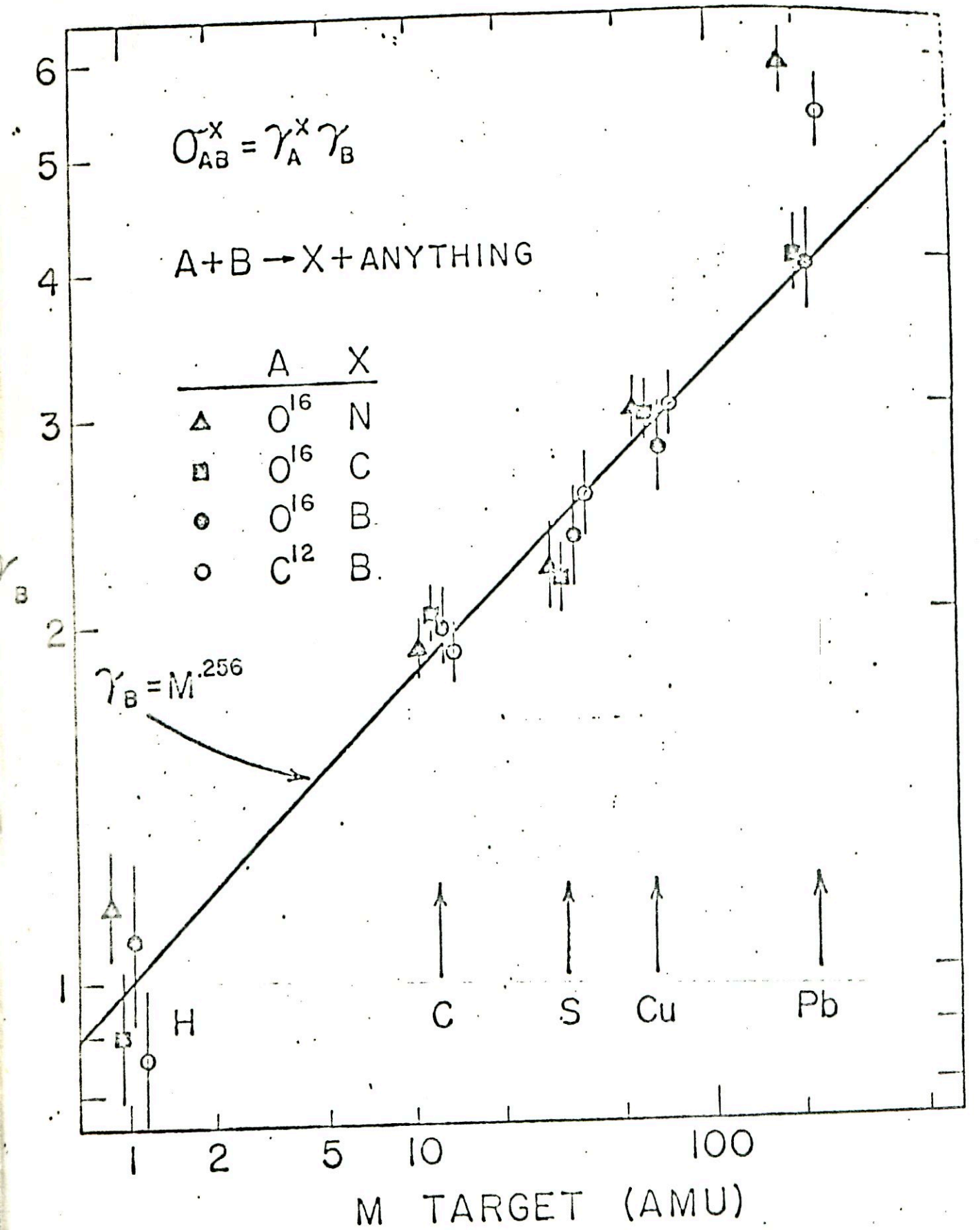
$\sigma^X_{AB} = \gamma^X_A \gamma_B$
A+B → X+ANYTHING
A X
O^{16} N
O^{16} C
O^{16} B.
C^{12} B.
$\gamma_B = M^{.256}$
γ_B
H
C
S
Cu
Pb
1
2
5
10
100
M TARGET (AMU)

Fig. 7.

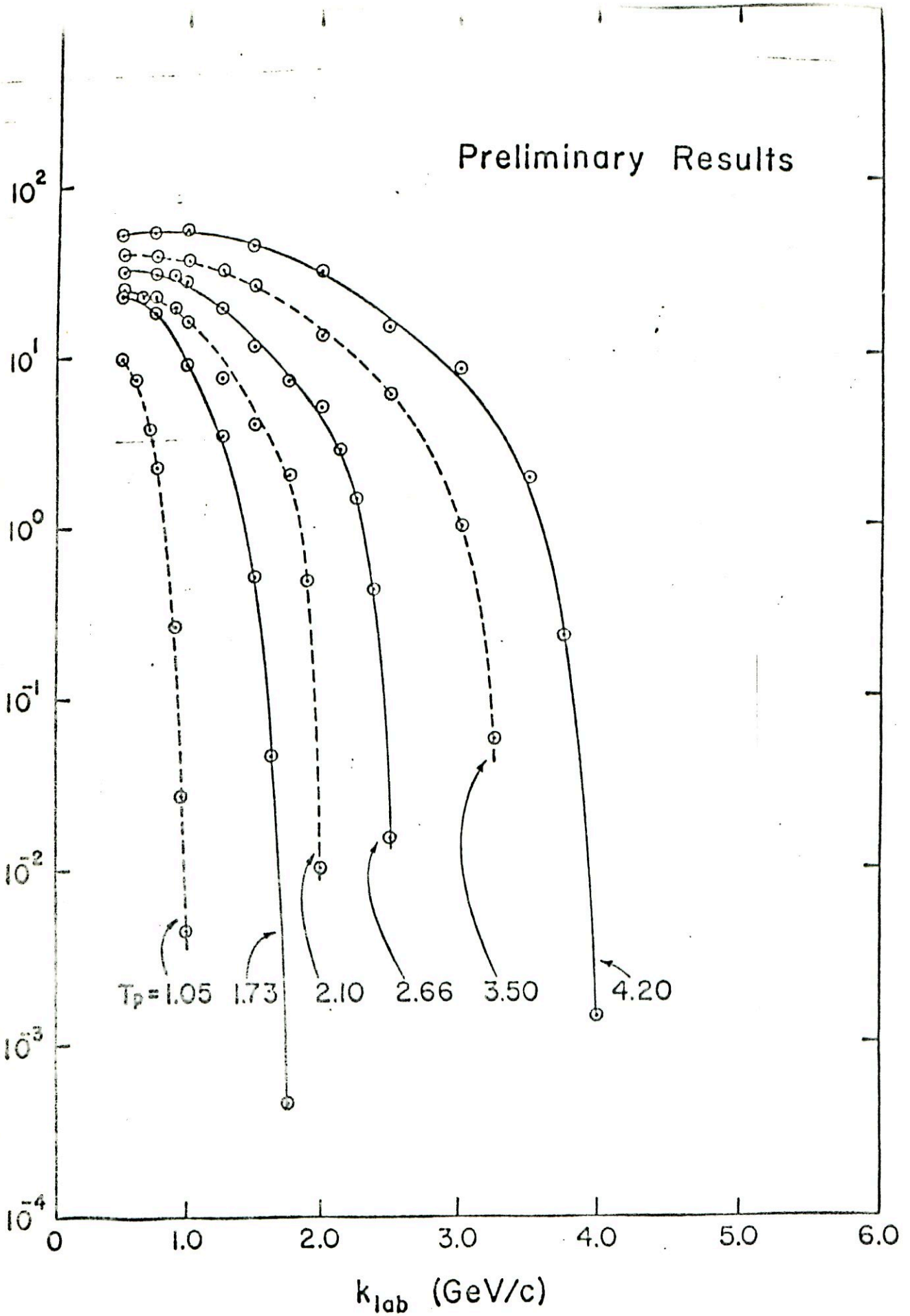
Preliminary Results
10^2
10^1
10^0
10^{-1}
10^{-2}
10^{-3}
10^{-4}
$\frac{d\sigma}{d\Omega dk}$ mb-sr^{-1}-$\left(\frac{c}{\quad}\right)$
T_p = 1.05
1.73
2.10
2.66
3.50
4.20
0
1.0
2.0
3.0
4.0
5.0
6.0
k_{lab} (GeV/c)

Fig. 8.

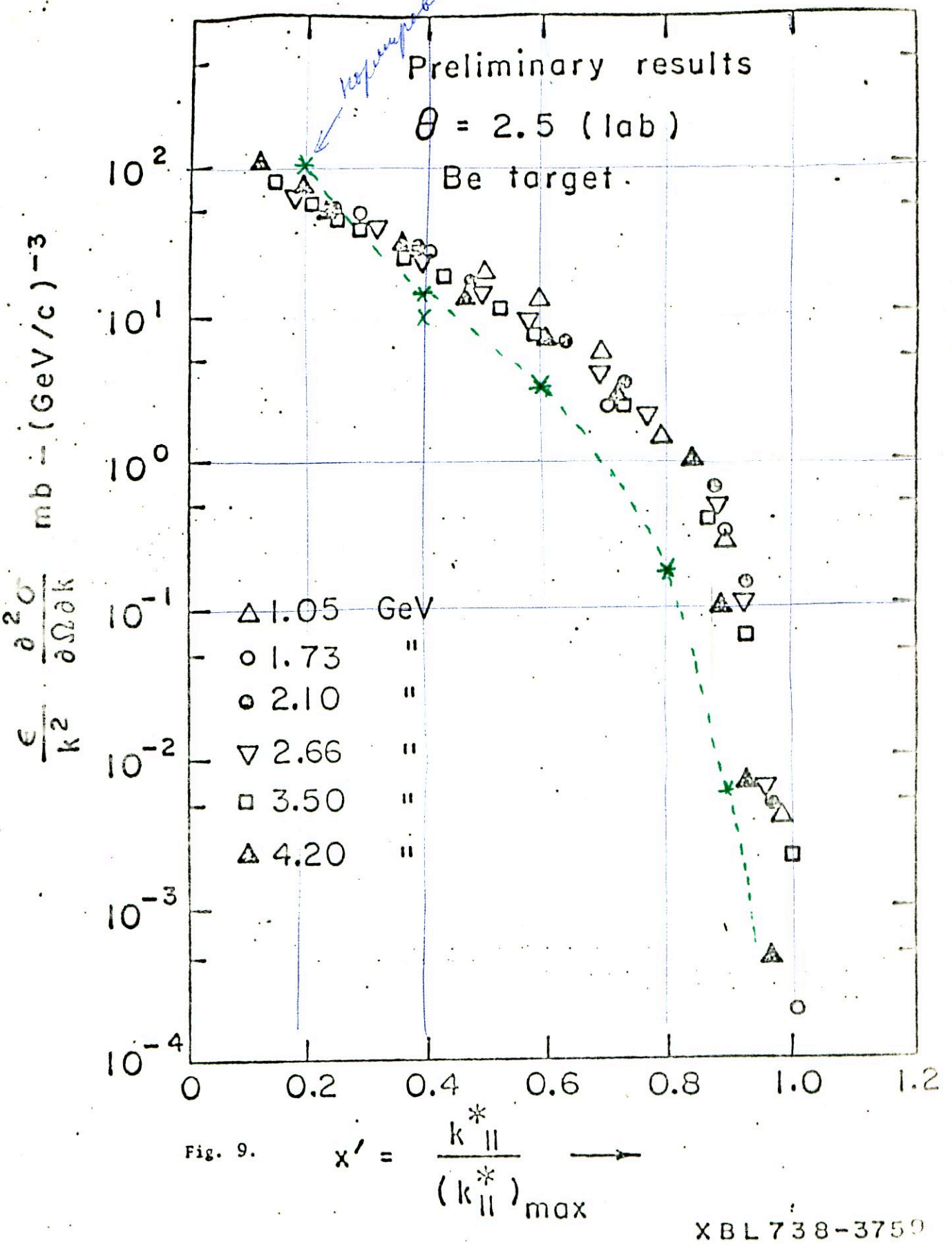
Preliminary results
θ = 2.5 (lab)
Be target
1.05 GeV
1.73 "
2.10 "
2.66 "
3.50 "
4.20 "
$\frac{\epsilon}{k^2}\frac{d^2\sigma}{d\Omega dk}$ mb (GeV/c)$^{-3}$
$x' = \frac{k^*_{\parallel}}{(k^*_{\parallel})_{max}}$
XBL738-3759

Fig. 9.

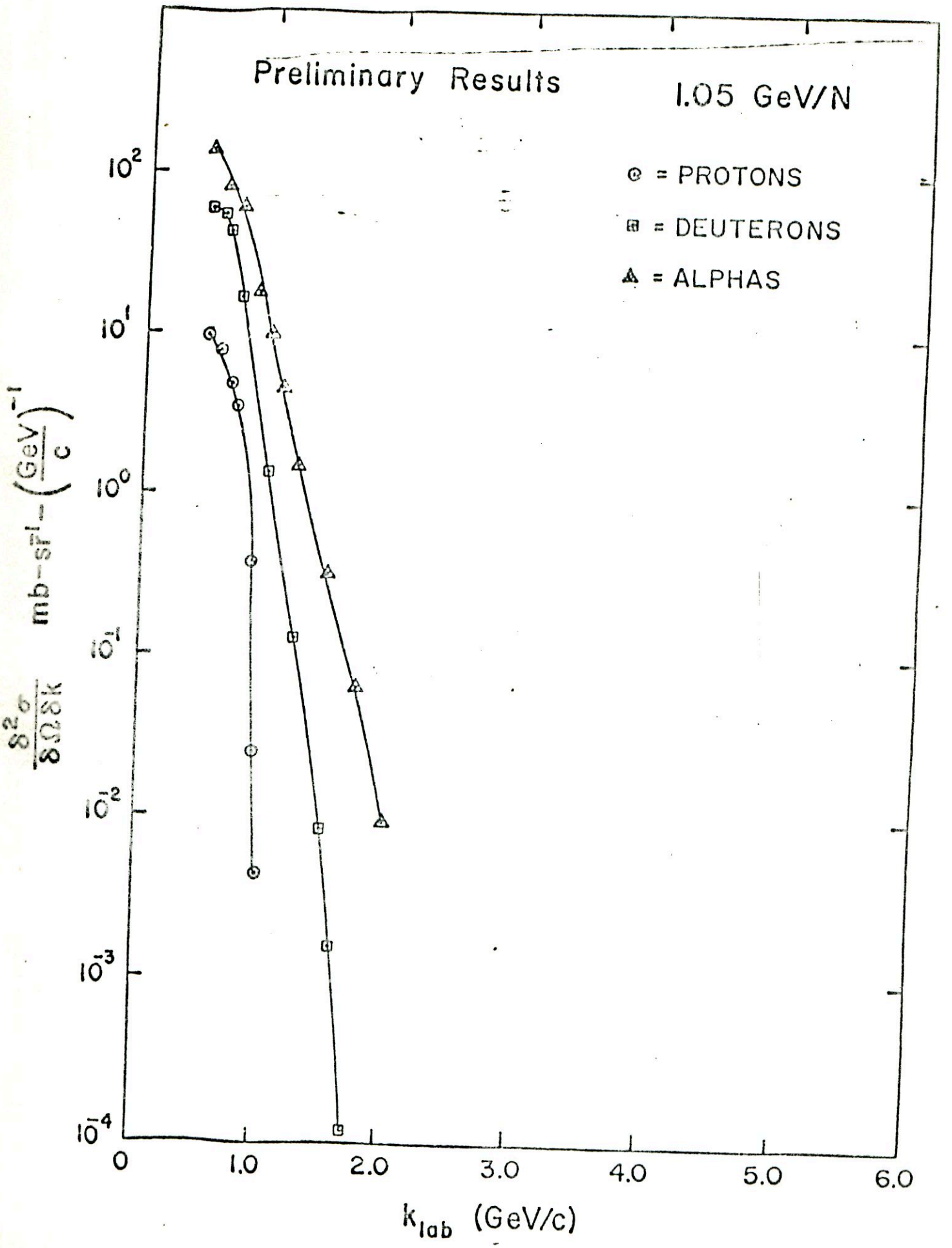
Preliminary Results
1.05 GeV/N
= PROTONS
= DEUTERONS
= ALPHAS
$\frac{\delta^2\sigma}{\delta\Omega\delta k}$ mb-sr^{-1}-$\left(\frac{GeV}{c}\right)^{-1}$
10^2
10^1
10^0
10^{-1}
10^{-2}
10^{-3}
10^{-4}
0
1.0
2.0
3.0
4.0
5.0
6.0
k_{lab} (GeV/c)

Fig. 10.

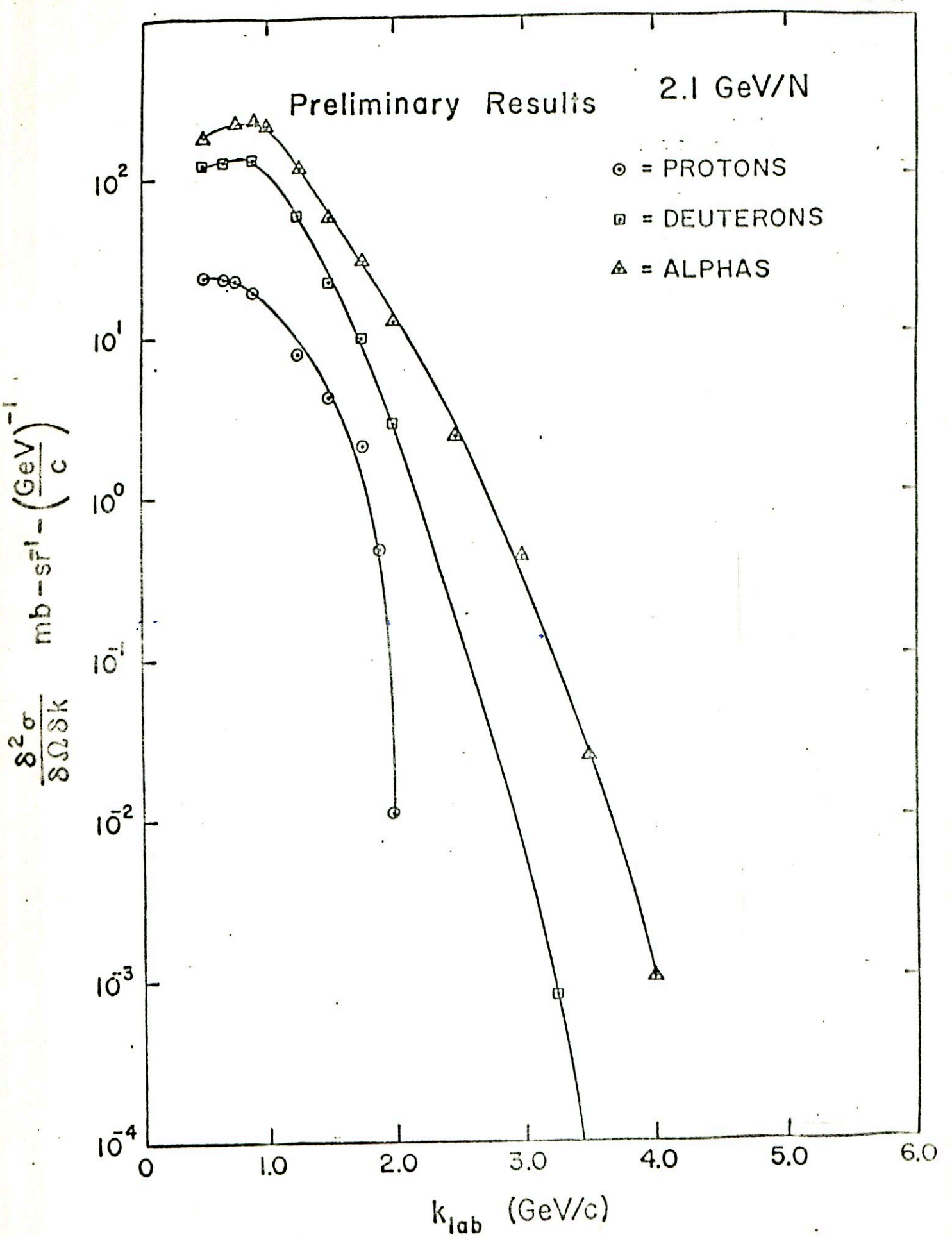
Preliminary Results
2.1 GeV/N
⊙ = PROTONS
⊡ = DEUTERONS
△ = ALPHAS
$\frac{\delta^2\sigma}{\delta\Omega\delta k}$ mb-sr^{-1}-$\left(\frac{GeV}{c}\right)^{-1}$
10^2
10^1
10^0
10^{-1}
10^{-2}
10^{-3}
10^{-4}
0
1.0
2.0
3.0
4.0
5.0
6.0
k_{lab} (GeV/c)

Fig.11.

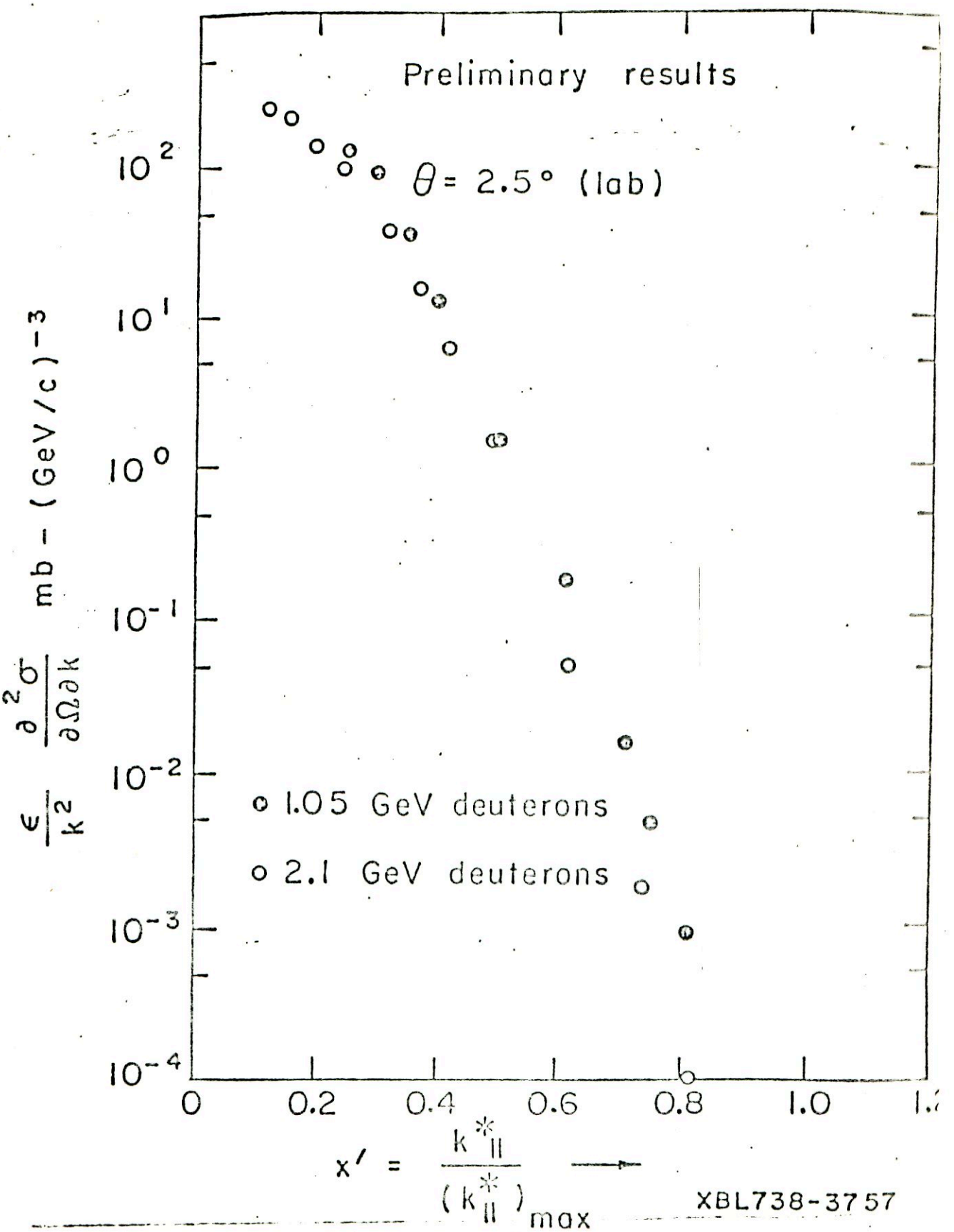
Preliminary results
θ = 2.5° (lab)
o 1.05 GeV deuterons
o 2.1 GeV deuterons
$\frac{\epsilon}{k^2}\frac{\partial^2\sigma}{\partial\Omega\partial k}$ mb - (GeV/c)$^{-3}$
10^2
10^1
10^0
10^{-1}
10^{-2}
10^{-3}
10^{-4}
0
0.2
0.4
0.6
0.8
1.0
$x' = \frac{k^*_{\parallel}}{(k^*_{\parallel})_{max}}$
XBL738-3757

Fig. 12.

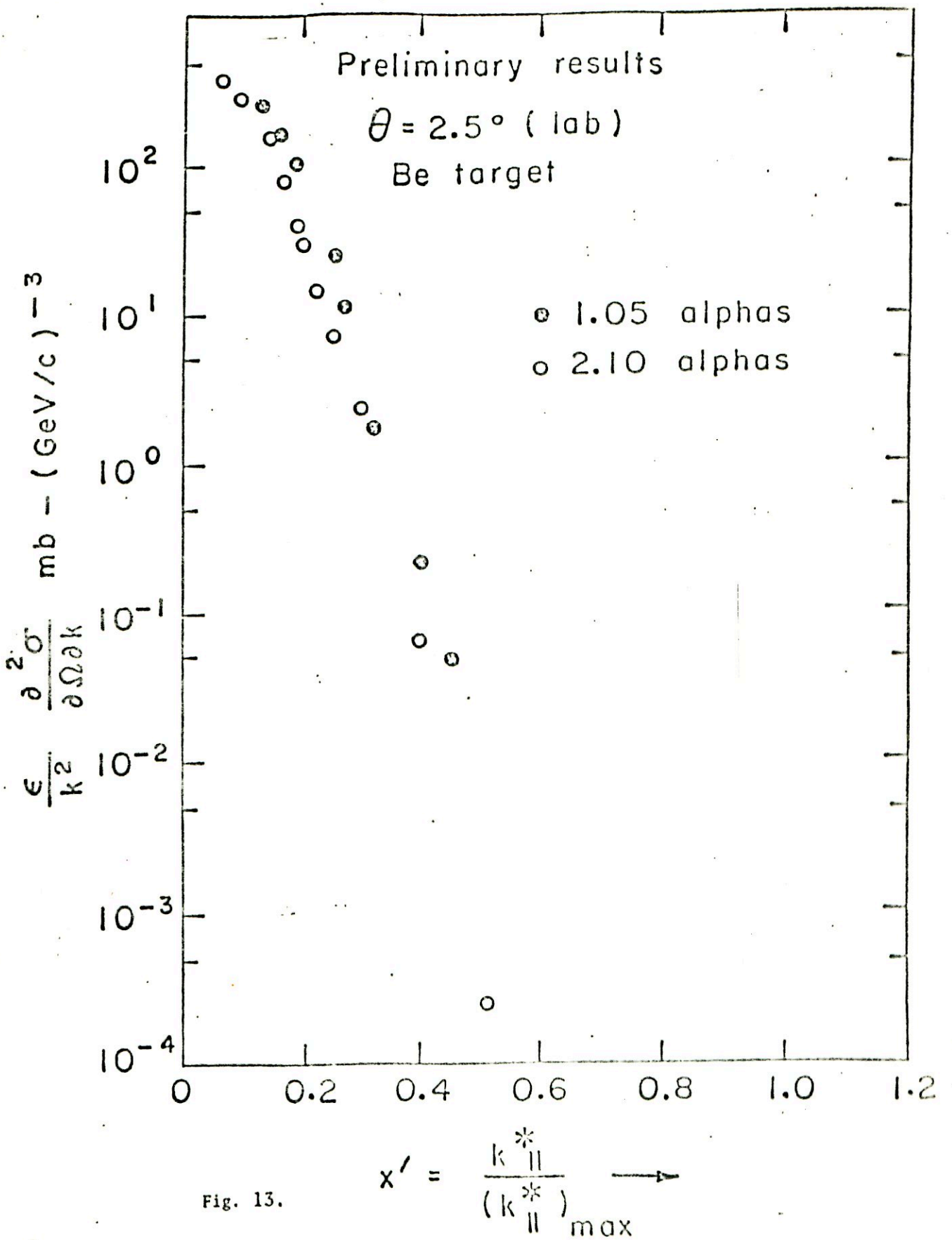
Preliminary results
θ = 2.5° (lab)
Be target
1.05 alphas
2.10 alphas
$\frac{\epsilon}{k^2}\frac{\partial^2\sigma}{\partial\Omega\partial k}$ mb − (GeV/c)$^{-3}$
10^2
10^1
10^0
10^{-1}
10^{-2}
10^{-3}
10^{-4}
0
0.2
0.4
0.6
0.8
1.0
1.2
$x' = \frac{k^*_{\parallel}}{(k^*_{\parallel})_{max}}$ ⟶

Fig. 13.

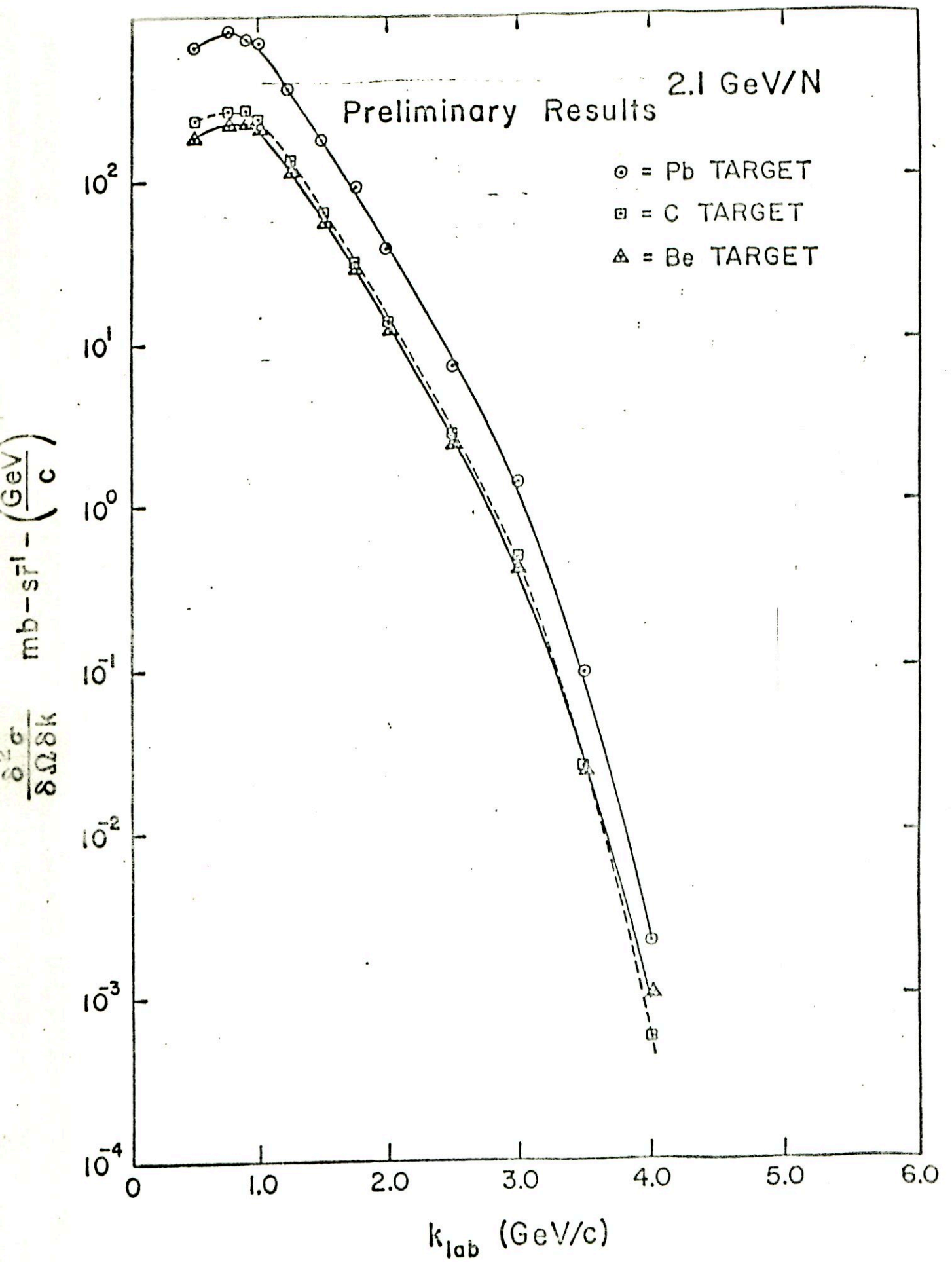
Preliminary Results
2.1 GeV/N
⊙ = Pb TARGET
⊡ = C TARGET
△ = Be TARGET
$\frac{d^2\sigma}{d\Omega dk}$ mb-sr^{-1}-$\left(\frac{GeV}{c}\right)^{-1}$
10^2
10^1
10^0
10^{-1}
10^{-2}
10^{-3}
10^{-4}
0
1.0
2.0
3.0
4.0
5.0
6.0
k_{lab} (GeV/c)

Fig. 14.

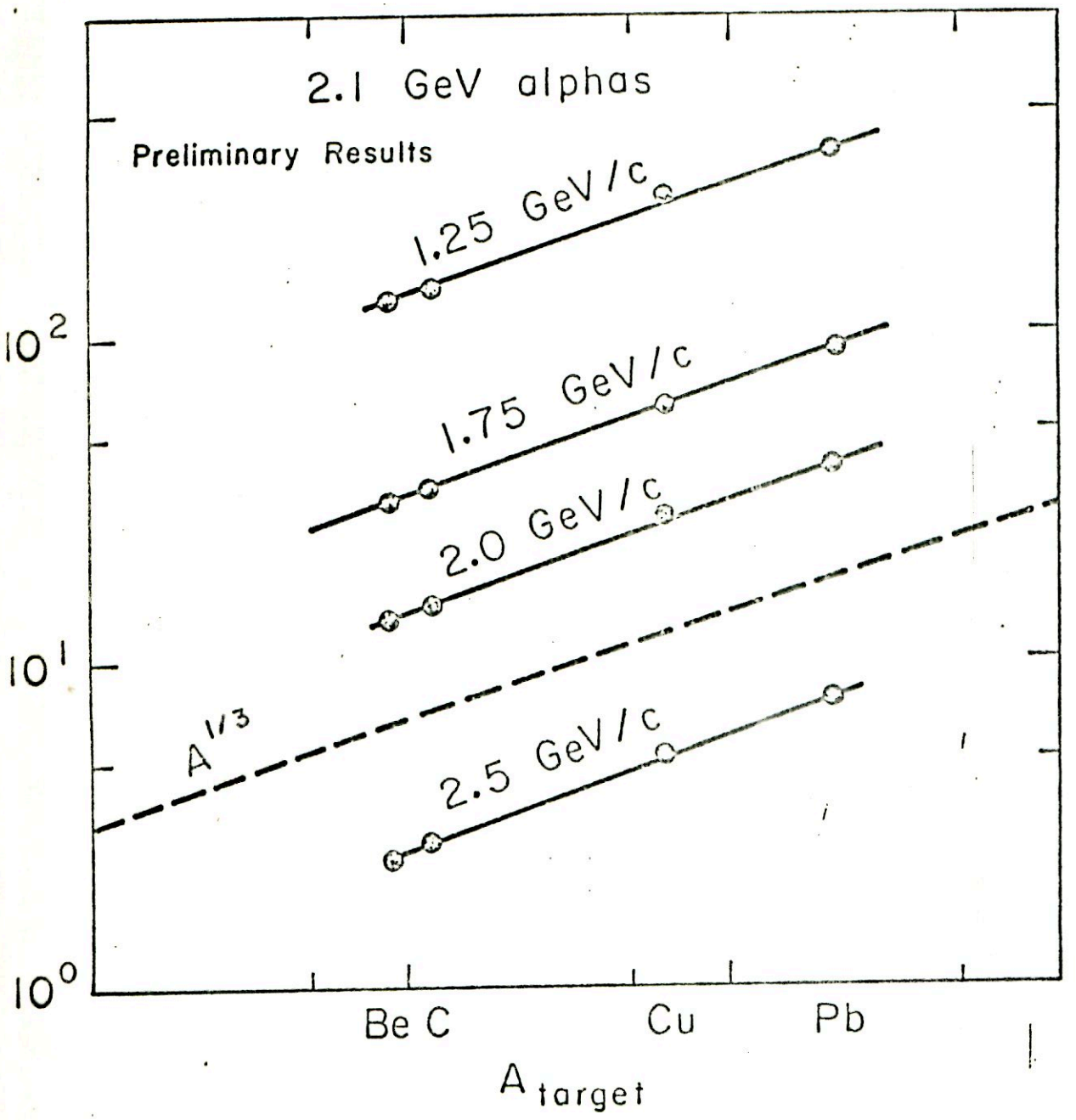
2.1 GeV alphas
Preliminary Results
1.25 GeV/c
1.75 GeV/c
2.0 GeV/c
2.5 GeV/c
A^1/3
10^2
10^1
10^0
Be C
Cu
Pb
A target
XBL738-3755

Fig. 15.

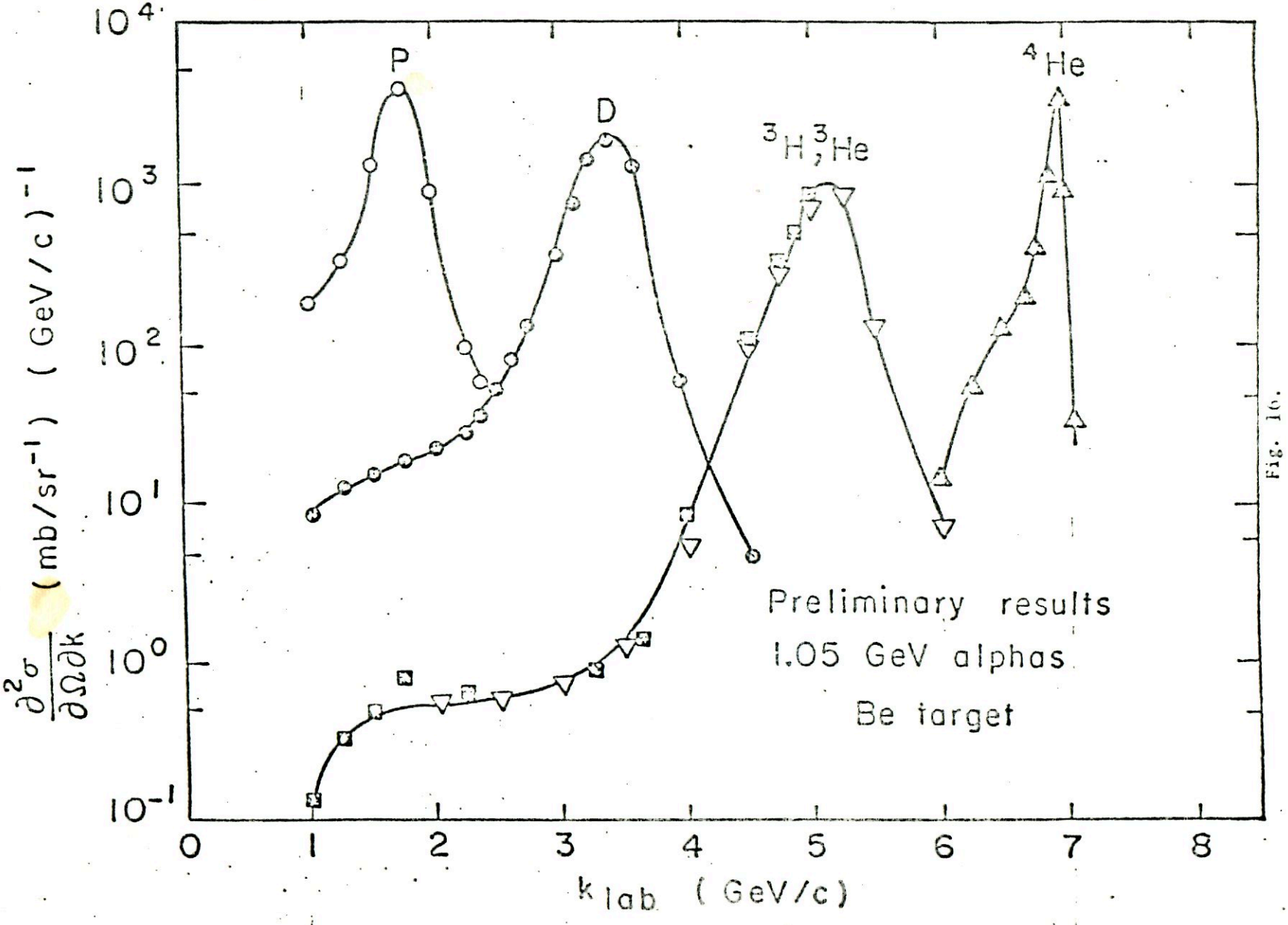
P
D
^{3}H,^{3}He
^{4}He
Preliminary results
1.05 GeV alphas
Be target
$\frac{\partial^2\sigma}{\partial\Omega\partial k}$ (mb/sr^{-1}) (GeV/c)$^{-1}$
k_{lab} (GeV/c)
10^4
10^3
10^2
10^1
10^0
10^{-1}
0
1
2
3
4
5
6
7
8

Fig. 10.

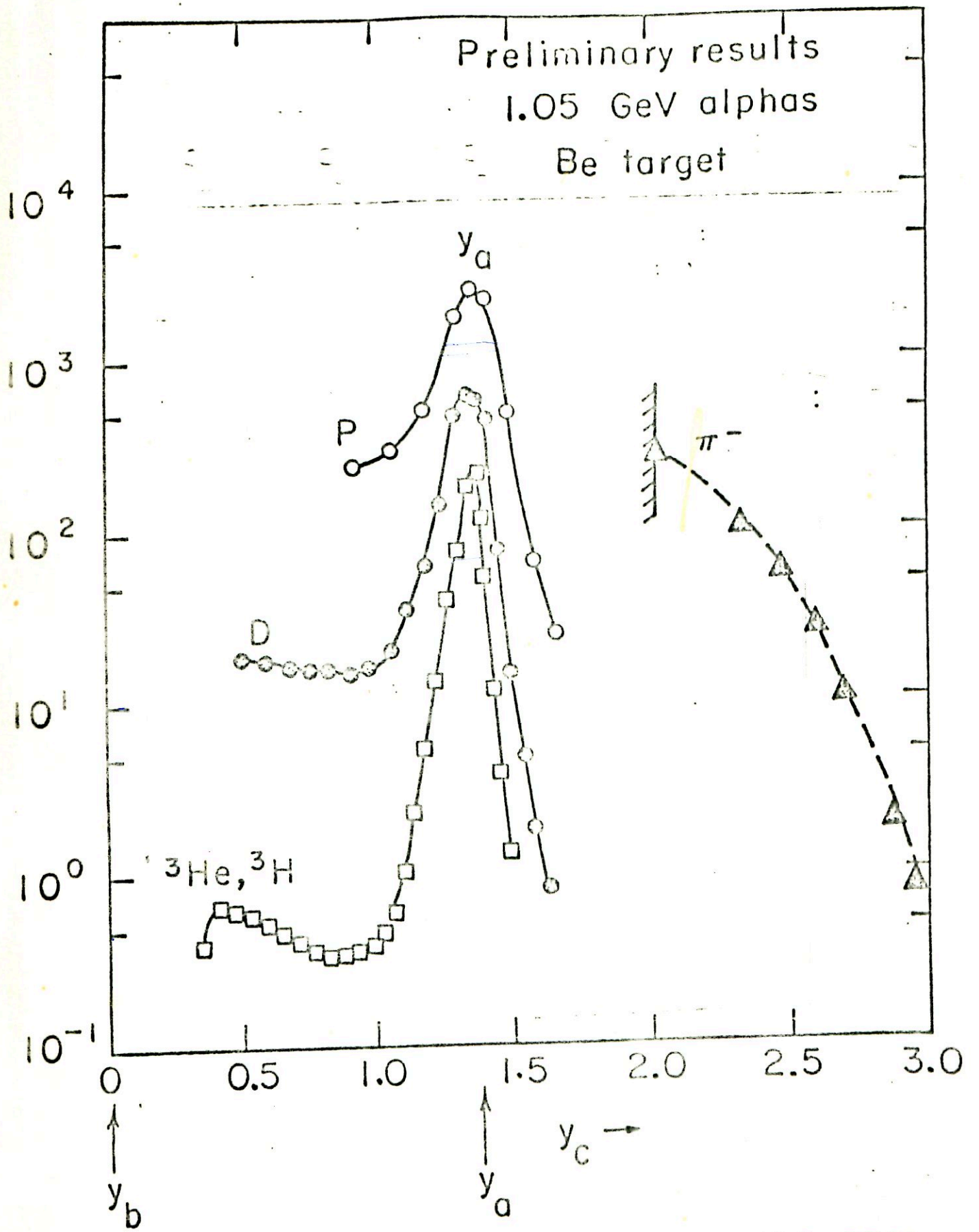

Fig. 17. XBL738-3751

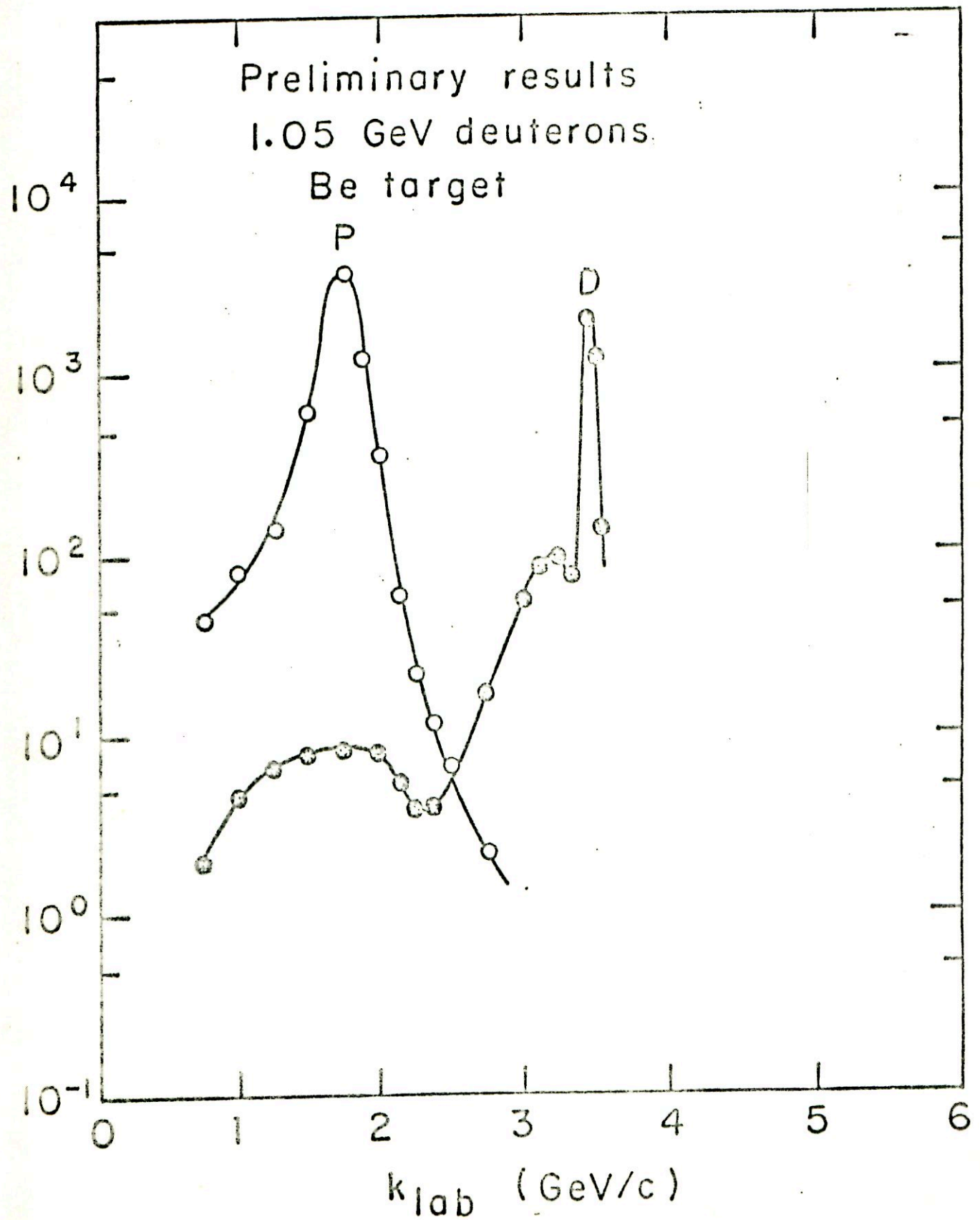

Fig. 18.

XBL738-3754

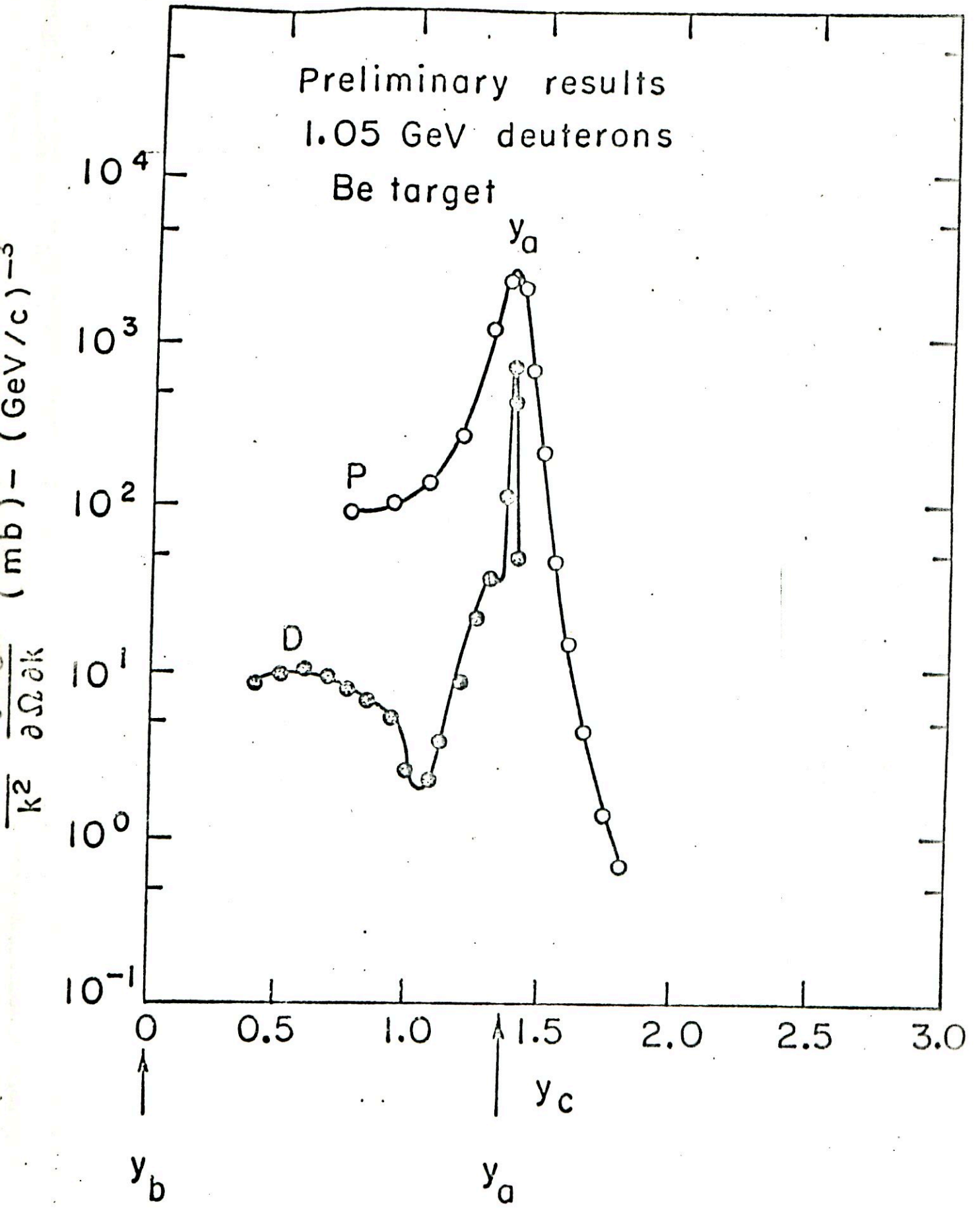

Fig. 19.

XBL738-3753

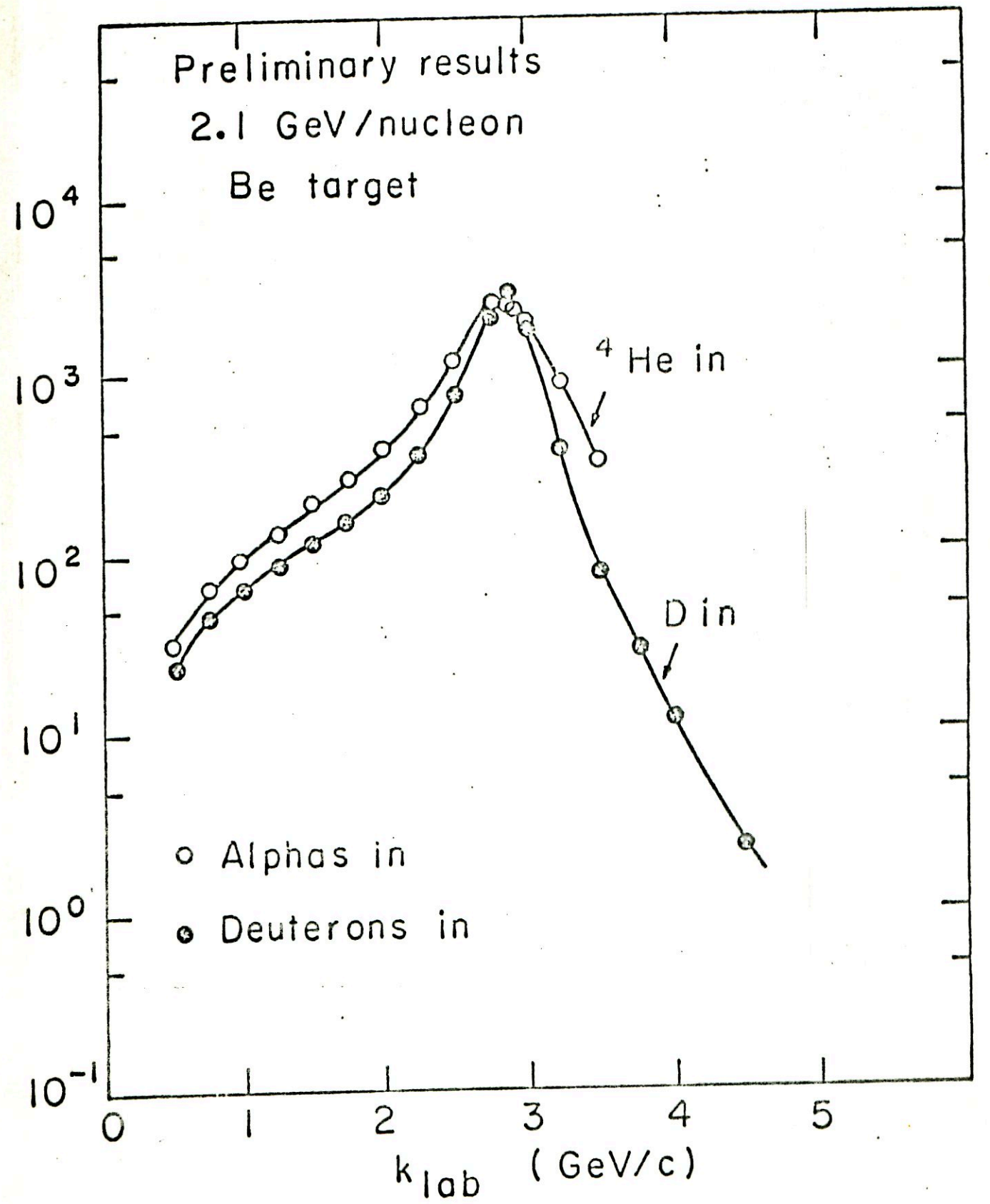

Fig. 20.

XBL738-3752

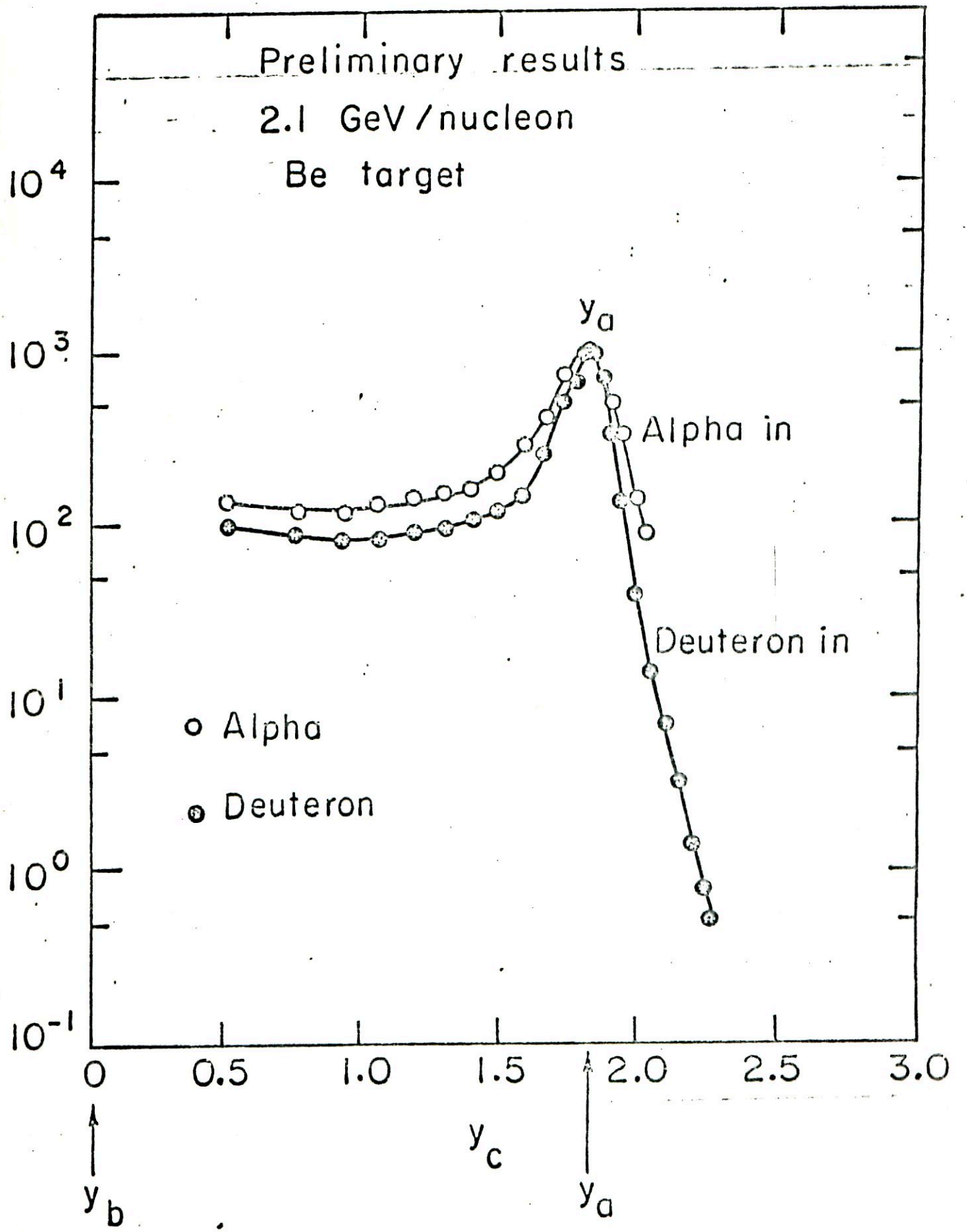

Fig. 21.

XBL738-3756

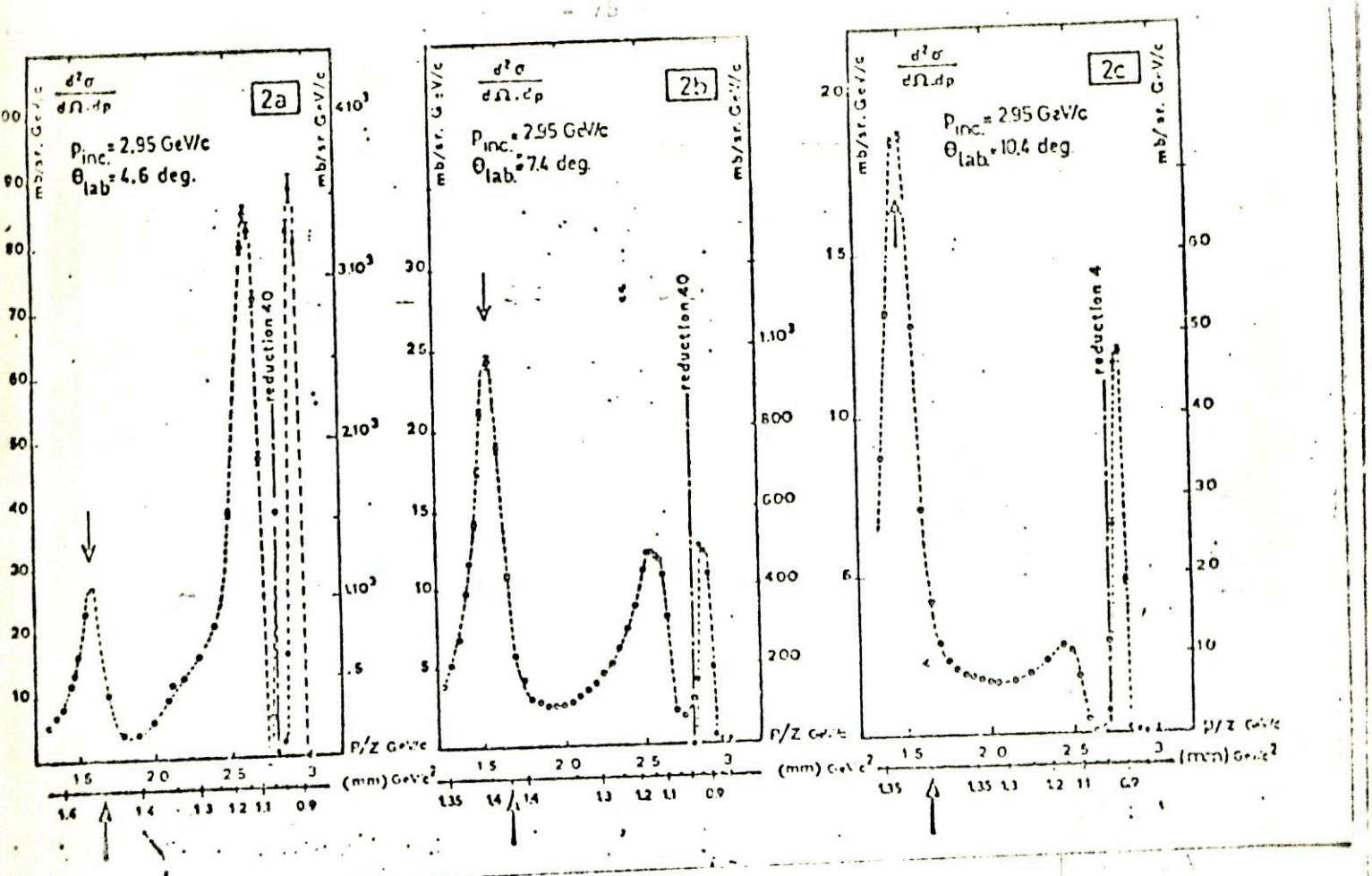
2a
$p_{inc.}$ = 2.95 GeV/c
θ_{lab} = 4.6 deg.
reduction 40
2b
$p_{inc.}$ = 2.95 GeV/c
θ_{lab} = 7.4 deg.
reduction 40
2c
$p_{inc.}$ = 2.95 GeV/c
θ_{lab} = 10.4 deg.
reduction 4
mb/sr. GeV/c
P/Z GeV/c
(mm) GeV/c²

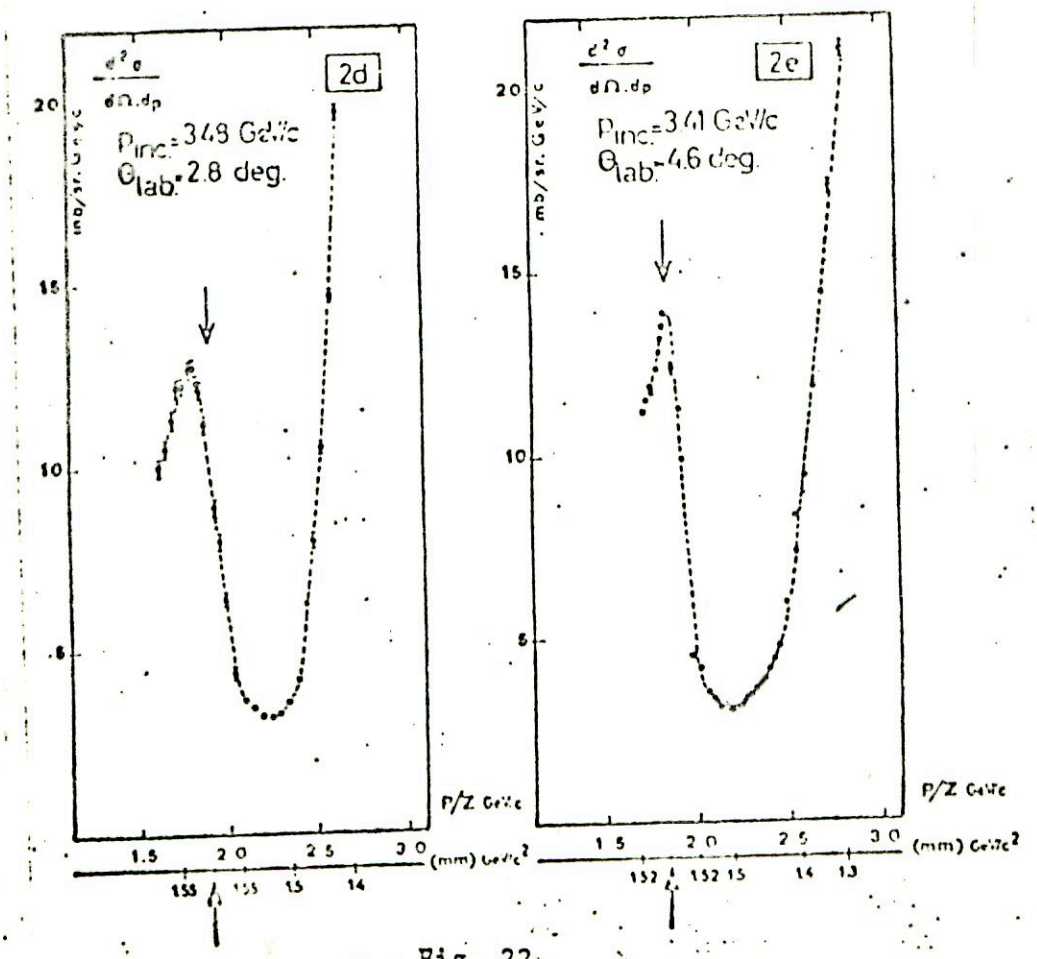
2d
$p_{inc.}$ = 3.48 GeV/c
θ_{lab} = 2.8 deg.
2e
$p_{inc.}$ = 3.41 GeV/c
θ_{lab} = 4.6 deg.
mb/sr. GeV/c
P/Z GeV/c
(mm) GeV/c²

Fig. 22

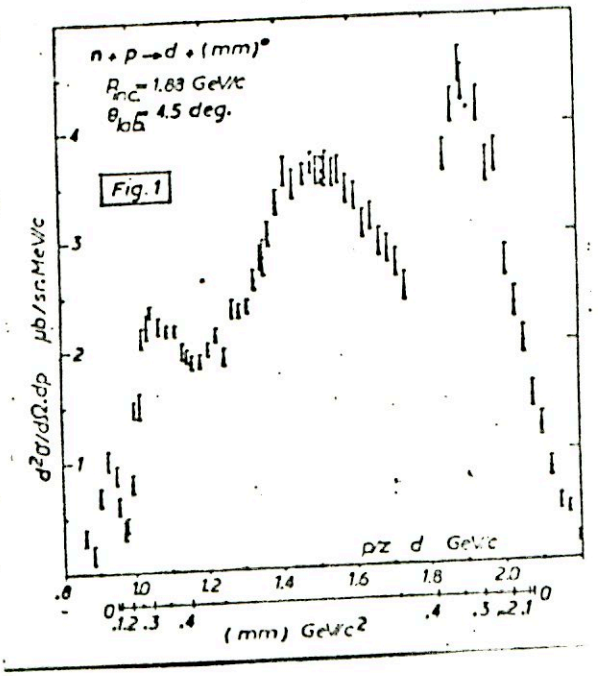
n + p → d + (mm)°
P_inc = 1.83 GeV/c
θ_lab = 4.5 deg.
Fig. 1
d²σ/dΩ.dp μb/sr.MeV/c
pz d GeV/c
(mm) GeV/c²

Fig. 23

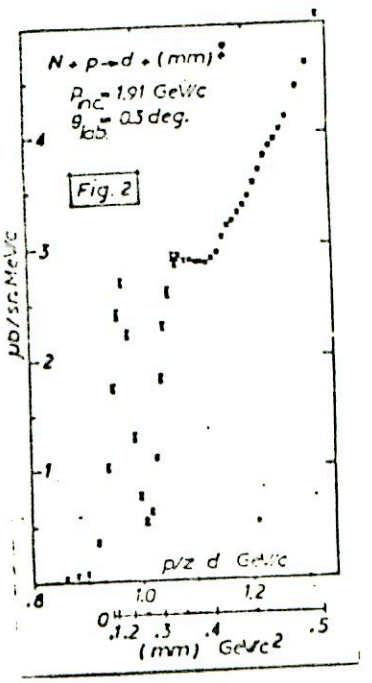
N + p → d + (mm)°
P_inc = 1.91 GeV/c
θ_lab = 0.5 deg.
Fig. 2
μb/sr.MeV/c
pz d GeV/c
(mm) GeV/c²

Fig. 24.

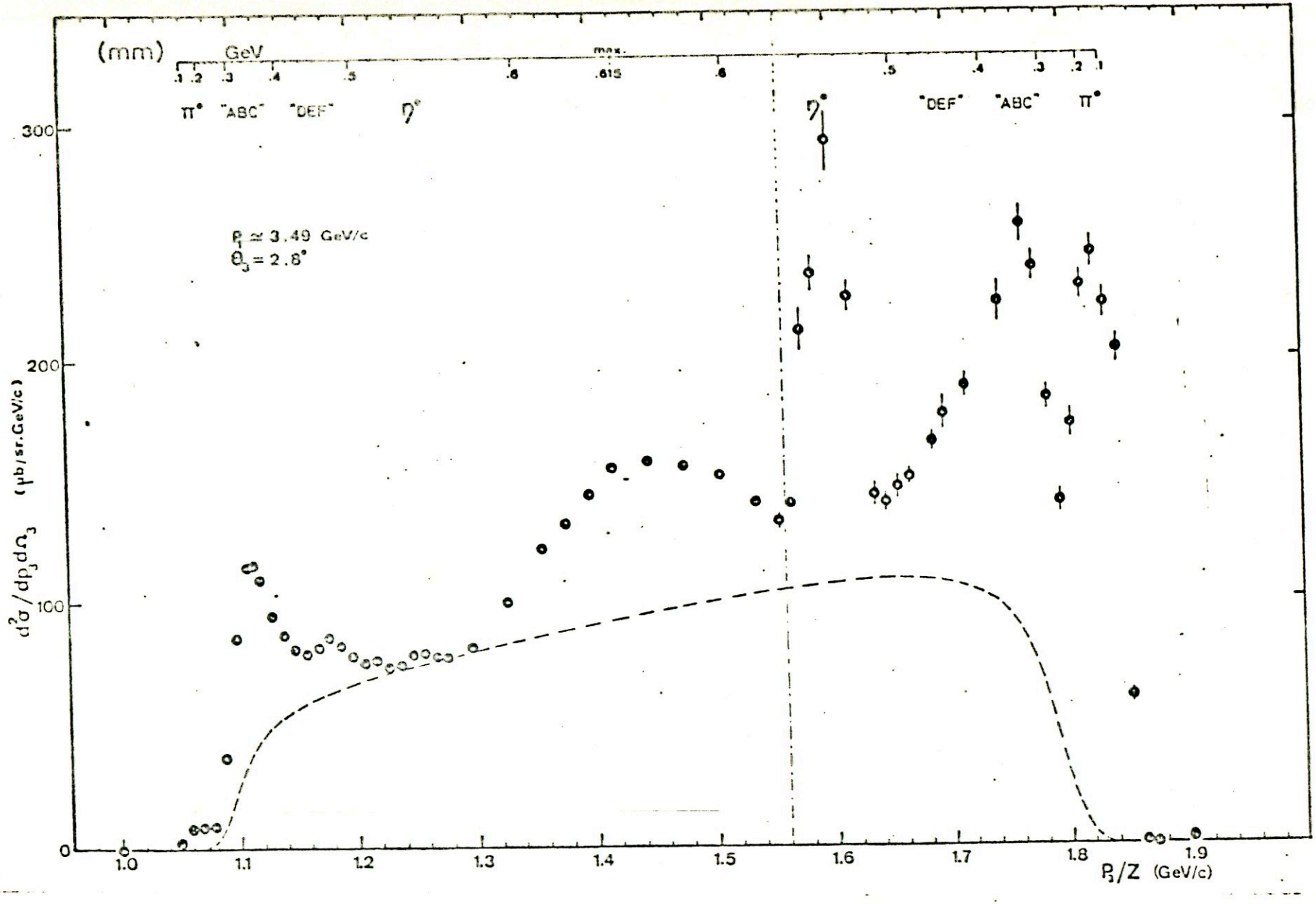
(mm)
GeV
max.
.615
π° "ABC" "DEF" η°
η° "DEF" "ABC" π°
$P_1 \simeq 3.49$ GeV/c
$\theta_3 = 2.8°$
$d^2\sigma/dp_3 d\Omega_3$ (μb/sr.GeV/c)
300
200
100
0
1.0
1.1
1.2
1.3
1.4
1.5
1.6
1.7
1.8
1.9
P_3/Z (GeV/c)

Fig. 25.

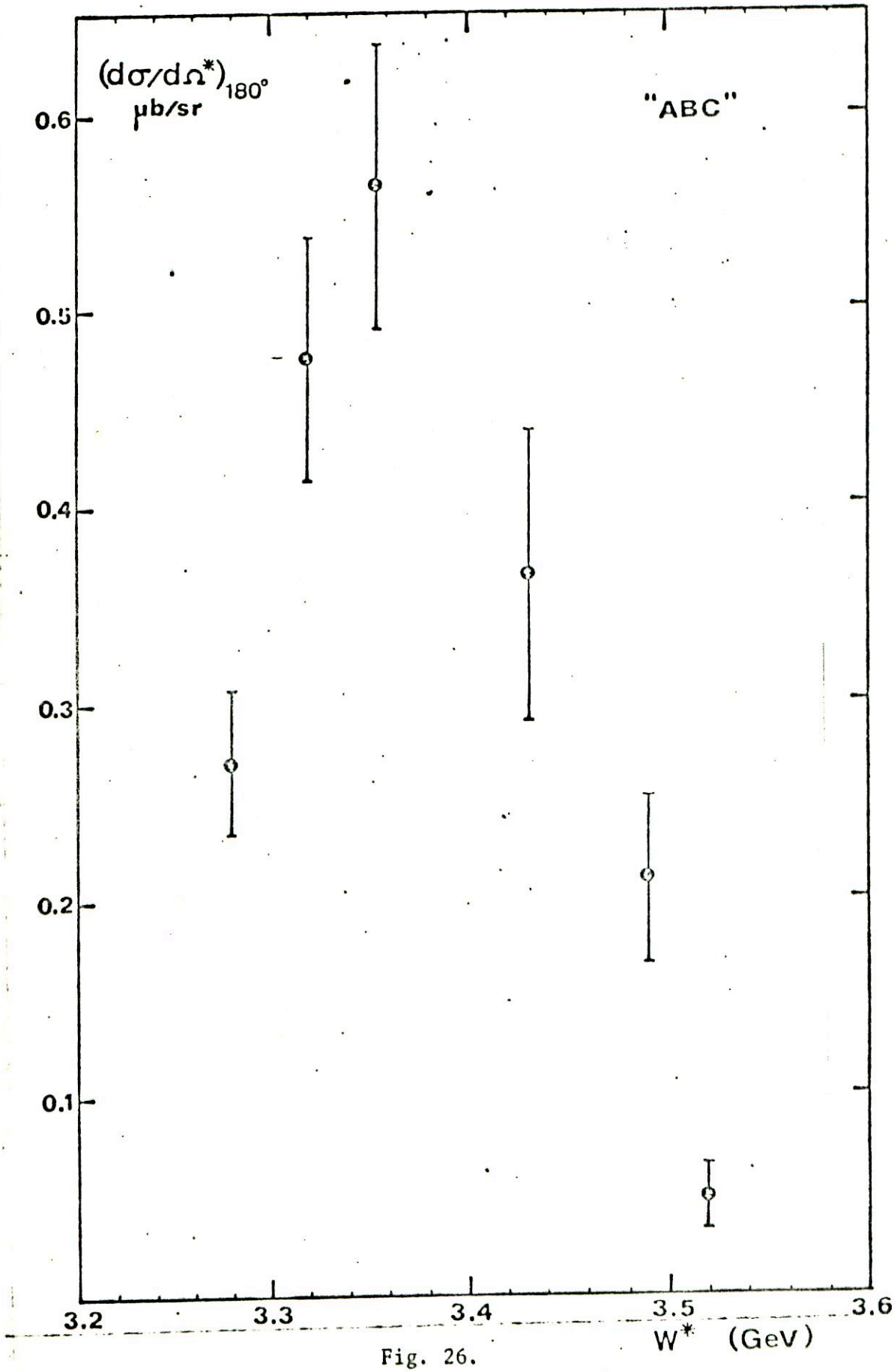

Fig. 26.

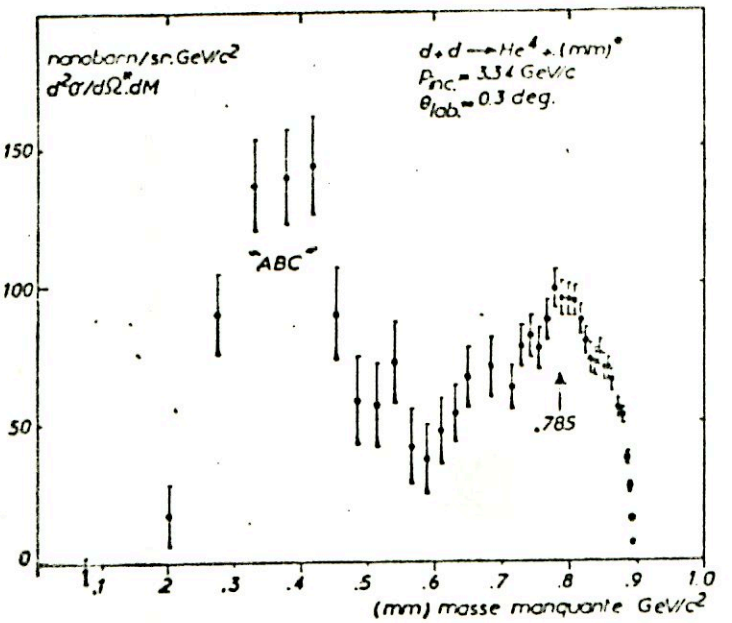
nanobarn/sr.GeV/c²
d²σ/dΩ.dM
d + d → He⁴ + (mm)°
P_inc. = 3.34 GeV/c
θ_lab. = 0.3 deg.
"ABC"
.785
150
100
50
0
.1
.2
.3
.4
.5
.6
.7
.8
.9
1.0
(mm) masse manquante GeV/c²

Fig. 27.

I - INTRODUCTION

The availability of high-energy heavy ion beams at the LBL Bevatron has made it possible to investigate experimentally the mechanism involved in nucleus - nucleus interactions. It is of main interest to make some progress in this field as it appears that heavy nucleonic probes will give us much information about the elementary processes involved in high - energy collisions.

The preliminary results we present here will be analyzed in order to test some important properties predicted by the quantized unitarity interaction model (ref. 1), especially the existence of coplanarities in high-energy production processes.

The experiment was done using nuclear emulsion detectors which present very high angular resolution in all space.

The emulsion stacks, irradiated by the 2.1 GeV/N oxygen beam, were made of normal K-5, 600 μ thick Ilford plates. They have been chosen for their sensibility that make it convenient to follow any emitted charged particle. Furthermore it will give us a sample of hydrogen, light and heavy, spin and spinless nucleus - nucleus interactions. We measured eight stars, the targets have been identified and selected according to the method developed in reference 2.

II - DATA PROCESSING

A. Improved measurement procedure

Very precise angle measurements have been performed by physicists on "LEITZ Orthoplan" microscopes which have been selected for their mechanical properties of vertical motion. Indeed their helicoïdal system for measuring dips is believed to be most insensitive to wear and to give a constant measurement unit, since integrated on a large number of screw steps.

All microscopes are kept at constant temperature during the measurements, the star being adjusted to the optical axis and the stage definitely blocked up in the (x,y) plane.

Measurements of azimuthal angles are made relatively to any arbitrary original direction of a goniometer which gives directly minutes of arc. Ten independant measurements are made by considering the parallelism between the reticle of the goniometer and each track.

HIGH-ENERGY ELEMENTARY PROCESSES IN NUCLEUS-NUCLEUS INTERACTIONS

D. KARAMANOUKIAN, C. JACQUOT, R. PFOHL, J.N. SUREN

Laboratoire de Physique Corpusculaire - Strasbourg

Groupe des Ions Lourds Relativistes

High resolution in angular distributions has been obtained for nucleus-nucleus interactions induced by the 2.1 GeV/n incident oxygen beam of the LBL bevatron. In the first part we present the technical improvements and the measurement procedure we have developed to this purpose. In the second part we analyze six events and conclude to the existence of geometrical correlations between the charged particles emitted in the first scattering process.

This set of particles includes the leading one and corresponds to the diffractive component of high-energy particle production. The dynamical origin of these correlations is discussed and the existence of internal parameters suggested.

NUCLEAR REACTION O^{16}, emulsion nuclei, E = 2.1 GeV/n, measured angular correlations, deduced elementary processes, leading particle effect, diffractive scattering, dynamical correlations.

For each one the ten independent dip measurements are made starting from the center of the star up to a determined point of the track by retaining the maximum contrast of the track grains. The micrometric screw is to be rotated slowly in the same direction in order to avoid mechanical play effects. By adjoining a vernier to the micrometric screw we are able to evaluate the tenth of a micron.

To reduce the depth of vision field we used 100 x object and 25 x ocular lens. A "LEITZ" goniometer is fixed on the binocular and a television camera on the central tube.

The dip measurements are made using a television screen in order to avoid the eyes' accomodation of the operator. The fixed micrometer has been mechanically dissociated from the exit centered lens system so to fourfold the television field. By the way we also get a better resolution on the micrometer system, a longer measurable track length and a smaller depth field.

B. Experimental biases and corrections

Table 1 shows the detail of measurements for one event. The two first columns contain each ten independent values, expressed in microns, of the relative dip position of two grains, one located near the center of the star, the other one on the track at about half a micrometer length. The exact projected distance between these two points is expressed in micrometer units. The third column shows ten independent values of the azimuthal angle, in degrees and minutes.

The values have been corrected for field curvature. Physical constraints such as emulsion distorsion are negligeably small because the volume containing the measured lengths is elementary enough in regards to such macroscopic effects. Further geometrical aberrations have not been considered since the star is adjusted on the optical axis and no noticeable distorsion was detected for the beam tracks.

III - DATA ANALYSIS

Our aim is to detect the existence of physical coplanarities in high-energy particle production. At this stage of our study we only know the angular distribution event by event and therefore are unable to transform laboratory variables into center-of-mass ones.

So we have to restrict ourselves to collisions which conserve the center-of-mass coplanarities. Furthermore, we had to reject two events with special configurations, i.e. with few tracks very strongly collimated in the forward direction and presenting large relative errors, which could favour too much the coming out of coplanarities.

One of the oxygen-hydrogen interactions is remarkable by its relativistic heavy ion emission. Though its asymmetryis larger than the one of the other stars, we have included it in our study in order to show that the coplanarity effect also exists in that specific case. But we should be a priori aware that it will be more difficult to conclude for physical effects in the case of that star.

We did an independent event analysis and a systematic search for coplanary tracks on six events, four oxygen-hydrogen interactions, one oxygen-light nucleus and one oxygen-heavy nucleus interaction satisfying the above criteria. We decided for coplanarity each time the box product of the directive cosines was both compatible with zero within the error and less than $1^{o}/oo$.

In each event we found coplanarities of 3, 4 and even 5 charged particles, which we divided into 2 groups.

type A : coplanarities, containing the incident track. They are invariant in the CMS to laboratory system transformation.

type B : coplanarities not containing the incident track. They are not invariant in such a transformation.

In order to extract the physical coplanarities of three particles out of casual ones, we deformed randomly our events in the following way :

- in order to conserve the kinematical constraints as well as possible the directive cosines were deformed so that the real angle between each track and the incident one remained constant.

- in order to avoid any too large geometrical deviation, the final asymmetryfactor was not allowed to change by more than 25 %.

1 - Coplanarities of three tracks

In Figures 1 A, 1 B, and 1 C, we plot the ratios $P_i^f(1)$, $P_i^f(t)$ and $P_i^f(t-1)$ definedas follows :

$$P_i^f(1) = \frac{\text{(number of coplanarities of type A) real event}}{\text{(number of coplanarities of type A)}_{i^{th}} \text{ deformed event}}$$

$$P_i^f(t) = \frac{\text{(number of coplanarities of types A and B) real event}}{\text{(number of coplanarities of types A and B)}_{i^{th}} \text{ deformed event}}$$

$$P_i^f(t-1) = \frac{\text{(number of coplanarities of type B) real event}}{\text{(number of coplanarities of type B)}_{i^{th}} \text{ deformed event}}$$

One can see that there is a large excess of real coplanarities including the incident track while the other real ones appear as more casual, essentially in the last ratio. The statistical excess in the case of Figure 1 C is mainly due to the physical constraints which remain while crudely substracting number of coplanarities.

Figure 2 A represents the frequency of the ratio R_i^f defined by :

$$R_i^f = \left(\frac{\text{number of coplanarities of type A}}{\text{number of coplanarities of type A and B}}\right)_{\text{real event}} \Bigg/ \left(\frac{\text{number of coplanarities of type A}}{\text{number of coplanarities of type A and B}}\right)_{i^{th} \text{ deformed even}}$$

Figure 2 B represents the frequency of the ratio R_i^s defined by :

$$R_i^s = \left(\frac{\text{number of coplanarities of type A}}{\text{number of coplanarities of type A and B}}\right)_{i^{th} \text{ deformed event}} \Bigg/ \left(\frac{\text{number of coplanarities of type A}}{\text{number of coplanarities of type A and B}}\right)_{(i+1)^{th} \text{ deformed event}}$$

Each event was deformed thirty times and the values $R^f = 1.0$ were equally distributed between the "statistical" (R<1) and the "physical" (R>1) sides. We immediately see that the ratios $R^f>1$ are about six times more frequent than the $R^f \leq 1$ ones ; on the other hand the ratios $R^s>1$ and $R^s<1$ are equally probable, as expected.

In order to determine what kind of particles are involved in these coplanarity effects we did a systematic cut-off analysis on white, grey, black, jet- and non jet - particles. We found that the most unbiased sample was made of the high-energy heavy ion tracks, if any, and of all the grey and white trakcs, i. e. of essentially the relativistic tracks. Figure 3 showing the R^f histogram for these relativistic tracks does not reveal any noticeable discrepancy with Figure 2.

2 - Phenomenological analysis of four tracks coplanarities

The next step was to look for high order coplanarities. Table 2 shows the frequency of four tracks coplanarities appearing in each event deformed thirty times in the same way as described before. There is a striking evidence for very high abundances in our real events.

Let us now begin with the event by event analysis, in order to get some more specific and relevant informations about the first step elementary process (FSEP).

$$\frac{(COP_4^1)\ \text{STAT.}}{(COP_4^1)\ \text{PHYS.}}$$

	0	0.1	0.2	0.3	0.4	0.5	0.6	0.7	0.8	0.9	1	2	3	4	5	≥1/<1
AgBr	20		7		2						1					1/29
CNO	12			9				6			2	1				3/27
H(1)	19										1					1/29
H(2)	18										8	1	1	1	1	12/18
H(3)	28										1	1				2/28
H(4)	20										5	2	3			10/20

Table 2

The number of realistic coplanarities have been deduced by assuming that a track cannot belong to more than one deduced coplanarity. Table 3 summarizes the characteristics of each event.

Comments on Table 3 :

1 - column 1 represents the configuration of the measured coplanarities. Each circle represents a charged particle contributing in coplanarities, the black one being the incident one.

2 - star N° is the identification number.

3 - target H1, H2, H3, H4 are 4 stars on hydrogen target.
CNO : Target belonging to C,N,O group
AgBr : Target belonging to Ag, Br group.

4 - column 4 represents the total number of charged particles in the final state.
W : means white (relativistic) tracks
G : means grey (relativistic) tracks
B : means black (low energy) tracks
HI : means relativistic heavy ions in the forward direction.

5-6 - columns (5,6) represent respectively the measured number of 3,4 tracks coplanarities including the incident one.

7 - column (7) represents the deduced number of 4 tracks coplanarities, where W, G, and B represents the nature of the tracks contributing in each of such coplanarities.

8 - column (8) represents the deduced number of 3 tracks coplanarities, including the incident particle.

9 - column (9) Number of 3 tracks coplanarities which do not interfer in the 4 tracks one.

10 - column (10) Number of coplanarities formed by more than 4 tracks.

11 - column (11) The ratio of the number of charged particles contributing in the coplanarities to the total number of charged particles in the final state.

12 - column (12) Number of elementary processes as explained in section (3.2).

13 - column (13) represents the configuration of the deduced coplanarities.

In the case of hydrogen targets we observe only one four-tracks coplanarity. This is to be expected if one assimilates the first step with the first scattering inside the projectile. In the case of CNO and Ag Br targets we may say that two, four scattering processes are generated in the first step.

MEASURED SCHEME	STAR N°	TARGET	TOTAL NUMBER OF TRACKS	N° OF MEAS. COP_1^3	N° OF MEAS. COP_1^4	N° OF DEDUCED COP_1^4	N° OF DEDUCED COP_1^3	N° OF FINAL COP_1^3	N° OF COP_1 > 4	N° OF TRACKS IN COPLANARITIES / TOTAL NUMBER	N° OF ELEM. PROCESSES	DEDUCED SCHEME	COMMENTS
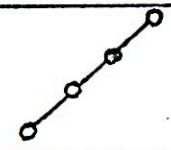	1991	H1	9 W = 2 G = 4 B = 3	3	1	1 W = 1 G = 1 B = 1	3	∅	0	3/9 = 0.33	1	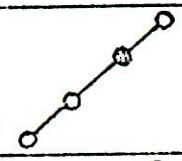	
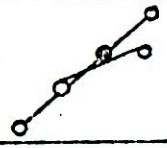	2869	H2	9 W = 3 G = 2 B = 4	4	1	1 W = 2 G = 1	3	0	0	3/9 = 0.33	1	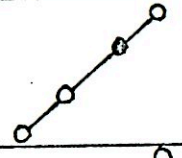	
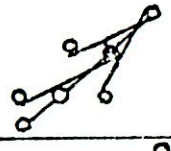	2294	H3	7 W = 2 G = 2 B = 3	6	1	1 W = 2 G = 1	3	0	0	3/7 = 0.42	1	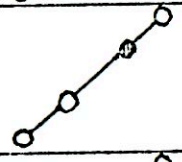	
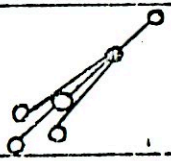	3182	H4	6 G = 4 B = 1 HI = 1	5	1	1 G = 2 HI = 1	3	0	0	3/6 = 0.5	1	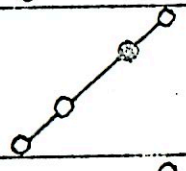	Heavy Ion in the forward direction
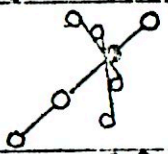	1418	C N O	11 W = 1 G = 7 B = 3	9	3	1 W = 1 G = 1 B = 1	4	1 G=1 B=1	0	5/11 = 0.45	2	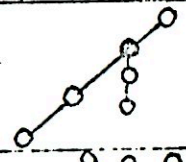	
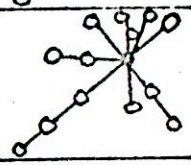	2672	Ag Br	25 W = 17 G = 3 B = 5	12	1	1 W = 2 G = 1	11	2 W=2 W=2	1 W=4	11/25 = 0.44	4	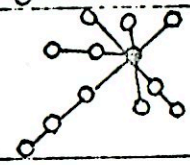	

Table 3

We now consider one sample of four-tracks coplanarities (FSEP4) which each presents the following characteristics :

- there is one FSEP4 in each star
- the track emitted in each star at the smallest angle is contained in the FSEP4. We shall call this track the leading track (LT).
- The incident (IN) and the leading track directions are included in the interval made of the two other coplanary track directions (A and B tracks).

In table 4 we present the FSEP4 angular schemes where the angles are computed from the leading track. We can then make the following comments :

- all FSEP4 have the same general configuration
- the leading track is always on the same side as the second smallest angle track (A-track).
- it seems that according to the relative A-and B - angle values, we could have two classes of FSEP4, the more symetric H3 and H4 ones on one hand, the less symmetric H1, H2, CNO and AgBr ones on the other hand.

	A	LT	IN	B	
	a	o	i	b	
H1	281	0	74	8769	(minutes of arc)
H2	200	0	80	6119	"
H3	54	0	40	115	"
H4	85	0	31	221	"
CNO	17	0	33	3624	"
AgBr	542	0	112	5704	"

Table 4

In the case of three tracks coplanarities we could not find any systematic configuration ; this may be due either to some neutral missing particle or to casual coplanarities of tracks which do not belong to the first step. Therefore we shall try only to interprete the FSEP4.

V - PHYSICAL INTERPRETATION

We are conscious that our statistics should be increased in order to confirm the generality of our results, nevertheless one can conclude to the existence of geometrical correlations.

In the following we shall call cluster any interacting subnuclear region and distinguish between projectile and target clusters.

A - Dynamical origin of the coplanarity effect

The coplanarities can be explained in a simple classical way by high momentum angular transfer to the first step clusters.

One can imagine two high-energy clusters colliding at a given impact parameter. The relative angular momentum will be converted into high spins of the two clusters in the final state. If the spins in the initial state are negligeably small the final state spins will be parallel to the relative angular momentum vector, perpendicular to the incident kinetic momentum and to the impact parameter vectors. Such spins will lead to the emission of particles in a plane including the incident track and conserved in the center-of-mass to laboratory system transformation. Figure 4 shows the symmetric emission of two particles with same mass.

One can see that the configuration A, IN, LT, B is holding in any case. Furthermore we can make the following comments :

- if the initial state spins are negligeably small, a and b remain small in regards to IN.
- for given spins, if a increases, b decreases and vice versa.
- high spins may explain large momentum transfers, backward emission and velocities in forward direction much larger than the incident one.

In a less classical way one could imagine that the incident particle is getting same planetary configuration while being accelerated. The collision with the target would make the satellites being ejected and emitted in the laboratory system. The orbital planes should then include the incident track so that the coplanarities are conserved in the center-of-mass to laboratory system transformation. This last picture could explain why cosmic-ray people (ref. 3,4) attribute the leading fragments to the incoming particle.

B - Properties of the diffractive component in particle production

Let us now look how the FSEP inserts in the generally reported phenomena.

The FSEP tracks are highly anisotropic and made of relativistic, very fast and medium fast particles going in opposite directions. This fact has to be considered as a sign of diffraction scattering. The mean-multiplicity FSEP is only weakly depending on energy and our value of 2.4 is in good agreement with the value of 2.5 reported (ref. 6) for 200 GeV proton-nucleus interactions.

It appears that the leading particle, which can be either an incident nucleon, or an incident cluster, induces the liberation of associated particles, fastly orbiting in a central force field. In this hypothesis the production characteristics could be described by some new parameters such as internal impact parameters.

To draw more precise conclusions we have undertaken granulometric and photometric measurements in order to identify the particles involved in these elementary processes. We are also increasing the statistics in order to get precise values for the angles between the FSEP planes

Already now it seems that the elementary processes are fundamental ones underlying the high-energy diffraction mechanism.

Especially in the case of hydrogen targets the FSEP will give us fruitful information on the cluster distribution inside the incident nuclei.

ACKNOWLEDGMENTS

We are most grateful to Dr H. HECKMANN for his very kind help during the experiment at the LBL beam. We wish to thank our collaboration from the Laboratorio de Fisica Corpuscular Universidad Autonoma de Barcelona for their help in the measurements.

The experiment has been supported by the NATO research grant nb. 145.

FIGURE CAPTIONS :

- Figure 1 A : represents the frequency of the ratio physical to statistical number of 3 tracks coplanarities including incident track, for six events deformed 30 times.

  B : represents the frequency of the ratio physical to statistical total number of 3 tracks coplanarities.

  C : represents the frequency of the same ratio for total number of coplanarities which do not include the coplanarities the incident track.

- Figure 2 A : represents the R^f physical ratio for 3 tracks coplanarities (all the tracks).

  B : represents the R^s statistical ratio for 3 tracks coplanarities (all the tracks).

Figure 3 : represents the R^f ratio for 3 tracks coplanarities (relativistic tracks only).

Figure 4 : Symmetric emission of two particles with same mass in high spin hypotheses.

Table 1 : Measurement sheet for one event

Table 2 : Frequencies of the ratio : number of four tracks coplanarities in deformed events over the same in measured events.

Table 3 : Analyse of the coplanarities of each event.

Table 4 : Angular values of the FSEP 4 tracks.

EVENT 1418 0 incident WGB (White, Grey, Black) UD (Up, Down)

OD		
50.5	51.	306.55
50.5	50.9	306.59
50.4	50.9	307.03
50.5	51.	307.01
50.0	50.4	306.54
50.5	51.	306.54
50.5	51.	306.56
50.5	51.	306.57
50.5	50.8	306.52
50.5	50.8	306.51

50 µm

BD		
50.2	63.5	182.48
50.5	63.5	182.40
50.5	63.8	182.47
50.5	64.1	182.40
50.5	64.	182.51
50.3	64.	182.49
50.3	63.9	182.44
50.4	64.1	182.56
50.4	63.9	182.49
50.5	64.	182.57

50.5 µm

WU		
51.9	29.	133.41
51.9	29.	133.45
51.8	29.	133.41
51.5	29.	133.38
52.0	29.3	133.58
52.5	29.	133.46
52.0	29.4	133.48
52.0	29.4	133.49
52.0	29.	133.45
52.0	29.	133.38

46 µm

WU		
50.8	24.3	100.33
50.5	24.2	100.37
50.5	24.2	100.30
50.8	24.4	100.31
50.5	24.3	100.32
50.5	24.	100.33
50.2	24.	100.35
50.5	24.3	100.37
50.3	24.	100.35
50.4	24.	100.36

47 µm

GD		
51.2	52.	127.25
51.2	52.	127.24
51.0	51.6	127.28
50.9	51.5	127.20
51.1	52.	127.19
51.2	52.	127.24
51.6	52.	127.25
51.3	52.1	127.22
51.5	52.1	127.25
51.5	52.1	127.22

48 µm

WD		
51.2	51.6	126.10
51.4	52.	126.10
51.3	51.7	126.12
51.1	51.5	126.09
50.9	51.2	126.10
50.9	51.3	126.09
50.8	51.3	126.06
50.9	51.3	126.08
50.8	51.3	126.14
50.8	51.2	126.11

43 µm

WU		
52.2	51.7	126.10
52.3	51.7	126.10
52.2	51.8	126.12
52.4	51.7	126.09
52.4	51.7	126.10
52.0	51.3	126.09
52.2	51.6	126.06
52.0	51.3	126.08
52.0	51.4	126.14
52.1	51.2	126.11

48.5 µm

WD		
47.7	74.6	344.33
47.9	74.	344.37
47.5	74.	344.30
47.6	74.2	344.34
47.7	74.2	344.39
47.7	74.2	344.34
47.5	74.2	344.40
47.5	74.3	344.36
47.7	74.5	344.29
47.6	74.	344.37

47.µm

WU		
51.0	39.9	111.40
51.2	39.9	111.36
51.2	39.9	111.43
51.0	40.	111.39
51.1	39.9	111.45
51.2	40.	111.42
51.2	39.9	111.38
49.9	39.6	111.38
51.3	39.5	111.39
51.0	39.6	111.46

45 µm

BD		
49.2	24.7	106.47
49.0	25.1	106.40
49.3	25.4	106.40
49.0	25.4	106.44
49.1	25.5	106.48
49.8	25.8	106.52
49.6	25.6	106.52
49.6	25.6	106.49
49.5	25.5	106.50
49.2	25.9	106.41

47 µm

WD		
49.9	66.2	100.54
50.0	66.	100.50
49.9	66.	100.51
49.9	66.	100.52
49.9	66.	100.56
49.8	66.3	100.48
50.0	66.9	100.58
49.8	65.8	100.55
49.8	66.	100.53
49.8	66.	100.52

44 µm

BD		
49.2	75.5	44.15
48.7	75.4	44.09
48.5	75.5	44.08
48.5	75.5	44.07
48.5	75.5	44.04
48.5	75.5	44.12
48.4	75.4	44.05
48.4	75.5	44.05
48.2	75.3	44.06
48.3	75.4	44.04

49 µm

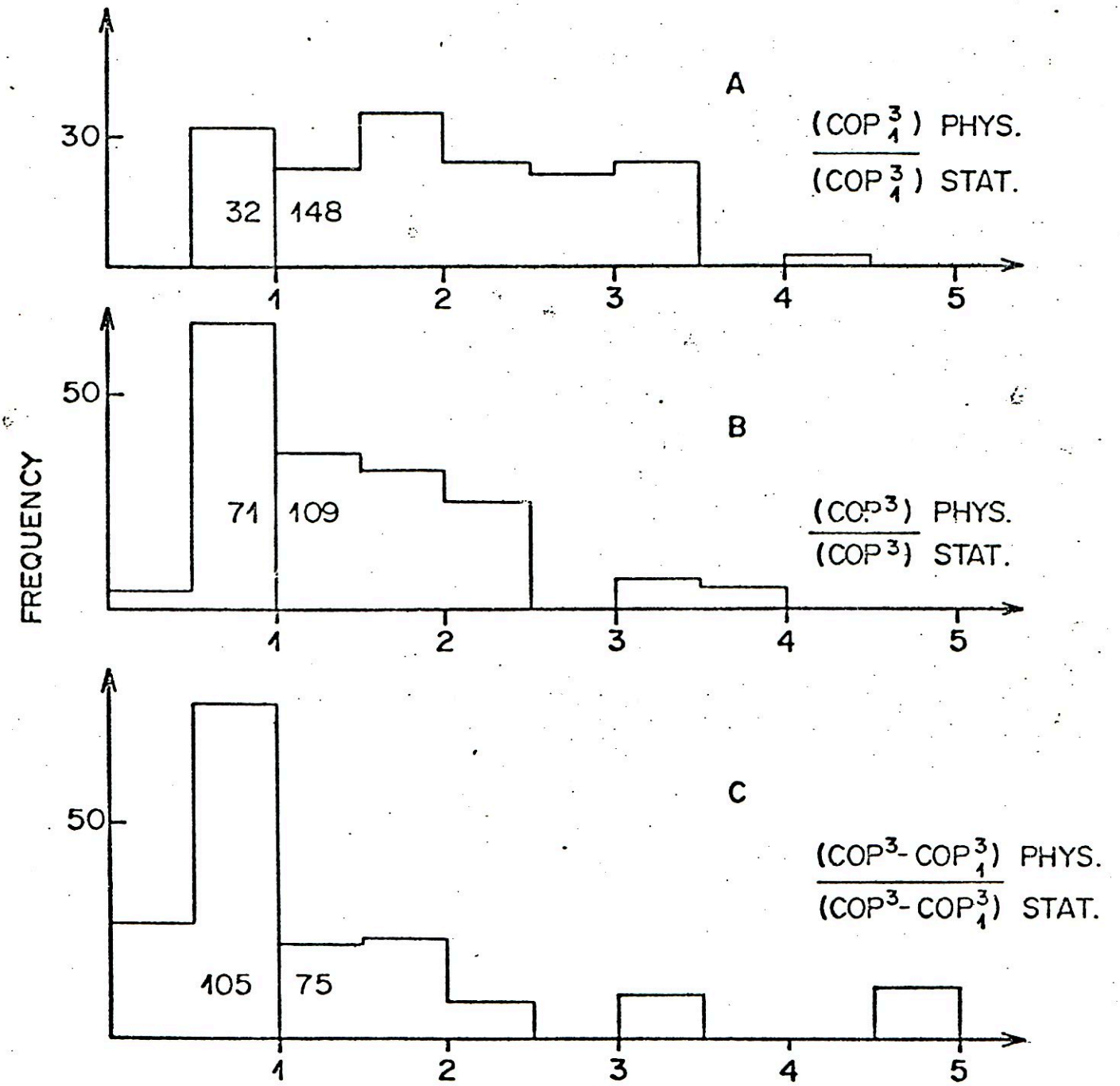
A
30
32
148
1
2
3
4
5
(COP 3 1) PHYS.
(COP 3 1) STAT.
B
50
71
109
FREQUENCY
(COP3) PHYS.
(COP3) STAT.
C
50
105
75
(COP3- COP 3 1) PHYS.
(COP3- COP 3 1) STAT.

fig 1

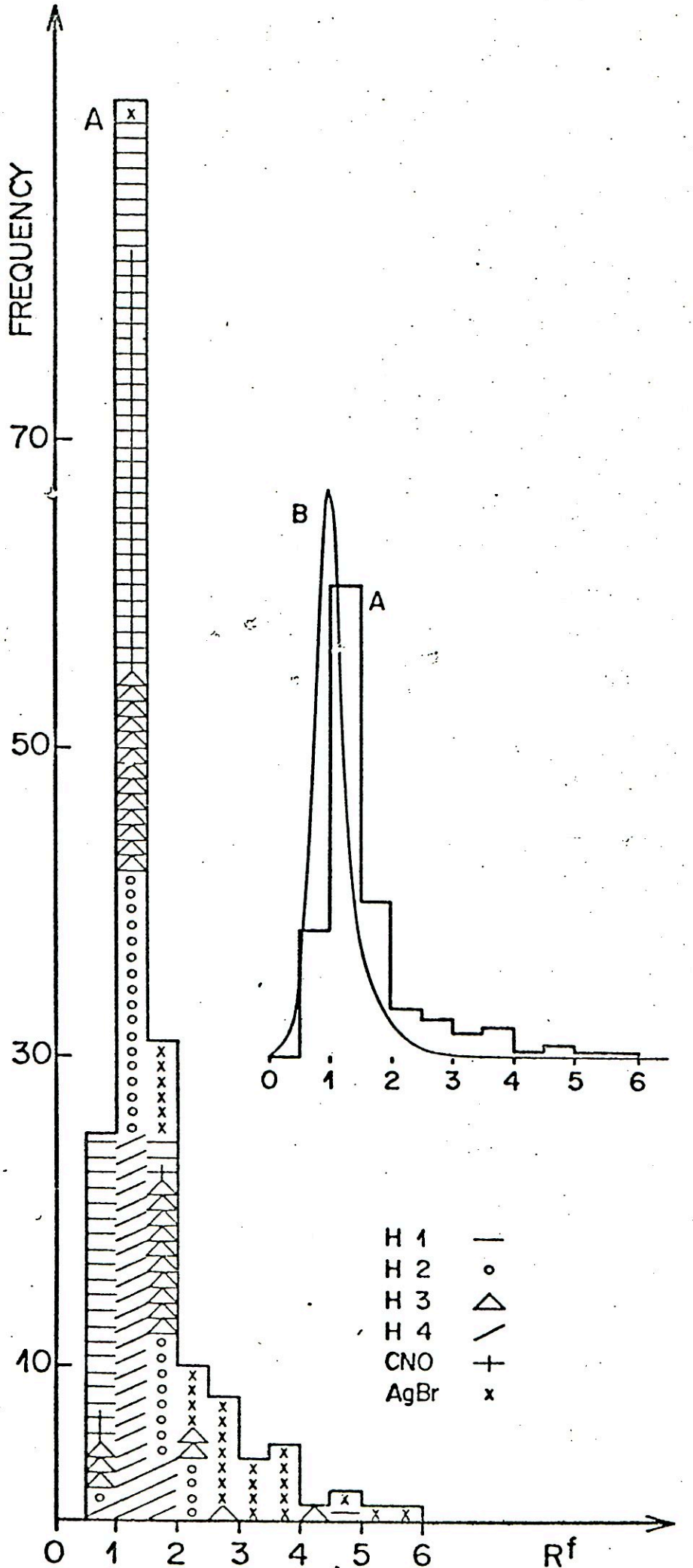

fig. 2

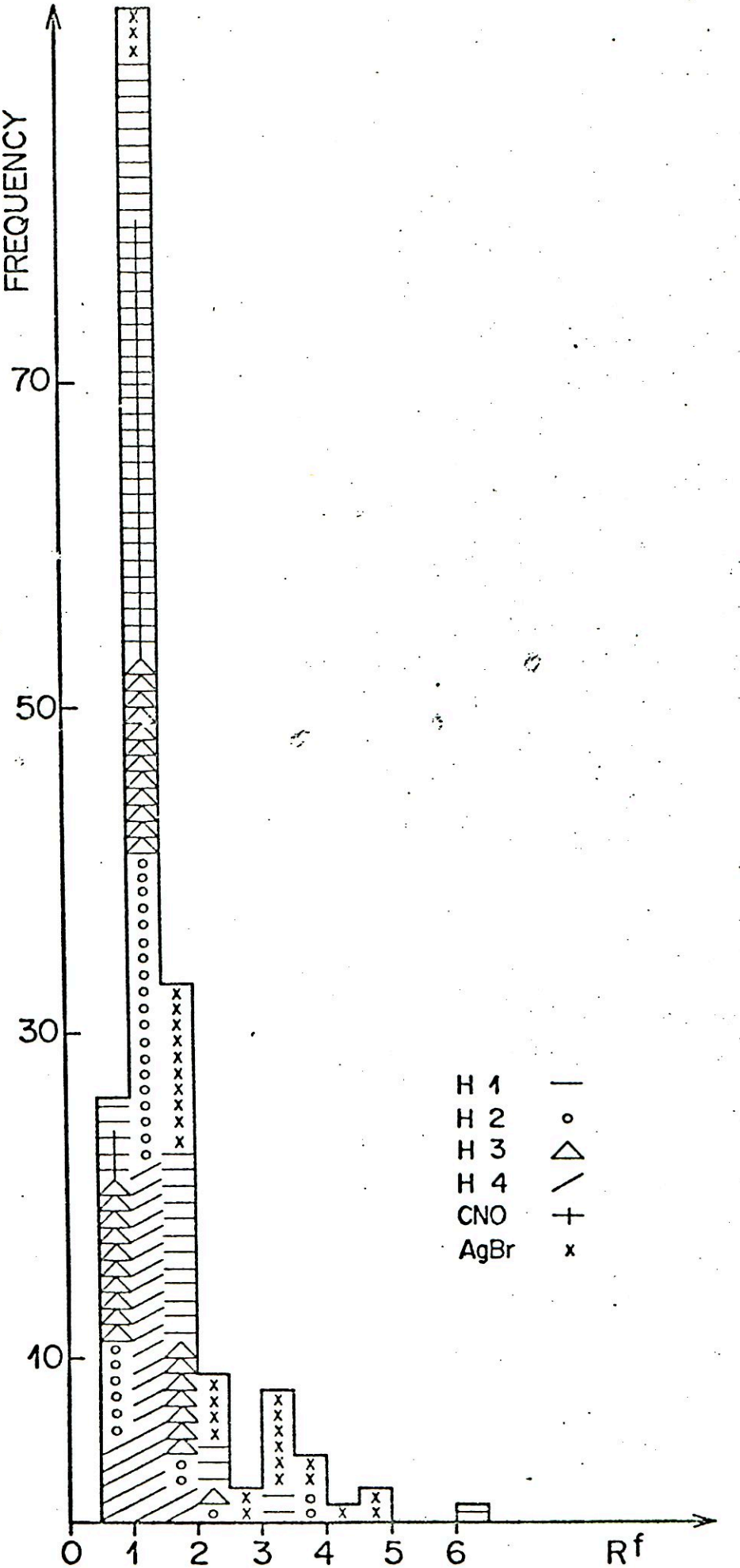

fig 3

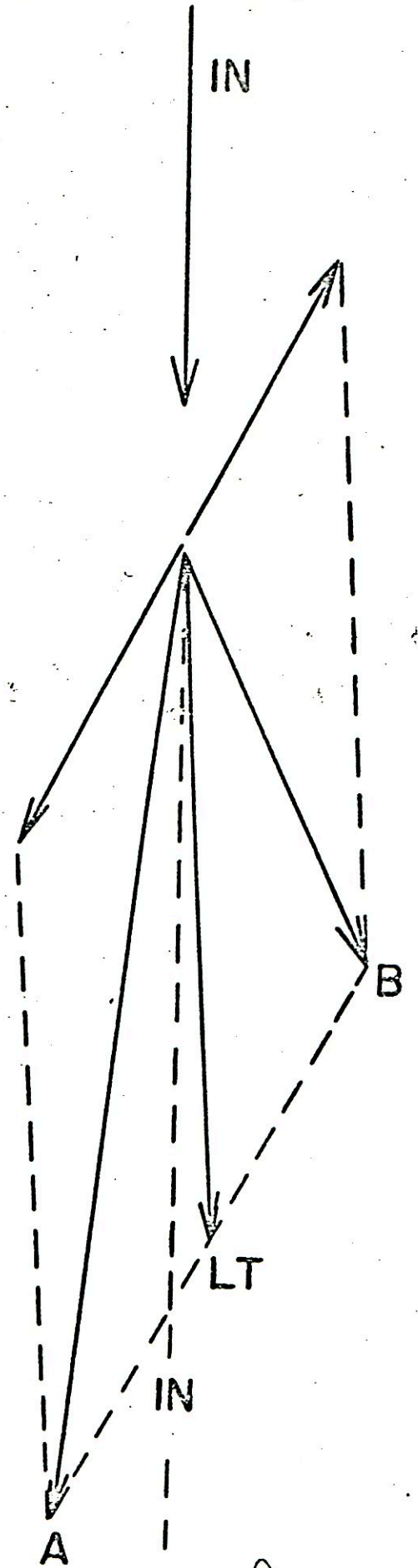

fig 4

REFERENCES

1 - SUREN J.N. et al.
Effets des singularités du canal q dans les interactions Noyau-Noyau.
Preprint Laboratoire de Physique Corpusculaire - Strasbourg.

2 - KARAMANOUKIAN D., JUNG M., GIRARDIN L.
Target selection in high-energy nucleus-emulsion nuclei interactions.
Submitted to Phys. Rev.

3 - D.H. PERKINS
Emission of heavy fragments in nuclear explosions.
Proc. Roy. Soc. A, 203, 399 (1950)

4 - H.H. HECKMANN, D.E. GREINER, P.J. LINDSTROM, F.S. BIESER
Fragmentation of ^{14}N Nuclei at 2.1 GeV/nucleon.
LBL 345 (1971).

5 - E.L. BERGER
Fragmentation models for Particle Production
Fourth International Conference on High Energy Collisions, Oxford (1972).

E.L. FEINBERG
Multiple production of hadrons at Cosmic ray energies (experimental results and theoretical concepts)
North-Holland Publishing Company.

6 - L. VAN HOVE
Particle Production in Complex Nuclei
Preprint Th 1746 - CERN, September 1973.

J. HEBERT et al.
Study of nuclear interactions of 200 GeV protons in emulsion, 5th International Conference on High Energy Physics and Nuclear Structure, Uppsala, June 1973.

7 - I. OTTERLUND
Studies of High Energy Nucleus-Nucleus interactions - Lund (1969).